ANALYTICAL MODELING OF REINFORCED CONCRETE PANEL ELEMENTS UNDER REVERSED CYCLIC LOADINGS

by

Denizhan Uluğtekin

B.S., Civil Engineering, Kocaeli University, 2007

Submitted to the Institute for Graduate Studies in
Science and Engineering in partial fulfillment of
the requirements for the degree of
Master of Science

Graduate Program in Civil Engineering

Boğaziçi University

2010

ANALYTICAL MODELING OF REINFORCED CONCRETE PANEL ELEMENTS UNDER REVERSED CYCLIC LOADINGS

APPROVED BY:

Assist. Prof. Kutay Orakçal (Thesis Supervisor) .....

Prof. Uğur Ersoy (Thesis Co-Supervisor) .....

Assoc. Prof. Alper İlki .....

Assoc. Prof. Hilmi Luş .....

Assoc. Prof. Cem Yalçın .....

DATE OF APPROVAL: 15/06/2010

To my first and real engineering coach,

My father . . .

ACKNOWLEDGEMENTS

I would like to express my sincere gratitude to my thesis supervisors Assistant Professor Dr. Kutay Orakçal and Professor Dr. Uğur Ersoy for their invaluable guidance and help during the preparation of this thesis. I would like to mention their patience, giving me inspiration and hope when I was at the darkest part of the black tunnel.

I would like to express my special thanks to Dr. Leonardo M. Massone for his kind and advisory guidance.

I would also like to thank Associate Professor Dr. Alper İlki, Associate Professor Dr. Hilmi Luş and Associate Professor Dr. Cem Yalçın for their kind and supportive attitude to me and showing high interests and valuable advices to my thesis.

I am also grateful to Associate Professor Dr. Şevket Özden, Dr. Onur Ertaş, Assistant Professor Dr. Seval Pınarbaşı and Assistant Professor Dr. Fuad Okay for their kind and unlimited supports during my whole thesis.

I would also like to thank Dr. Mohammad Mansour for his sharing attitude shown by sharing his test data with our research group.

I would also like to thank Dr. Selçuk Altay and Dr. Osman Kaya for their kind and supportive attitudes during the endless discussions. I have also very much benefited from the discussions with my dear “Civil Engineer” friends; Mustafa Cömert, Umut Karacadağlı, Mehmet Ülker, Erkan Yılan, Mehmed Çakkol and Bernard Adam. I thank them all for their support and friendship throughout the preparation of this thesis.

I am grateful to my parents for the endless support, encouragement and love they have given me throughout my life.

This research has been financially supported by Boğaziçi University Research Fund, under Project numbers 08A403 and 09S110.

ABSTRACT

ANALYTICAL MODELING OF REINFORCED CONCRETE PANEL ELEMENTS UNDER REVERSED CYCLIC LOADINGS

A novel constitutive model – named as the Fixed Strut Angle Model (FSAM) – is proposed in this study for simulating the cyclic shear behavior of reinforced concrete panel elements. The constitution of the FSAM is based on interpretation of previously-developed reinforced concrete panel models, as well as the results of panel tests available in the literature. The FSAM, with its assumptions and limitations clearly stated; is capable of predicting the nonlinear shear behavior and axial-shear response coupling of reinforced concrete panels subjected to generalized and reversed cyclic loading conditions in plane.

The main inherent assumption underlying the formulation of the FSAM is that upon cracking of concrete in a reinforced concrete panel, principal stress directions in concrete do not rotate and coincide with fixed crack directions, implying zero shear stresses along cracks and therefore zero shear aggregate interlock. Although this type of behavior have been consistently observed in panel tests, a modeling methodology which assumes fixed principal stress directions for concrete has not been proposed to this date.

State-of-the art constitutive material relationships were implemented in the formulation of the proposed model and a nonlinear analysis solution strategy was used for conducting nonlinear quasi-static analyses using the model. Correlation studies were conducted to compare the model predictions with results of cyclic reinforced concrete panel tests available in the literature. The model was shown to capture, with reasonable accuracy, overall behavioral attributes of RC panels, including cyclic shear stress versus shear strain behavior, shear stress capacity, stiffness, cyclic stiffness degradation, pinching, ductility, and failure mode. The model has also yielded promising results on local deformation predictions.

The proposed constitutive model is expected to be a feasible candidate for implementation into a two-dimensional finite-element analysis formulation, for efficient and practical response prediction of reinforced concrete walls with various geometries and reinforcement details.

ÖZET

TERSİNİR TEKRARLI GENELLEŞTİRİLMİŞ YÜKLER ALTINDAKİ BETONARME PANEL ELEMANLARIN ANALİTİK MODELLEMESİ

Bu çalışmada, betonarme panel elemanların tekrarlı kesme davranışlarını benzeştiren, Sabit Payanda Açısı Modeli (SPAM) adında bir model sunulmuştur. Modelin oluşumunda, literatürde bulunan bugüne kadar sunulmuş betonarme panel eleman modellerinin ve deneylerinin değerlendirilmesi temel alınmıştır. SPAM, açık bir şekilde belirlenmiş kabulleri ve kısıtlamaları ile betonarme panel elemanların genelleştirilmiş tersinir tekrarlı yükler altındaki doğrusal olmayan kayma ve eksenel-kayma etkileşimli davranışlarını öngörme kapasitesine sahiptir.

SPAM ın en temel kabulü, betonarme panel elemanda çatlak oluşması halinde, asal gerilme doğrultusunun, çatlak yüzeylerinde oluşan kayma gerilmelerini sıfıra eşit olduğu kabulünü de yaparak, asal birim şekil değiştirmeler ile birlikte dönmeye devam etmemesi ve çatlak doğrultusunda sabit kalmasıdır. Yapılan deneylerde bahsi geçen türde davranışlar gözlenmiş olduğu halde, betonda sabit asal gerilme doğrultusu kabulü yapan başka bir model bulunmamaktadır.

Modele en yeni malzeme modelleri eklenmiş ve modelin doğrusal olmayan "kısmi durağan" analiz yapabilmesi için bir "doğrusal olmayan çözüm stratejisi" kullanılmıştır. Tekrarlı betonarme panel eleman testleri ile model tahminleri arasında yapılan karşılaştırmalar literatürde bulunmaktadır. Model betonarme panel elemanların tekrarlı kayma gerilmesi-kayma birim şekil değiştirmesi, kayma gerilmesi kapasitesi, rijitlik, tekrarlı rijitlik kaybı, daralma, süneklik ve göçme modları gibi davranışsal özelliklerini makul hata sınırları içerisinde tahminedebildiğini göstermiştir. Ayrıca model bölgesel şekil değiştirme tahminlerinde de ümit verici sonuçlar vermiştir.

Sunulan modelin, çeşitli geometri ve donatı detaylarına sahip olan betonarme duvar davranışlarının, pratik ve etkili bir şekilde tahmininde kullanılabilecek olan iki boyutlu bir Sonlu Elemanlar programında kullanılmaya aday bir model olduğu düşünülmektedir.

TABLE OF CONTENTS

ACKNOWLEDGEMENTS…… iv
ABSTRACT…… v
ÖZET…… vii
TABLE OF CONTENTS…… ix
LIST OF FIGURES…… xii
LIST OF TABLES…… xviii
LIST OF SYMBOLS…… xix
1. INTRODUCTION…… 1
1.1. General …… 1
1.2. Literature Review …… 3
1.2.1. Overview…… 3
1.2.2. Monotonic Constitutive Panel Models…… 6
1.2.2.1. Modified Compression Field Theory (Vecchio and Collins 1986)…… 6
1.2.2.2. Rotating Angle Softened Truss Model (Pang and Hsu 1995). 7
1.2.2.3. Fixed Angle Softened Truss Model (Pang and Hsu 1996)…. 7
1.2.2.4. Softened Membrane Model (Hsu and Zhu 2002)…… 9
1.2.2.5. Disturbed Stress Field Model (Vecchio 2000)…… 9
1.2.3. Cyclic Constitutive Panel Models…… 11
1.2.3.1. Stevens et el. (1991)…… 11
1.2.3.2. Mansour and Hsu (2005)…… 14
1.2.3.3. Ohmori et el. (1989)…… 14
1.2.3.4. Palermo and Vecchio (2003)…… 15
1.2.3.5. Gérin and Adebar (2009)…… 15
1.2.4. Assumptions, Limitations and Applicability of Available Models…. 15
1.3. Research Significance …… 17
1.4. Objectives…… 18
1.5. Scope …… 18
1.6. Thesis Outline …… 19
2. MODEL DESCRIPTION…… 20

2.1. Overview 20
2.2. Uncracked Panel Response 24
2.3. Panel Response after formation of First Crack 27
2.4. Panel Response after formation of the Second Crack 30
2.5. Nonlinear Analysis Solution Strategy 35
2.5.1. Incrementation Cycle (First Iteration Cycle)..... 35
2.5.2. Equilibrium Iteration Cycles..... 38
3. MATERIAL CONSTITUTIVE MODELS 41
3.1. Constitutive Model for Reinforcement 41
3.2. Constitutive Model for Concrete 45
3.2.1. Compression Envelope Curve..... 45
3.2.2. Tension Envelope Curve..... 49
3.2.3. Hysteretic Properties of the Model..... 51
3.3. Compression Softening of Concrete 56
3.3.1. Vecchio and Collins (1993)..... 57
3.3.1.1. Model A..... 56
3.3.1.2. Model B..... 57
3.3.2. Belarbi and Hsu (1995)..... 58
3.4. Tension Stiffening Effect on Concrete and Steel 59
3.5. Biaxial Damage on Concrete 62
4. COMPARISON OF MODEL RESULTS WITH EXPERIMENTAL DATA 65
4.1. Cyclic Panel Tests in the Literature 65
4.1.1. Tests by Stevens (1987)..... 65
4.1.2. Tests by Mansour and Hsu (2005)..... 67
4.2. Comparisons of Model Results with Test Results of Stevens 69
4.2.1. Global Comparisons..... 69
4.2.1.1. Specimen SE8..... 69
4.2.1.2. Specimen SE9..... 70
4.2.1.3. Specimen SE10..... 71
4.2.2. Local Response Comparisons..... 71
4.2.2.1. Specimen SE8..... 72
4.2.2.2. Specimen SE9..... 74
4.2.2.3. Specimen SE10..... 79

4.3. Comparisons of Model Results with Test Results of Mansour and Hsu (2005)..... 82
4.3.1. Global Comparisons……...……. 83
4.3.1.1. Specimen CA2……..... 83
4.3.1.2. Specimen CA3……..... 83
4.3.1.3. Specimen CA4……..….. 84
4.3.2. Local Response Comparisons…….....…... 84
4.3.2.1. Specimen CA2……..... 85
4.3.2.2. Specimen CA3……...… 86
4.3.2.3. Specimen CA4…….……..... 87
4.4. General Discussion of Model Results and Effectiveness..... 89
4.5. Parametric Sensitivity Studies on the Fixed Strut Angle Model..... 90
4.5.1. Effect of Concrete Parameters…….…… 91
4.5.1.1. Effect of Concrete Post Peak Behavior on Overall Behavior……...….. 91
4.5.1.2. Effect of Peak Compressive Stress (Strength) of Concrete on Overall Behavior……...…… 93
4.5.1.3. Effect of Modulus of Elasticity of Concrete on Overall Behavior……. 95
4.5.2. Effect of Steel Parameters……... 97
4.5.2.1. Effect of Yield Stress of Reinforcing Steel on Overall Behavior……. 98
4.5.2.2. Effect of Strain Hardening Properties of Reinforcing Steel on Overall Behavior…..……. 100
4.5.2.3. Effect of Bauschinger's Effect Properties of Reinforcing Steel on Overall Behavior…….....….. 102
5. SUMMARY AND CONCLUSIONS..... 104
5.1. Overview..... 104
5.2. Conclusions..... 104
5.3. Recommendations for Future Research..... 106
REFERENCES…… 107

LIST OF FIGURES

Figure 2.1. Applied strain field and corresponding principal strains on an uncracked panel ……...…….. 24

Figure 2.2. Visualization of a rotating strut assumption..... 25

Figure 2.3. Calculation of stresses in concrete using the monotonic constitutive model 25

Figure 2.4. Back transformation of principal stresses on an un-cracked panel 27

Figure 2.5. Deviation of principal strain and fixed strut directions after formation of first crack 28

Figure 2.6. Calculation of stresses in concrete using the hysteretic constitutive model after formation of the first crack. 29

Figure 2.7. Representation of the single fixed strut mechanism after formation of the first crack 29

Figure 2.8. Back transformation of concrete stresses along and perpendicular to the first strut, into the x-y state of concrete stress 30

Figure 2.9. Deviation of principal strain and fixed strut directions after formation of the second crack..... 32

Figure 2.10. Calculation of stresses in concrete using the hysteretic constitutive model after formation of the second crack. 32

Figure 2.11. Representation of the two-fixed-strut mechanism after formation of the second crack 33

Figure 2.12. Back transformation of concrete stresses along the first and second strut, into the x-y state of concrete stress 34

Figure 2.13. Representation of the nonlinear analysis solution strategy for a single degree of freedom system 40

Figure 2.14. Representation of iterative equilibrium cycles 40

Figure 3.1. Constitutive model for steel (Menegotto and Pinto, 1973) 42

Figure 3.2. Degradation of cyclic curvature 44

Figure 3.3. Illustration of Menegotto Pinto model 44

Figure 3.4. Compression and tension envelope curves of the model by Chang and Mander (1994) 46

Figure 3.5. Hysteretic parameters of the model by Chang and Mander (1994) 53

Figure 3.6. Unloading from the compression envelope curve 55

Figure 3.7. Continuous hysteresis in compression and tension 56

Figure 3.8. Softening effect modeled with Model B 58

Figure 3.9. Comparison of tension stiffening models 62

Figure 3.10. Comparison of tension stiffening effects 63

Figure 4.1. Panel and loading geometry for Stevens (1987) specimens 66

Figure 4.2. Shell Element Tester (University of Toronto) 66

Figure 4.3. Configuration of panel tests by Mansour and Hsu (2005) 68

Figure 4.4. Universal Element Tester (University of Houston)..... 68

Figure 4.5. Specimen SE8, shear stress vs. shear strain comparison..... 70

Figure 4.6. SpecimenSE9, shear stress vs. shear strain comparison..... 71

Figure 4.7. Specimen SE10, shear stress vs. shear strain comparison..... 72

Figure 4.8. Specimen SE8, comparison of normal strains in x direction 72

Figure 4.9. Specimen SE8, comparison of normal strains in y direction 73

Figure 4.10. Specimen SE8, comparison of principal strain directions..... 73

Figure 4.11. Specimen SE8, comparison of shear stress vs. normal strains in y direction 75

Figure 4.12. Specimen SE8, comparison of principal strain direction vs. shear strain .. 75

Figure 4.13. Specimen SE8, comparison of principal stress direction in concrete vs. shear stress..... 76

Figure 4.14. Specimen SE9, comparison of normal strains in x direction 76

Figure 4.15. Specimen SE9, comparison of normal strains in y direction 77

Figure 4.16. Specimen SE9, comparison of principal strain directions..... 77

Figure 4.17. Specimen SE9, comparison of shear stress vs. normal strains in y direction.....78

Figure 4.18. Specimen SE9, comparison of principal strain direction vs. shear strain .. 78

Figure 4.19. Specimen SE9, comparison of principal stress direction in concrete vs. shear stress..... 79

Figure 4.20. Specimen SE10, comparison of normal strains in x direction 79

Figure 4.21. Specimen SE10, comparison of normal strains in y direction 80

Figure 4.22. Specimen SE10, comparison of principal strain directions..... 80

Figure 4.23. Specimen SE10, comparison of shear stress vs. normal strains in y direction……...……...…..……..... 81

Figure 4.24. Specimen SE10, comparison of principal strain direction vs. shear strain 81

Figure 4.25. Specimen SE10, comparison of principal stress direction in concrete vs. shear stress..... 82

Figure 4.26. Specimen CA2, shear stress vs. shear strain comparison..... 84

Figure 4.27. Specimen CA3, shear stress vs. shear strain comparison..... 85

Figure 4.28. Specimen CA4, shear stress vs. shear strain comparison..... 85

Figure 4.29. Specimen CA2, comparison of shear stresses vs. normal strains in x direction..... 86

Figure 4.30. Specimen CA2, comparison of shear stresses vs. normal strains in y direction……..... 86

Figure 4.31. Specimen CA3, comparison of shear stresses vs. normal strains in x direction……..... 87

Figure 4.32. Specimen CA3, comparison of shear stresses vs. normal strains in y direction……..... 87

Figure 4.33. Specimen CA4, comparison of shear stresses vs. normal strains in x direction……..... 88

Figure 4.34. Specimen CA4, comparison of shear stresses vs. normal strains in y direction……..... 88

Figure 4.35. Effect of used post peak parameters on the compressive envelope of concrete……..... 92

Figure 4.36. Effect of parameter x_{cr} on the overall response prediction of the FSAM... 93

Figure 4.37. Effect of parameter *f'c* on the compressive stress-strain envelope of concrete……..... 94

Figure 4.38. Effect of concrete compressive strength on the overall response prediction of the FSAM..... 95

Figure 4.39. Effect of parameter E_c on the compressive stress-strain envelope of concrete……..... 96

Figure 4.40. Effect of concrete elastic modulus on the overall response prediction of the FSAM 97

Figure 4.41. Effect of yield strength parameters on the tensile envelope of steel reinforcement 98

Figure 4.42. Effect of steel yield stress on overall response of the FSAM 99

Figure 4.43. Effect of steel strain hardening parameters on the cyclic stress-strain behavior of reinforcing steel 100

Figure 4.44. Effect of steel strain hardening on the overall response predicted by the FSAM 101

Figure 4.45. Effect of Bauschinger's effect on the cyclic stress-strain behavior of reinforcing steel 102

Figure 4.46. Effect of Bauschinger's Effect in reinforcing steel on overall response predicted by the FSAM 103

LIST OF TABLES

Table 4.1. Test Parameters of Stevens……..……..... 67

Table 4.2. Test Parameters of Mansour and Hsu…….……...… 69

LIST OF SYMBOLS

a_1 and a_2	Experimentally determined parameters that represent the degradation of the curvature within subsequent cycles.
C_b	Bond effectiveness coefficient.
C_t	A coefficient equal to 75 mm
d_b	Bar diameter
E_0	Slope of elastic asymptote (Modulus of Elasticity)
E_1	Slope of yield asymptote
E_{new}	New tangent modulus
E_{re}	Reloading tangent modulus
f_{cr}	Cracking stress of concrete
f_l	Steel stress in longitudinal direction
f_{new}	New stress
f_{re}	Reloading stress
f_t	Steel stress in transverse direction
f_t	Concrete tensile strength,
f_{un}	Unloading stress
f_y	Yield strength of the bare reinforcing steel bars
$f_{y\,eff}$	Effective (reduced) average yield strength of bars embedded in cracked concrete
k_ε	A coefficient 0 for sequential loading and 500 for proportional loading

R	Parameter that influences the curvature of the transition curve between the two asymptotes
R_0	The value assigned to the parameter R for initial (or monotonic) loading,
$\{R\}$	Residual force vector
x^+	Non-dimensional strain on the tension envelope curve,
x^+_{cr}	Critical strain on the tension envelope curve (used to define a tangent line up to the cracking strain), and
x_{crk}	Concrete cracking strain
x^-	Non-dimensional strain on the compression envelope
x_{cr}^-	Non-dimensional critical strain on the compression envelope curve (used to define a tangent line up to the spalling strain)
x_{sp}	Non-dimensional spalling strain
$y(x)$	Non-dimensional stress function
$z(x)$	Non-dimensional tangent modulus function (Figure 3.4)
β	Compression softening coefficient
β_m	Compression softening coefficient
$\{\delta_1\}$	The tangent displacement vector
$\Delta\lambda$	The initial load increment
$\{b_n\}$	Vector with a unity term along the degree-of-freedom to be incremented for the displacement-controlled analysis,
$\Delta\delta_n$	The initial displacement increment
$\Delta\delta$	Displacement increment

$\Delta\delta_R$	Residual displacement increment
$\Delta\theta$	The difference between θ_ε and θ_σ
Δf_{ycr}	Magnitude of strength drop as a result of tension stiffening
ε_t	Normal strain in transverse direction
ε_l	Normal strain in longitudinal direction
ε_1	Principal strain in direction1
ε_2	Principal strain in direction2
ε_x	Normal strain in x direction
ε_y	Normal strain in y direction
$\varepsilon_{x'}$	Arbitrary strain transformed to x' direction
$\varepsilon_{y'}$	Arbitrary strain transformed to y' direction
ε_r	Strain at the point of strain reversal,
ε_0	Strain at the point of intersection of the two asymptotes
ε_0	Strain at the current intersection point of the two asymptotes, and
ε_y	Strain at monotonic yield point
ε_t	Concrete tensile strain at peak tension stress,
ε_{un}	Unloading strain.
ε_m	Maximum or minimum strain, at the previous point of strain reversal,
ε_{pl}	Plastic strain upon unloading
ε_{un}	Upon return to unloading strain from the envelope curve
ε_{re}	Reloading strain

ε_r	Tensile strain perpendicular to the compressive stress direction.
$\varepsilon_{\perp max}$	Maximum value of the compressive strain experienced
$\varepsilon_{\perp}$	Current compressive strain(if any) in the direction perpendicular to the compressive (strut) direction considered,
γ_{21}	Shear strain along crack surface
γ_{xy}	Shear strain
γ_s	Sliding shear strain along crack surface
$\gamma_{x'y'}$	Arbitrary shear strain transformed to x'y' direction
σ_l	Normal stress in longitudinal direction
σ_t	Normal stress in transverse direction
σ_1^c	Principal stress in direction 1
σ_2^c	Principal stress in direction 2
σ_{c2}	Concrete stress in principal direction 2
σ_{c1}	Concrete stress in principal direction 1
σ_{c1soft}	Softened concrete stress in principal direction 1
σ_{c2soft}	Softened concrete stress in principal direction 2
σ_{cx}	Concrete normal stress in x direction
σ_{cy}	Concrete normal stress in y direction
σ_x	Total normal stress in x direction
σ_y	Total normal stress in x direction
$\sigma_{cx'}$	Concrete stress in x' direction

$\sigma_{cy'}$	Concrete stress in y' direction
$\sigma_{cx'soft}$	Softened concrete stress in x' direction
$\sigma_{cy'soft}$	Softened concrete stress in y' direction
σ_r	Stress at the point of strain reversal
σ_0	Stress at the point of intersection of the two asymptotes
σ_{cAx}	Concrete normal stress in x direction transformed from the Fixed Strut Direction A
σ_{cAy}	Concrete normal stress in y direction transformed from the Fixed Strut Direction A
σ_{cBx}	Concrete normal stress in x direction transformed from the Fixed Strut Direction B
σ_{cBy}	Concrete normal stress in y direction transformed from the Fixed Strut Direction B
τ_{lt}	Global shear stress
τ_{21}^{c}	Shear stress along crack surface
τ_{cxy}	Concrete shear stress
$\tau_{cx'y'}$	Concrete shear stress in x'y' direction
τ_{cAxy}	Concrete shear stress transformed from the Fixed Strut Direction A
τ_{xy}	Total shear stress
τ_{cBxy}	Concrete shear stress transformed from the Fixed Strut Direction B
θ_2	The crack angle
θ_2	The crack angle.
θ_ε	Principal direction of apparent strains

θ_{σ}	Principal direction of concrete stresses
θ_{cr}	Concrete Crack direction or Fixed Strut Angle
$\theta_{cr\text{-}per}$	Perpendicular direction to concrete crack direction or Fixed Strut Angle
θ_{crA}	Concrete Crack direction A or Fixed Strut Angle A
θ_{crB}	Concrete Crack direction B or Fixed Strut Angle B
ρ_{l}	Reinforcement ratio in longitudinal direction
ρ_{t}	Reinforcement ratio in transverse direction
ρ_{s}	Steel reinforcement ratio
ξ	The absolute strain difference between the current asymptote intersection point and the previous maximum or minimum strain reversal point.
$\xi_{\sigma o}$	Stress softening coefficient
$\xi_{\varepsilon o}$	Strain Softening coefficient

1. INTRODUCTION

1.1. General

With the introduction of performance-based methodologies for design and evaluation of reinforced concrete (RC) structures subjected to earthquake actions, analytical modeling of the behavior of individual reinforced concrete members under generalized and cyclic loading effects has recently gained substantial importance among researchers. Improved analysis and computation capabilities of available structural analysis software has made it possible for simulation of the hysteretic and time-dependent behavior of complete structural systems subjected to earthquake-induced dynamic effects. However, a reliable prediction of the nonlinear inelastic earthquake response of such structural systems inherently requires the use of analytical models that can accurately capture the hysteretic behavior of individual structural members under generalized loading conditions, as well as their interaction within the structural system.

In seismic-resistant design of reinforced concrete buildings, in particular, use of structural walls has been proven to be a very feasible alternative for resisting earthquake actions. Structural walls provide substantial strength and stiffness, as well as the deformation capacity needed to meet the demands of strong earthquake ground motions. To resist such actions, slender walls are properly designed and detailed to yield in flexure, and to undergo inelastic flexural deformations without loss of lateral load capacity. Their design is usually oriented toward supplying sufficient shear strength to promote flexural yielding; therefore, a modeling methodology that appropriately accounts for nonlinear flexural behavior (e.g., a moment-curvature-analysis based plastic hinge model or a model based on fiber formulation fiber-based model) becomes sufficient for design and evaluation purposes. However, shear-controlled squat walls (with aspect ratios typically less than 1.5) are also common in low-rise construction and at lower levels of tall buildings (for example, parking-level walls or basement walls). They can also be found in perimeter walls with perforations due to window and door openings, resulting in wall segments between openings. For low aspect-ratio walls or wall segments, behavior is often dominated by nonlinear shear responses, and the modeling parameters selected for shear

stiffness and strength can have a significant impact on the predicted distribution of member forces and on building lateral drift.

Extensive research, both analytical and experimental, has been carried out to study the behavior of both slender and squat walls. Recent research has shown that the lateral force versus deformation response of slender walls in flexure can be captured reasonably well using simple (moment-curvature based) analytical models and improved predictions can be obtained using more detailed (fiber-based) models. However, such models usually consider uncoupled shear and flexural responses; which has been shown to be inconsistent with recent experimental observations, even for relatively slender walls. There is a need for relatively simple modeling approaches that consider interaction (coupling) between axial, flexural, and shear responses, and capture important hysteretic response features for a wide range of wall geometries and reinforcing details.

Analytical modeling of the inelastic response of structural wall systems can be accomplished by using microscopic (finite element) or macroscopic (behavioral) models. For finite element modeling, although a number of constitutive model elements (e.g., the Modified Compression Field Theory and the Disturbed Stress Field Model) have been proposed for simulating the nonlinear shear behavior and the coupled axial-shear responses of reinforced concrete panels, these models are not implemented in commonly-used structural analysis platforms due to complexities in their formulation. Therefore, development of new constitutive models, which can provide sufficiently accurate response predictions, yet are simplistic in formulation, would be desirable for implementation into widely-used analysis programs, providing researchers and engineers with improved modeling capabilities for the simulation of coupled axial-shear-flexural load-deformation responses of RC walls under generalized reversed-cyclic loading conditions.

Therefore, in this study, a new constitutive panel model was proposed – based on interpretation and simplification of previous modeling approaches – for simulating the behavior of RC panel elements under generalized, in-plane, reversed-cyclic loading conditions. The proposed constitutive model is presented as a feasible candidate for implementation into a two-dimensional finite-element analysis formulation, for efficient

and practical response prediction of walls with various geometries and reinforcement details.

1.2. Literature Review

1.2.1. Overview

In the late 1970's and early 1980's, two research groups, one led by Thomas Hsu from the University of Houston, and the other led by Michael Collins and Frank Vecchio from University of Toronto, focused on the issue of modeling and prediction of shear-dominated panel behavior. When the Diagonal Compression Field Theory (DCFT) was proposed (Mitchell and Collins, 1974), the objective was to predict whole monotonic load-deformation behavior of an RC panel, instead of merely its capacity, with an incremental solution strategy.

After development of this theory, Collins and Vecchio developed the "Membrane Element Tester" and conducted a comprehensive test program on numerous RC panel specimens. Based on results of this test program, the Modified Compression Field Theory (MCFT) (Vecchio and Collins, 1986) was proposed. In this theory, although the main features of the DCFT (e.g., coinciding principal strain and stress directions, perfect bond) were preserved, a number of additional behavioral parameters (e.g., compression softening, tension stiffening, and shear transfer along crack surfaces) were introduced in the formulation.

During the same period, Mau and Hsu (1986) proposed a new approach on the analysis and shear design for low-rise structural walls. In this study, without using any test results and only based on equilibrium, compatibility and material stress-strain relationships (essentially same stress-strain relationships used for the MCFT), a new design approach was proposed and boundaries among different failure modes were identified. In 1987, the methodology was improved for predicting the behavior of vertically-loaded wall panels (Mau and Hsu, 1987) In this approach, cracked concrete was treated as a new material working in diagonal compression strut directions, as also assumed in the MCFT .

In 1988, Hsu proposed his first theory, named the Softened Truss Model (STM) (Hsu 1988), for predicting the shear response of RC panels under monotonic loading. In this theory, using equilibrium, compatibility, and material stress-strain relationships, a systematic method was developed for solving nonlinear shear and torsion problems. Unlike the MCFT, shear transfer along cracks was not formulated discretely, but represented using a smeared crack approach using tension stiffening relationships.

In 1989, Kajima Institute of Construction Technology conducted an experimental research program in their newly-developed test facility. Within the scope of this project, several reversed-cyclic panel tests were performed and a nonlinear cyclic analysis strategy was developed (Ohmori et al. 1989). This theory was essentially the cyclic version of MCFT, using improved and hysteretic stress-strain models for the materials.

In the same year, another cyclic model was proposed by Stevens et al. (1991), based on experimental results of three panel specimens. In this model, a new approach was proposed, which considers the deviation between principal strain and stress direction for the first time. An approach was proposed for tracking and collection of the history parameters of hysteretic concrete stress-strain model applied along rotating compression directions, and a solution strategy was developed.

In 1995, the Rotating Angle Softened Truss Model (RA-STM) was proposed by Pang and Hsu (1995), as the first robust theory of the research group led by Hsu. Based on results of 13 panel specimens tested, new constitutive material models were proposed, together with new parameters to represent compression softening and tension stiffening behavior. Another important feature of this work was that it identified and considered the "kinking effect", (representing the softening effect on reinforcing bars caused by the dowel action) in the analysis.

In 1996, Pang and Hsu proposed a new theory called the Fixed Angle Softened Truss Model (FA-STM) (1996). In this theory, unlike the MCFT or RA-STM, the direction of the cracks was assumed to coincide with the fixed angle following the principal directions of the applied stresses. Sliding shear stresses along cracks surfaces, which develop as a result of this assumption, were calculated using a newly-developed shear modulus.

In 2000, Vecchio proposed a new theory called the Disturbed Stress Field Model (DSFM). In this theory, it was assumed that principal stress and strain directions deviate from each other and the crack directions coincide with the principal stress direction. On the other hand, principal stress directions rotate relative to (deviate from) principal strain directions with a fixed "lag". Shear strains developing along cracks as result of this "lag" are taken in to account as partially slip deformations along cracks.

In 2002, Hsu and Zhu proposed a new model called Softened Membrane Model (SMM) (Hsu and Zhu, 2002). The only difference of this model with the FA-STM was that it considered the Poisson's effect. It was also concurred that the influence of the "kinking effect" on the response, which had been identified in development of the FA-STM, was not as important as stated previously.

In 2005 a cyclic version of the SMM was proposed by Mansour and Hsu (Mansour and Hsu, 2005). In this study, 12 panel specimens were tested under reversed cyclic loading for development of the formulation of the proposed model, as well as for assessment its prediction capabilities.

The most recent constitutive panel model proposed is the one proposed by Gérin and Adebar (2009). In this model, it is assumed that principal strain and stress directions coincide, while the crack directions are fixed. This model formulation separates strains due to crack deformations from strains on concrete between the cracks, and allows the principal direction of the total (applied) strains to deviate from the principal stresses on concrete. Crack deformations are assumed to be independent of concrete stresses and to occur as needed to maintain compatibility of the strains in the reinforcement and total strains.

The constitutive panel models mentioned above are described more detail in the following subsections. Model formulations are categorized in two groups, as Monotonic Models and Cyclic Models.

1.2.2. Monotonic Constitutive Panel Models

1.2.2.1. Modified Compression Field Theory (Vecchio and Collins 1986): This was the pioneering study on predicting the behavior of a RC membrane element under arbitrarily-applied in-plane stresses. The model treated cracked concrete as a new material using smeared crack approach, which considers average stress and strain states to satisfy equilibrium equations. In addition, compatibility and stress-strain relationships were also incorporated in the model formulation. Therefore, unlike the Diagonal Compression Field Theory (DCFT), which was proposed by Mitchell and Collins (1974), the Modified Compression Field Theory (MCFT) allowed conducting an incremental analysis of a membrane element, for predicting both the pre- and post-peak branches of load-deformation behavior, with its well-defined constitutive laws for steel and concrete. These constitutive laws were capable of simulating monotonic material behavior under tension or compression. Tensile behavior of concrete, which was neglected in the Diagonal Compression Field Theory as a simplification, was considered in the MCFT, not only to represent the so-called "created tie effect", but also to be able to consider the softening effect along the compression strut, due to the existence of tensile strains in the perpendicular direction. Although this softening effect was proposed by well-known Kupfer, Hilsdorf and Rüsch failure envelope, Vecchio and Collins derived a simple equation, which was calibrated with the tests conducted, for simulating the softening effect of tensile strains developed perpendicular to the compressive stress direction.

Another main assumption in the MCFT was related to principal stress, principal strain and crack directions. According to the MCFT, principal strain, principal stress and crack directions coincide. Although, it was stated by the Vecchio and Collins that principal strain and stress directions can deviate for some cases, the deviation was found to be negligible, for piratical purposes, for monotonic loading. MCFT therefore neglected this deviation for the sake of simplification. In addition to this idealization, it was also assumed that in every stage of analysis; the strain field on concrete is equal to the strain field on reinforcing steel (indicating perfect bond), and the reinforcing steel bars cannot resist shear stresses (indicating no dowel action).

Although it was a pioneering work, its monotonic formulation limited the applicability of the MCFT. The theory was not suitable for a cyclic analysis, since monotonic constitutive material models were used in the formulation. In addition, assuming rotating principal strain and therefore stress directions was also presented difficulties for cyclic analysis. Even if cyclic material constitutive models are used, during incremental analysis, cyclic damage histories in the constitutive models cannot be tracked along newly-formed principal stress directions. Finally, representation of the tension stiffening effect and the definition of shear stress transfer across cracks (defined by local stress criteria) was subject to misinterpretation by other researchers.

1.2.2.2. Rotating Angle Softened Truss Model (Pang and Hsu 1995): Another important research project was conducted by David Pang and Thomas Hsu, and a new constitutive panel formulation called the Rotating Angle Softened Truss Model (RA-STM) was proposed. The Rotating Angle Softened Truss Model was an improvement of the Softened Truss Model proposed by Hsu (1988). This model depended on a pure mechanical (equilibrium and compatibility) approach, without the requirement to use a particular material constitutive model. However, after the publication of Softened Truss Model (STM), researchers conducted a series of comprehensive panel tests in order to develop new constitutive material models, using the new "Universal Panel Tester" (Belarbi and Hsu 1994), (Belarbi and Hsu 1995). As a result of numerous stress-controlled tests, the Rotating Angle Softened Truss Model (RA-STM) was proposed. While Rotating Angle Softened Truss Model formulation used rotating principal strain, principal stress, and crack directions, together with a smeared crack approach similar to the MCFT; unlike the MCFT, it incorporated an empirical tension stiffening approach, with its new constitutive models for concrete and reinforcing steel. The model also considered the effect of compression softening in the analysis. Despite all these features, this model formulation was also monotonic like the MCFT, not allowing cyclic response predictions for RC panel behavior.

1.2.2.3. Fixed Angle Softened Truss Model (Pang and Hsu 1996): As mentioned previously, although deemed not realistic by researchers, the coincident principal stress, principal strain and crack direction assumption was used in previous constitutive panel model formulations, for the sake of simplicity and also because the assumption was found to be sufficiently reasonable for monotonic loading. The first monotonic model aimed

towards overcoming this limitation was developed by David Pang and Thomas Hsu, and was named the "Fixed Angle Softened Truss Model" (FA-STM). Unlike the Rotating Angle Softened Truss Model, the Fixed Angle Softened Truss Model was not fully rotating-stress field model, where the direction of the cracks is assumed to incline at the fixed angle following the principal stress of the applied loading. One of the main differences of the model from previous formulations was the implementation of a stress strain model for concrete in shear. Although the model used the same principals with the Rotating Angle Softened Truss model when the reinforcement ratios of a panel element are same in both directions, when the ratios were not equal, shear stresses were developing at crack surfaces as a consequence of aggregate interlock. In order to consider this effect, the researchers proposed a shear modulus, representing shear behavior along the crack surfaces. (Equation 1.1).

$$\gamma_{21} = -(\varepsilon_t - \varepsilon_l) \cdot sin2\theta_2 + (\varepsilon_1 - \varepsilon_2) \cdot cot2\theta_2 \tag{1.1}$$

where γ_{21} is shear strain along crack surface, ε_t is the normal strain in transverse direction, ε_l is the normal strain in longitudinal direction, θ_2 is the crack angle, ε_1 is the principal strain in direction1, and ε_2 is the principal strain in direction2 .

$$\tau_{21}^{c} = \frac{1}{2} \cdot \left[(\sigma_l - \rho_l f_l) - (\sigma_t - \rho_t f_t) \right] \cdot sin2\theta_2 + \tau_{lt} \cdot cos2\theta_2 \tag{1.2}$$

where; $\tau_{21}{}^{c}$ is shear stress along crack direction, σ_l is the normal stress in longitudinal direction, ρ_l is reinforcement ratio in longitudinal direction, f_l is steel stress in longitudinal direction, σ_t is the normal stress in transverse direction, ρ_t is reinforcement ratio in transverse direction, f_t is steel stress in transverse direction, τ_{lt} Global shear stress and θ_2 is the crack angle.

Although the FA-STM was considered the deviation between principal stress, principal strain, and crack directions, it was also not suitable for cyclic response predictions, due to its monotonic formulation.

1.2.2.4. Softened Membrane Model (Hsu and Zhu 2002): The most recent monotonic constitutive panel model proposed by researchers at the University of Houston was the Softened Membrane Model (SMM). This model was for the most part an extension of the FA-STM, with two main modifications. The first was consideration of the Poisson's effect. Hsu and Zhu have performed an extensive experimental program on investigating the influence of the Poisson's effect and the kinking effect, which considers the strength degradation triggered by dowel action in reinforcing steel. It was previously stated by the Pang and Hsu (1996) that the kinking effect has an important influence on the shear behavior of membrane elements. As result of tests conducted, the researchers concluded that the kinking effect can be neglected in the analysis, whereas the Poisson's effect should be considered. As a result, the formulation of the FA-STM was modified to consider Poisson's effect using coefficients named as Hsu/Zhu ratios. In addition to consideration of Poisson's effect, the shear modulus used in FA-STM was also modified in the Softened Membrane Model, using the empirical relationship below:

$$\tau_{21}^{c} = \frac{\sigma_1^{c} - \sigma_2^{c}}{2 \cdot (\varepsilon_1 - \varepsilon_2)} \gamma_{21} \tag{1.3}$$

Where; $\tau_{21}{}^{c}$ is the shear stress along the crack surface, $\sigma_1{}^{c}$ is the principal stress in direction 1, $\sigma_2{}^{c}$ is the principal stress in direction 2, ε_1 is the principal strain in direction 1, ε_2 is the principal strain in direction 2, γ_{21} is the shear strain along crack surface

1.2.2.5. Disturbed Stress Field Model (Vecchio 2000): As described previously, the MCFT was a monotonic model, and there were some inherent restrictions (e.g., tracking of cyclic material damage parameters) on cyclic implementation of this model. In order to overcome this limitation of the MCFT, Vecchio has made some cyclic implementation efforts (Vecchio 1999). As a result of these studies, a new theory called the "Disturbed Stress Field Model" was proposed (Vecchio, 2000). In this new theory, Vecchio focused on the two main deficiencies of MCFT, including the "coinciding angles of principal strain and stress directions" and "localized stress definitions". In the theory, "apparent" shear deformations has been separated into two main components; the first being the "average constitutive response" calculated using a smeared crack approach for concrete and the

second being the “local rigid body slip” defined along the cracks. According to the theory, this rigid body slip is the reason of the deviation between principal strain and principal stress directions named as “lag”. In order to consider these components in the model formulation, Vecchio has derived new sets of equilibrium, compatibility and constitutive equations (Equation 1.4, 1.5 and 1.6).

$$\theta_{\varepsilon} = \frac{1}{2} \cdot tan^{-1} \cdot \left[\frac{\gamma_{xy}}{\varepsilon_x - \varepsilon_y} \right] \tag{1.4}$$

$$\theta_{\sigma} = \frac{1}{2} \cdot tan^{-1} \cdot \left[\frac{\gamma_{cxy}}{\varepsilon_{cx} - \varepsilon_{cy}} \right] \tag{1.5}$$

$$\Delta\theta = \theta_{\varepsilon} - \theta_{\sigma} \tag{1.6}$$

At that point, the critical issue was the definition or calculation of amount of slip deformation, which would need to be considered in compatibility equations. On the other hand, previously-derived equations for calculation of shear slip across a crack were not suitable for this model. Therefore, the theory derived the slip deformation in an inverse manner. Since the reason of the angle “lag” between principal strain and principal stress directions was associated the rigid body slip, then if the “lag” is predicted, the “rigid body slip” can be calculated, and finally “average constitutive response” can be determined for deformations which are obtained from the subtraction of “rigid body slip” from “apparent” (global) shear deformation.

In the formulation, the principal strain angle calculated using “apparent (global) deformations” was calculated as:

$$\theta_{\varepsilon} = \frac{1}{2} \cdot tan^{-1} \cdot \left[\frac{\gamma_{xy}}{\varepsilon_x - \varepsilon_y} \right] \tag{1.7}$$

Since the "lag" between strain and stress angle was empirically known, principal stress angle was calculated as:

$$\theta_\sigma = \theta_\varepsilon - \Delta\theta \tag{1.8}$$

If the angle of principal stress direction is known, the following equation yields the slip deformation along the crack surfaces:

$$\gamma_s = \gamma_{xy} \cdot cos2\theta_\sigma + \left(\varepsilon_x - \varepsilon_y\right) \cdot sin2\theta_\sigma \tag{1.9}$$

As a result of tests performed, this angle "lag", was predicted as an angle oscillating between 0° and 10°, and was associated with reinforcement characteristic of member (5° for bi-axially reinforced members, 7.5° for uni-axially reinforced members and 10° for reinforced members).

Another component of this theory was the revision of the compression softening effect with respect to the shear slip deformations considered. Since slip deformations are subtracted from the "apparent" shear deformations, the compression softening equations derived based on "apparent" deformations, predicted overestimated softening behavior. Under the light of this fact, the theory proposed that for the models considering slip deformations, softening effect should be decreased to 0.55 of the original formulation. Although this was a very impressive model which considers both slip deformations and aggregate interlocking, with the effects implemented also in the compression softening behavior, its cyclic implementation has not yet been done.

1.2.3. Cyclic Constitutive Panel Models

1.2.3.1. Stevens et el. (1991): In addition to monotonic panel tests performed using the "Membrane Element Tester", researchers at the University of Toronto have also conducted reversed cyclic panel tests using a new testing facility named as the "Shell Element Tester", to be able to visualize the difference between the monotonic and reversed cyclic behavior (Stevens 1987). As results of these tests, some behavioral differences between

monotonic and cyclic panel responses were identified. Under the light of performed reversed cyclic tests, the researchers made the following remarks;

- During the increasing deformation cycles, while the principal strain directions progressively decayed and rotated, principal stress directions returned to virtually the same orientation at each deformation cycle.

- Additionally, it was observed that crack directions were not coinciding with principal strain directions; they were coincident with the principal stress directions which deviated from principal strain directions.

Based on these observations, a new theory was developed upon modifying the formulation of the MCFT via using the concept of "incremental directions". In this theory, Stevens claimed that principal stress and strain directions may not coincide; however, the principal stress increment directions and the principal strain increment directions should coincide, and defined the following incremental compatibility equations:

$$\Delta\varepsilon_x = \varepsilon_x^{\,i} - \varepsilon_x^{\,i-1} \tag{1.10}$$

$$\Delta\varepsilon_y = \varepsilon_y^{\,i} - \varepsilon_y^{\,i-1} \tag{1.11}$$

$$\Delta\gamma_{xy} = \gamma_{xy}^{\,i} - \gamma_{xy}^{\,i-1} \tag{1.12}$$

$$tan2\theta_{\Delta} = \frac{\Delta\gamma_{xy}}{\Delta\varepsilon_x - \Delta\varepsilon_y} \tag{1.13}$$

In this theory, the second issue that was resolved was the inability of the MCFT to track strain (damage) in rotating principal strain directions. The solution proposed was a trial and error technique; since the principal directions of each strain increment will differ from one load stage to the next, the stress and strain values reached on the concrete stress-strain relationship at the end of each load increment will not be directionally-compatible

with the stress and strain values at the beginning of the load stage load increment. This meant that instead of using one stress-strain curve to define a certain region of the response, a whole family of curves was required to track and store directional damage history variables. As well, the effect of tension stiffening was considered on both cracked concrete and reinforcing steel in this model. In order to consider the reduction effect of tension stiffening on the average yield strength reinforcing steel bars, the following yield strength reduction relationships were used:

$$f_{y\,eff} = f_y - \Delta f_{ycr} \tag{1.14}$$

where f_y is the yield strength of the bare reinforcing steel bars, $f_{y\,eff}$ is the effective (reduced) average yield strength of bars embedded in cracked concrete, and,

$$\Delta f_{ycr} = \frac{C_t}{d_b} \cdot f_{cr} \cdot C_b \tag{1.15}$$

where C_t is 75 mm, d_b is the rebar diameter, f_{cr} is the cracking stress of concrete, and C_b is defined as the bond effectiveness coefficient.

To consider the influence of the tension stiffening effect on concrete, the following relationship was used, where the tensile behavior of concrete was affected by a so-called intensity factor (ρ_s/d_b):

$$f_c = f_{cr} \cdot \left[(1-\alpha) \cdot e^{-\lambda_t (\varepsilon_c - \varepsilon_{cr})} + \alpha \right] \tag{1.16}$$

where $\alpha = C_t \cdot \frac{\rho_s}{d_b}$ and $\lambda_t = \frac{270}{\sqrt{\alpha}}$

and C_t is 75 mm, d_b is the rebar diameter, and ρ_s is the reinforcement ratio

As well, in addition a new compression softening parameter, a damage coefficient, which represents the accumulated damage on concrete along a compression strut due to the history of compressive strains in the perpendicular direction, was derived expirically from the test results. This damage coefficient was found to considerably affect the post-peak load-deformation behavior of RC panels.

1.2.3.2. Mansour and Hsu (2005): Cyclic Fixed Angle Softened Truss Model: After the development of FA-STM researchers at the University of Houston commenced a new experimental program to develop a set of reversed cyclic material models. In the scope of this experimental program, 12 cyclic panel tests were conducted, where three specimens were oriented at 90° angle relative to the testing equipment (the angle represents the orientation of reinforcing bars relative to panel edges), five specimens oriented at 45°, three at 68.2° and one at 79.8°. Proportionally-applied reversed cyclic load tests on three 45° panels were used as reference test specimens during the calibration of the model proposed in this study. As a result of this research program, a new model, which was a cyclic extension of the FA-STM, was proposed, together with new cyclic constitutive material relationships both for steel and concrete. (Mansour et al. 2002)

Cyclic Softened Membrane Model: Results of the same experimental program results were also used to calibrate the Cyclic Softened Membrane Model, which was an extension of the original SMM with cyclic constitutive material relationships implemented for both steel and concrete. However, in addition to the cyclic material models, a damage coefficient, which defines the effect of the compressive strain history in the perpendicular direction to a compressive strut, was also implemented into the model. This damage coefficient was similar to that derived by Stevens with minor differences in formulation (Mansour and Hsu 2005, Hsu and Mansour 2002).

1.2.3.3. Ohmori et el. (1989): Another research groups also conducted cyclic panel tests at the Kajima Institute of Construction Technology facilities. In early 1980's the Kajima Institute of Construction had developed a larger version of the Membrane Element Tester of University of Toronto. Under the light of cyclic tests performed, Ohmori et al. (1989) proposed a model based on the Modified Compression Field Theory, with new and uniquely-defined cyclic constitutive models for concrete and reinforcing steel.

1.2.3.4. Palermo and Vecchio (2003): Another cyclic extension of the Modified Compression Field Theory was proposed by Vecchio and Palermo in 2003. In this formulation, new constitutive material relationships were developed. The model was implemented into nonlinear finite element analysis platform and some wall tests in the literature were simulated. (Palermo and Vecchio 2003)

1.2.3.5. Gérin and Adebar (2009): One of the most recent cyclic panel constitutive models is the one proposed by Gérin and Adebar. This model formulation separates strains due to crack deformations from strains on concrete between the cracks, and allows the principal direction of the total (applied) strains to deviate from the principal stresses on concrete. Crack deformations are assumed to be independent of concrete stresses and to occur as needed to maintain compatibility of the strains in the reinforcement and total strains. The concrete direction stress rotates to maintain equilibrium, whereas the crack direction is fixed. According to this model, crack deformations with respect to smeared strains are defined as the difference between total strains and stains in concrete. If there are two cracks in different directions, strains in concrete are defined as the total strain parallel to the open cracks minus the crack strain normal to closed cracks. The model uses cyclic multi-linear stress strain relationships for reinforcing steel and concrete, in addition to a new compression softening relationship.

1.2.4. Assumptions, Limitations and Applicability of Available Models

Based on review of the constitutive panel models available in the literature, the general assumptions, limitations, and applicability previously-proposed models are summarized in this section.

The smeared crack modeling approach for concrete is adopted by a majority of the model formulations, due to its practicality in implementation. The perfect bond assumption was also adopted by most of the researchers, as the panel specimens tested did not possess anchorage deficiencies.

Although compression softening and tension stiffening parameters have been adopted for almost all of the models, there is a reasonable amount of inconsistency, especially in the definition of tension stiffening effect, in the model formulations.

Except Hsu and Zhu (2002), none of researchers considered the effect of dowel action of the reinforcing steel bars on RC panel behavior. Hsu and Zhu, upon examining the "kinking effect" of reinforcing bars in particular, concluded that the effect is not considerably influential on panel behavior.

Most importantly, in all of the model formulations proposed, principal stress directions of concrete are assumed to rotate with the principal directions of the applied strain field, although models define a shifting between the principal strain and stress directions. Validity and effectiveness of this approach is questionable due to two main complications.

First, as revealed after each cyclic panel tests, while the principal strain direction keeps rotating during the entire test duration (since the applied strain field is general or test-specific), after the occurrence of cracking, the principle stress direction in concrete fluctuates within a very narrow range for each direction of loading. As such, although the principle strain and stress directions coincide assumption may be acceptable for monotonic loading, for cyclic loading, the directions may deviate by up to 30° from each other (Gérin and Adebar, 2009). In addition, based on test observations and physical intuition, once a cracked has formed at a particular location, the direction (inclination) of the crack will not change (rotate) during subsequent loading. This implies a physical inconsistency in model formulations where cracks are assumed to rotate together with the principal stress and strain directions (all except Gérin and Adebar 2009), with real behavior.

Second, a formulation based on a rotating principal stress direction assumption is problematic in terms of numerical stability and simple implementation into an analysis code for application. The formulation of cyclic biaxial constitutive models for concrete (applied in principal stress directions in a panel model) typically involve history parameters associated with the strain histories collected in the direction they are applied. Therefore, when the domain (direction) of the constitutive model for concrete changes with

the applied load, difficulties and inconsistencies arise in tracking and storage of strain histories in rotating directions.

Although all of the cyclic models described above assume rotating principal concrete stress directions, Stevens (1987) clearly describes the solution method developed to resolve this problem. His solution is in the form of a trial and error technique; since the principal directions of each strain increment will differ from one load stage to the next, the stress and strain values reached on the concrete stress strain relationship at the end of each load increment will not be directionally the same as the values at the beginning of the load increment, necessitating using a whole set of stress-strain curves in multiple for tracking the history variables in appropriate directions. Although this is a physical and rational approach, considering that test results indicate that principal stress directions in concrete fluctuate within a very narrow range, this level of complication in the formulation seems unnecessary.

Finally, the relatively complex formulations of the available cyclic constitutive panel models make them difficult for use by other researchers and for simple implementation into commonly-used structural analysis platforms.

1.3. Research Significance

For performance-based design and evaluation of RC systems with structural walls, there is a need for relatively simple modeling approaches that consider coupling between axial, flexural, and shear responses, and capture important cyclic response features. Although a number of constitutive model elements (e.g., the Modified Compression Field Theory and the Disturbed Stress Field Model) have been proposed for simulating, the nonlinear shear behavior and the coupled axial-shear responses of RC panels, these models are not implemented in commonly-used structural analysis platforms to allow RC system studies, due to their behavioral inconsistencies and complexities in their formulation. Therefore, development of new constitutive element models, which can provide sufficiently accurate response predictions, yet are simplistic in formulation, are needed to provide researchers and engineers with improved modeling capabilities for the predicting

the load-deformation responses of RC walls with a wide range of configurations, under generalized and reversed-cyclic loading conditions.

1.4. Objectives

Based on the shortcomings above, the objective of this study is to develop, based on interpretation and simplification of previous modeling approaches, a new constitutive RC panel model, called the "Fixed Strut Angle Model" (FSAM), for simulating the behavior of RC panel elements under generalized, in-plane, reversed-cyclic loading conditions.

The constitutive model proposed is aimed to be simplistic in formulation, with the assumptions and limitations clearly stated; yet capable of predicting, with reasonable accuracy, the nonlinear shear behavior and axial-shear response coupling of RC panels. The model formulation is also aimed to be flexible to allow further revisions for improving its effectiveness or accuracy.

The proposed constitutive model is expected to be a feasible candidate for implementation into a two-dimensional finite-element analysis formulation, for efficient and practical response prediction of walls with various geometries and reinforcement details.

1.5. Scope

In light of the objectives above, the scope of this study includes:

A detailed review of available constitutive panel models in the literature, identifying their behavioral attributes and idealizations as well as their shortcomings and inconsistencies,

Development of a new and simple constitutive panel model formulation, which can simulate with reasonable accuracy, the cyclic behavior of reinforced concrete panel elements with different reinforcement configurations under generalized in-plane loading conditions,

Implementation of a nonlinear solution strategy and comparison of model results with the results of cyclic panel tests available in the literature at both local and global response levels,

Conducting parametric studies to identify the sensitivity of the model results to variation and uncertainties in material parameters.

1.6. Thesis Outline

This thesis summarizes the scope and findings of the analytical study conducted on development and evaluation of the constitutive panel element proposed. In Chapter 1, an introduction and a literature review, as well as the objectives and scope of this study were provided. Description of the model and details on the model formulation are presented in Chapter 2, together with the nonlinear analysis solution strategy implemented for response simulations. Detailed descriptions of the hysteretic material constitutive models incorporated in the model for reinforcing steel and concrete, as well as the empirical formulations used for compression softening, tension stiffening, biaxial damage behavior, are given in Chapter 3. Chapter 4 presents information on experimental calibration of the model and detailed comparison of the model results with test results from the literature on six RC panel specimens, as well as results of the parametric sensitivity studies conducted. Finally in Chapter 5, the analytical results are discussed, concluding remarks are presented, and future studies on improvement and application of the model are recommended.

2. MODEL DESCRIPTION

2.1. Overview

The Fixed Strut Angle Model proposed in this study is a constitutive panel model for simulating the behavior of RC panel elements under generalized, in-plane, reversed-cyclic loading conditions. The formulation of the model is based on interpretation of previously-developed RC panel models, as well as the results of panel tests available in the literature. The model is simplistic in formulation, with the assumptions and limitations clearly stated. A description of the model formulation is provided in this chapter, together with the nonlinear analysis solution strategy implemented for conducting displacement-controlled quasi-static analysis of individual RC panels, using the model.

As assumed by all other RC panel models available in the literature, in the Fixed Strut Angle model, the strain field acting on concrete and reinforcing steel components of an RC panel is assumed to be equal to each other, implying perfect bond assumption between concrete and reinforcing steel bars. Further, reinforcing steel bars are assumed to develop zero shear stresses perpendicular to their longitudinal direction, implying no dowel action on reinforcement.

While the reinforcing steel bars develop only uniaxial stresses under uniaxial strains in their longitudinal direction, the behavior of concrete is defined using stress–strain relationships in biaxial directions, and the orientation of those biaxial directions is governed by the state of cracking in concrete.

In the un-cracked state of concrete, the stress–strain behavior of concrete is represented with a rotating strut approach (similar to the Modified Compression Field Theory, Vecchio and Collins (1986) and the Rotating Angle Strut and Tie Model, Pang and Hsu (1995)). The strain field imposed on concrete is transformed into principal strain directions, which are assumed to coincide with principal stress directions, and uniaxial stress–strain relationships for concrete are applied along the principal strain directions in order to obtain the principal stresses in concrete. It should be mentioned that although the

stress–strain relationships used for concrete in principal directions are fundamentally uniaxial in nature, they also incorporate biaxial softening effects including compression softening and biaxial damage, as described in Chapter 3 of this thesis. At this stage of the behavior, monotonic stress–strain relationships for concrete are used, since it is reasonable to assume that concrete behavior follows a monotonic (virgin) stress–strain relationship, prior to first cracking under a biaxial state of stress. This assumption was also made to overcome the difficulties (e.g., Stevens, 1987) to track and store history variables in the hysteretic stress–strain relationship for concrete, along rotating stress and strain directions in a panel.

When the value of the principal tensile strain in concrete exceeds the monotonic cracking strain of concrete for the first time, the first crack is formed, and for following loading stages, the principal strain direction corresponding to first cracking in concrete is assigned as the first "Fixed Strut" direction for the panel. After formation of this first crack, while principal directions of the applied strain field continues to rotate based on the applied strain field, the principal stress directions in concrete are assumed to be along and perpendicular to the first Fixed Strut direction. This implies that the first crack (or strut) direction coincides with the principal stress directions in concrete, implying zero shear stresses developing along the crack. This physically implies zero shear aggregate interlock along a crack, which is an inherent assumption of the model formulation.

Since the direction of the first strut is fixed, a uniaxial hysteretic stress–strain relationship for concrete can now be applied in principal stress directions (parallel and perpendicular to the first strut), and history variables in the concrete stress-strain relationship can be easily tracked and stored in the two fixed directions. It should be mentioned that for calculation of concrete stresses in principal directions, the applied strain field in concrete should be transformed into strain components that are parallel and perpendicular to the first fixed strut direction, instead of principal strain directions.

The analysis is continued in the form of a single fixed strut mechanism until the formation of the second crack, after which the second strut will develop in the panel model. During the first fixed strut stage of the analysis, the model tracks the concrete stress–strain behavior along the first strut direction, and when the strains along the first

strut direction first exceeds the cyclic cracking strain (which depends on both the monotonic cracking strain and the plastic strain upon reversal from a compressive stress state), the second crack is formed. Due to the zero aggregate interlock assumption, the second crack will develop in perpendicular direction to the first crack, according to a stress-based cracking criterion, since the first strut direction is a principal stress direction and the concrete stress–strain relationship is assumed to be uniaxial along the first strut direction. It should be mentioned that although other cracking criteria may be used for defining the direction of the second crack (e.g., associating the formation and/or direction of the second crack with principal strains), this was found to be the simplest and mechanically-consistent approach.

After formation of this second crack, the second "Fixed Strut" will develop in the direction of the second crack (in perpendicular direction to the first strut), and for further loading stages, the concrete mechanism consists of two independent struts, working interchanging compression and tension struts in the two Fixed Strut directions, based on the applied strain field. While principal directions of the applied strain field continues to rotate based on the applied strain field, the principal stress directions in concrete are assumed to be along the two Fixed Strut directions, again implying zero shear stresses (zero shear aggregate interlock) developing along the two cracks. Since the direction of both struts are fixed, the uniaxial hysteretic stress–strain relationship for concrete can be applied in principal stress directions (parallel to the first and second strut directions), and history variables in the concrete stress-strain relationship can be tracked and stored in the two fixed directions. Again, for calculation of concrete stresses in the two principal directions, the applied strain field in concrete should be transformed into strain components that are parallel to the first and second fixed strut directions, instead of principal strain values.

As described above, the main inherent assumption underlying the formulation of the Fixed Strut Angle model is that the principal stress directions in concrete coincide with crack directions, implying zero shear stresses action along cracks, and therefore zero shear aggregate interlock.

In an RC member, sliding along crack surfaces is known to develop an aggregate interlocking action, resulting in shear stress along the crack, the magnitude of which is affected by the crack width and the amount of slip deformation along the crack. However, in the proposed model, shear strains along crack surfaces, developing due to the deviation between principal strain directions and the principal stress (crack) directions in concrete, are considered as shear slip (sliding) deformations and are assumed not to develop shear stresses due to aggregate interlocking along crack surfaces.

This inherent assumption of the model is based on interpretation of existing panel tests in the literature. Available test results in the literature typically indicate that for an RC panel, after formation of cracks, the principal stress direction in concrete does not change significantly with loading, although the principal strain direction on a panel may undergo significant variation (e.g., Stevens, 1987). The principal stress directions in concrete being insensitive to loading may imply that after formation of cracks, the principal stress directions in concrete follow approximately the fixed crack directions, indicating that shear stresses along a crack (and thus shear aggregate interlocking along a crack) has marginal influence on the panel behavior. Although this type of behavior has been consistently observed in experiments, a modeling methodology which assumes fixed principal stress directions for concrete has not yet been proposed.

Second, this assumption allows the flexibility to incorporate a suitable cyclic shear aggregate interlock constitutive model (shear stress versus shear strain along a crack) in the Fixed Strut Angle model, since the formulation of the model allows calculating shear strains along a crack. In the present study, however, such an aggregate interlock model was not implemented, for the purpose of evaluating the accuracy of the proposed model with the zero aggregate interlock assumption. The present model formulation also assumes that no shear stress is resisted by the reinforcing steel bars, indicating no dowel action on the reinforcement. However, the model also provides the flexibility to implement dowel effects into its formulation.

With all the assumptions described above, the present formulation of the proposed Fixed Strut Angle model is simple, yet mechanically complete and self-contained. A more detailed description of the model is presented in the following sections.

2.2. Uncracked Panel Response

At the initial stage of the analysis corresponding to the uncracked state, the stress–strain behavior of concrete is represented with a rotating strut approach. For a given (applied) strain field, the following steps are involved in the analysis:

First, the principal strain direction for the uncracked panel (θ_p) is calculated based on the applied (imposed) strain field (Figure 2.1).

$$\theta = \frac{1}{2} \cdot tan^{-1} \cdot \left(\frac{\gamma_{xy}}{\varepsilon_x - \varepsilon_y} \right) \tag{2.1}$$

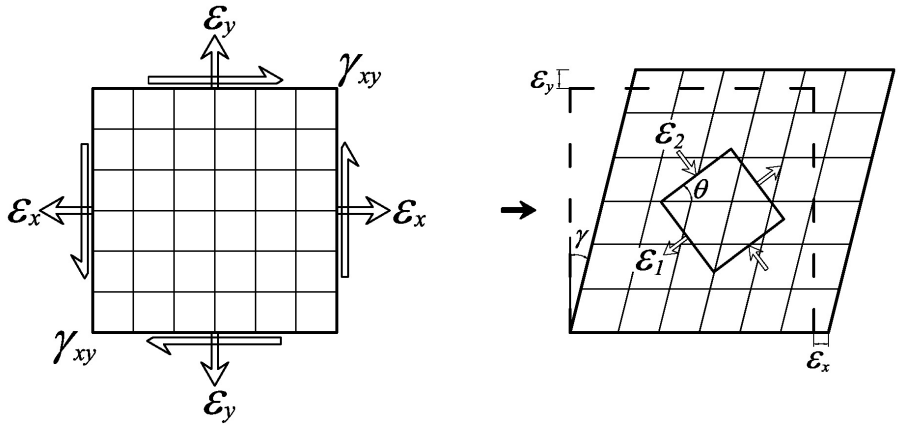

Figure 2.1. Applied strain field and corresponding principal strains on an uncracked panel

After calculation of the principal strain direction, the principal strains (ε_1 and ε_2) are calculated, as shown in Figure 2.2.

$$\varepsilon_1 = \frac{\varepsilon_x + \varepsilon_y}{2} + \frac{\gamma_{xy}}{2 \cdot sin2\theta} \tag{2.2}$$

$$\varepsilon_2 = \frac{\varepsilon_x + \varepsilon_y}{2} - \frac{\gamma_{xy}}{2 \cdot sin2\theta} \tag{2.3}$$

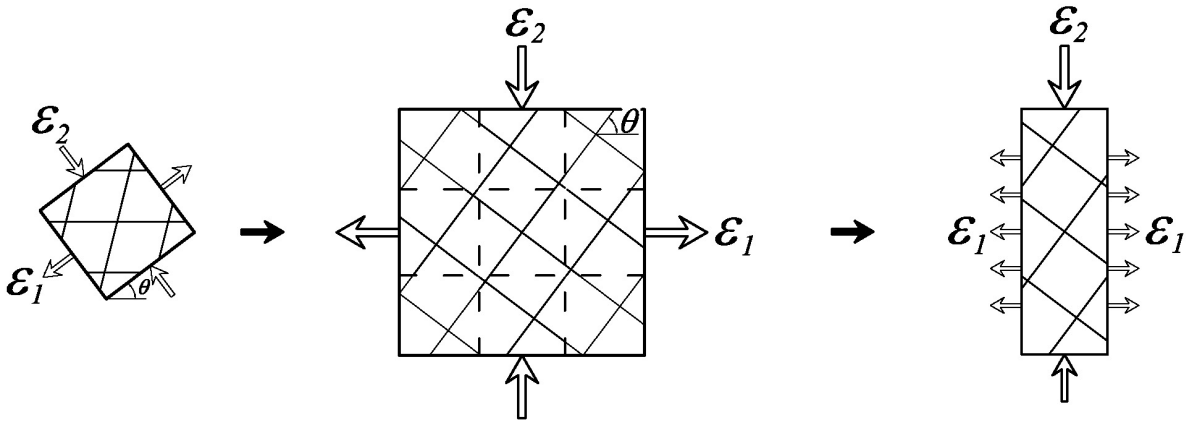

Figure 2.2. Visualization of a rotating strut assumption

Next step is the calculation of unsoftened principal stresses in concrete (σ_{c1} and σ_{c2}), which coincide with the principal strains directions, using the monotonic envelope of the constitutive material model used for concrete (Figure 2.3). Details of the concrete constitutive model are described in Chapter 3 of this thesis.

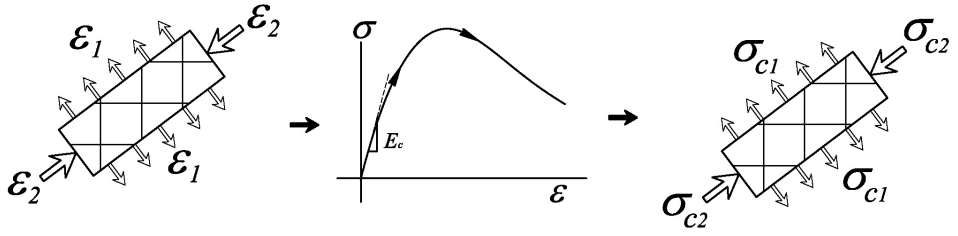

Figure 2.3. Calculation of stresses in concrete using the monotonic constitutive model

After the concrete stresses are calculated from the concrete constitutive model, the compressive stresses are reduced by appropriate compression softening parameters (beta, described in Chapter 3), and the final stress values are back-transformed into the x-y coordinate system to obtain the concrete stress state in the x-y coordinates, σ_{cx}, σ_{cy} and τ_{cxy}. (Figure 2.4).

$$\sigma_{c1soft} = \beta \cdot \sigma_{c1} \tag{2.4}$$

$$\sigma_{c2soft} = \beta \cdot \sigma_{c2} \tag{2.5}$$

$$\sigma_{cx} = \frac{\sigma_{c1soft} + \sigma_{c2soft}}{2} + \frac{\sigma_{c1soft} - \sigma_{c2soft}}{2} \cdot cos2\theta \tag{2.6}$$

$$\sigma_{cy} = \frac{\sigma_{c1soft} + \sigma_{c2soft}}{2} - \frac{\sigma_{c1soft} - \sigma_{c2soft}}{2} \cdot cos2\theta \tag{2.7}$$

$$\tau_{cxy} = \frac{\sigma_{c1soft} - \sigma_{c2soft}}{2} \cdot sin2\theta \tag{2.8}$$

After determination of the concrete stress state in x-y coordinates, uniaxial stresses in the reinforcing steel bars developed as a result of normal strains in their longitudinal direction, should also be calculated. For this purpose, the monotonic envelope of the uniaxial constitutive material model for reinforcing steel (described in Chapter 3) is applied in each of the two orthogonal (x and y) directions of reinforcement. It must be mentioned that the geometry of the panel model should be arranged such that orthogonal reinforcement directions should coincide with the x and y directions, of the panel.

Finally, the calculated stress fields for concrete and reinforcing steel are superimposed to obtain the resulting x-y state of stress in the panel, corresponding to the applied strain field.

$$\sigma_x = \sigma_{cx} + \rho_{sx} \cdot \sigma_{sx} \tag{2.9}$$

$$\sigma_y = \sigma_{cy} + \rho_{sy} \cdot \sigma_{sy} \tag{2.10}$$

$$\tau_{xy} = \tau_{cxy} \tag{2.11}$$

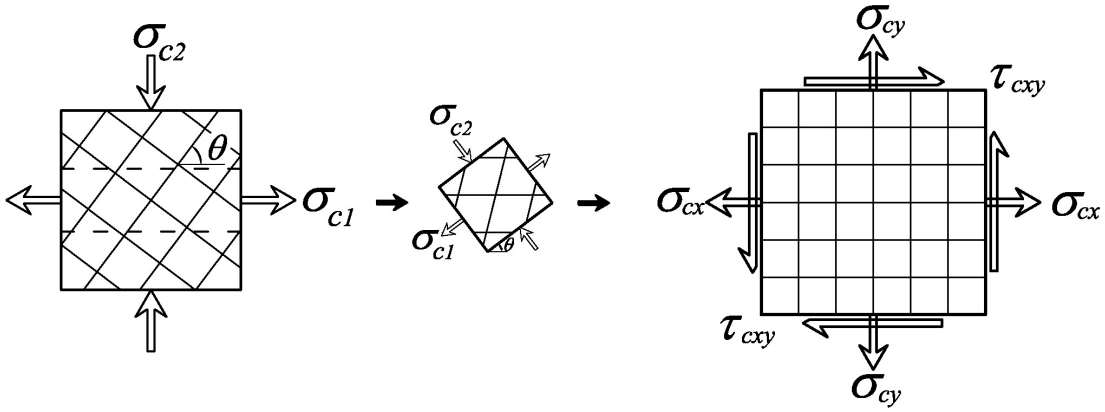

Figure 2.4. Back transformation of principal stresses on an un-cracked panel

2.3. Panel Response after formation of First Crack

When the value of the principal tensile strain in concrete exceeds the monotonic cracking strain of concrete for the first time, the first crack is formed, and for following loading stages, the principal strain direction corresponding to first cracking in concrete is assigned as the first "Fixed Strut" direction for the panel. After formation of this first crack, while principal directions of the applied strain field continues to rotate based on the applied strain field, the principal stress directions in concrete are assumed to be along and perpendicular to the first Fixed Strut direction. For a given (applied) strain field, the following steps are involved in the analysis:

As a first step, the applied strain field is transformed into directions parallel and perpendicular to the first strut direction. (Figure 2.5). It should be mentioned that, θ_{crA}, which represents the first fixed strut direction is obtained from the state of strain at the instant of first cracking (when the value of the principal tensile strain in concrete exceeds the monotonic cracking strain of concrete) using Equation 2.12.

$$\theta_{crA} = \frac{1}{2} \cdot tan^{-1} \cdot \left(\frac{\gamma_{xy}}{\varepsilon_x - \varepsilon_y} \right) \qquad \text{(at first cracking)} \quad (2.12)$$

$$\varepsilon_{x'} = \frac{\varepsilon_x + \varepsilon_y}{2} + \frac{\varepsilon_x - \varepsilon_y}{2} \cdot cos2\theta_{cr} + \frac{\gamma_{xy}}{2} \cdot sin2\theta_{cr} \qquad (2.13)$$

$$\varepsilon_{y'} = \frac{\varepsilon_x + \varepsilon_y}{2} + \frac{\varepsilon_x - \varepsilon_y}{2} \cdot cos2\theta_{cr-per} + \frac{\gamma_{xy}}{2} \cdot sin2\theta_{cr-per} \tag{2.14}$$

where,

$$\theta_{cr-per} = \theta_{cr} \pm \frac{\pi}{2} \tag{2.15}$$

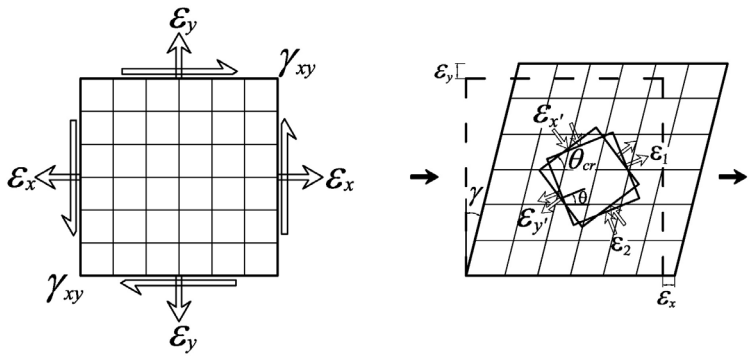

Figure 2.5. Deviation of principal strain and fixed strut directions after formation of first crack

Next step is the calculation of unsoftened principal stresses in concrete ($\sigma_{cx'}$ and $\sigma_{cy'}$), along and perpendicular to the fixed strut direction (Figure 2.7), using the hysteretic constitutive material model used for concrete (Figure 2.6). Details of the hysteretic concrete constitutive model are described in Chapter 3 of this thesis. It should be mentioned that the shear strains along the first fixed strut direction ($\gamma_{cx'y'}$) are assumed not to develop any shear stresses, because of the zero shear aggregate interlock assumption.

After the concrete stresses are calculated from the concrete constitutive model, the compressive stresses are reduced by appropriate compression softening and biaxial damage parameters (described in Chapter 3), and the final stress values are back-transformed into the x-y coordinate system to obtain the concrete stress state in the x-y coordinates (Figure 2.8).

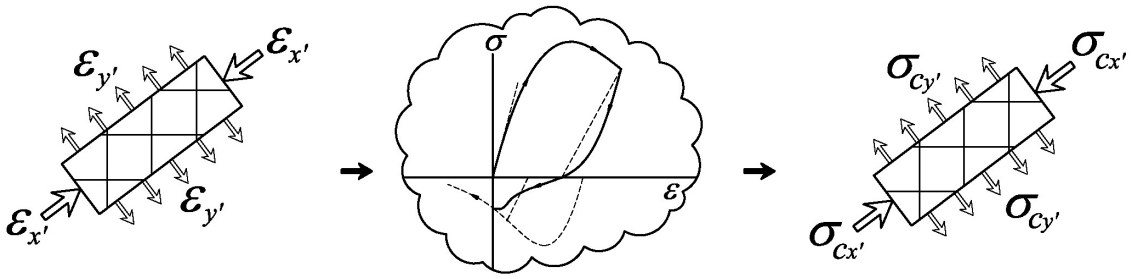

Figure 2.6. Calculation of stresses in concrete using the hysteretic constitutive model after formation of the first crack.

$$\sigma_{cx'soft} = \beta \cdot \sigma_{cx'} \tag{2.16}$$

$$\sigma_{cy'soft} = \beta \cdot \sigma_{cy'} \tag{2.17}$$

$$\sigma_{cx} = \frac{\sigma_{cx'soft} + \sigma_{cy'soft}}{2} + \frac{\sigma_{cx'soft} - \sigma_{cy'soft}}{2} \cdot cos2\theta_{cr} \tag{2.18}$$

$$\sigma_{cy} = \frac{\sigma_{cx'soft} + \sigma_{cy'soft}}{2} - \frac{\sigma_{cx'soft} - \sigma_{cy'soft}}{2} \cdot cos2\theta_{cr} \tag{2.19}$$

$$\tau_{cxy} = \frac{\sigma_{cx'soft} - \sigma_{cy'soft}}{2} \cdot sin2\theta_{cr} \tag{2.20}$$

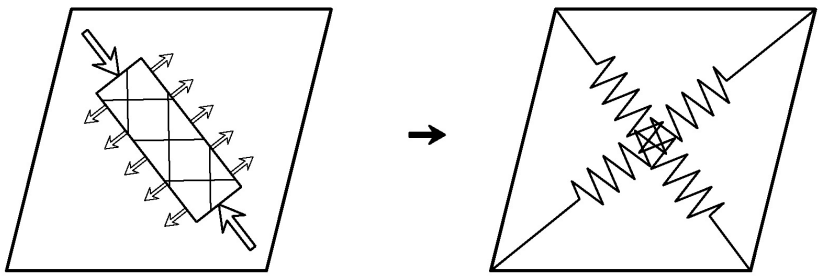

Figure 2.7. Representation of the single fixed strut mechanism after formation of the first crack

After determination of the concrete stress state in x-y coordinates, uniaxial stresses in the reinforcing steel bars developed as a result of normal strains in their longitudinal

direction are calculated. For this purpose, the hysteretic uniaxial constitutive material model for reinforcing steel (described in Chapter 3) is applied in each of the two orthogonal (x and y) directions of reinforcement.

Finally, the calculated stress fields for concrete and reinforcing steel are superimposed to obtain the resulting x-y state of stress in the panel, corresponding to the applied strain field.

$$\sigma_x = \sigma_{cx} + \rho_{sx} \cdot \sigma_{sx} \tag{2.21}$$

$$\sigma_y = \sigma_{cy} + \rho_{sy} \cdot \sigma_{sy} \tag{2.22}$$

$$\tau_{xy} = \tau_{cxy} \tag{2.23}$$

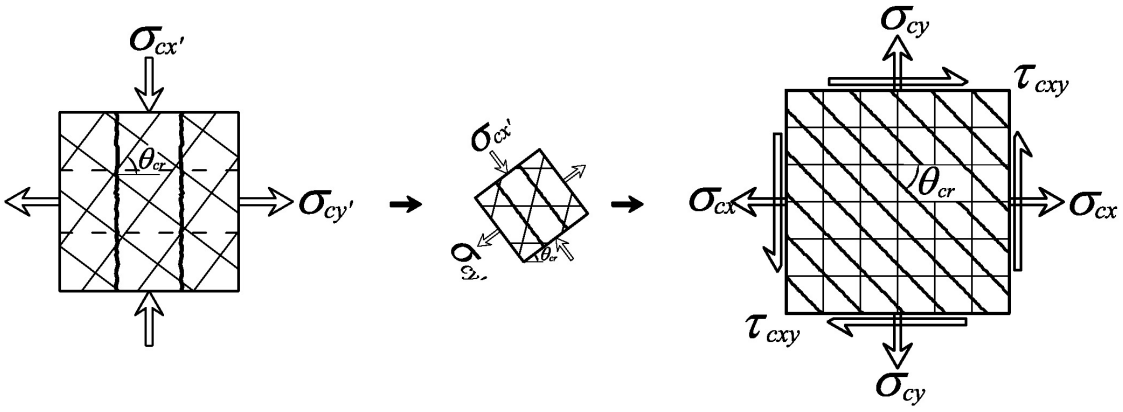

Figure 2.8. Back transformation of concrete stresses along and perpendicular to the first strut, into the x-y state of concrete stress

2.4. Panel Response after formation of the Second Crack

The single-fixed-strut analysis described in the previous section is continued until the formation of the second crack, after which the second strut will develop in the panel model. During the first fixed strut stage of the analysis, the model tracks the concrete stress–strain behavior along the first strut direction, and when the strains along the first strut direction first exceed the cyclic cracking strain (which depends on both the monotonic

cracking strain and the plastic strain upon reversal from a compressive stress state), the second crack is formed. Due to the zero aggregate interlock assumption, the second crack will develop in perpendicular direction to the first crack, according to the stress-based cracking criterion, since the first strut direction is a principal stress direction, as described in Section 2.1. For a given (applied) strain field, the following steps are involved in the analysis:

As a first step, the applied strain field is transformed into directions parallel to the first and second strut directions. (Figure 2.9). It should be mentioned that θ_{crB} represents the direction of the second strut.

$$\theta_{crB} = \theta_{crA} \pm \frac{\pi}{2} \tag{2.24}$$

$$\varepsilon_{x'} = \frac{\varepsilon_x + \varepsilon_y}{2} + \frac{\varepsilon_x - \varepsilon_y}{2} \cdot cos2\theta_{crA} + \frac{\gamma_{xy}}{2} \cdot sin2\theta_{crA} \tag{2.25}$$

$$\varepsilon_{y'} = \frac{\varepsilon_x + \varepsilon_y}{2} + \frac{\varepsilon_x - \varepsilon_y}{2} \cdot cos2\theta_{crB} + \frac{\gamma_{xy}}{2} \cdot sin2\theta_{crB} \tag{2.26}$$

Next step is the calculation of unsoftened principal stresses in concrete along the first and second fixed strut directions, using the hysteretic constitutive material model used for concrete (Figure 2.10). It should be mentioned that the shear strains along the first and second fixed strut directions are assumed not to develop any shear stresses, because of the zero shear aggregate interlock assumption.

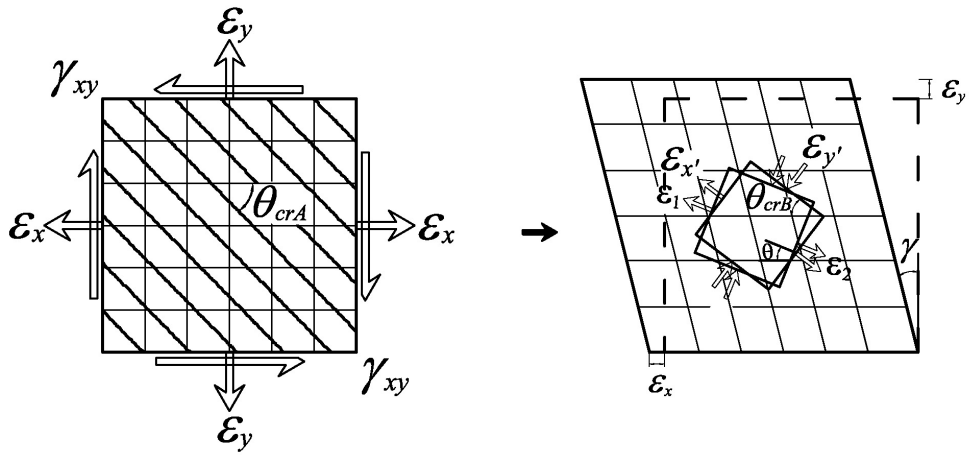

Figure 2.9. Deviation of principal strain and fixed strut directions after formation of the second crack

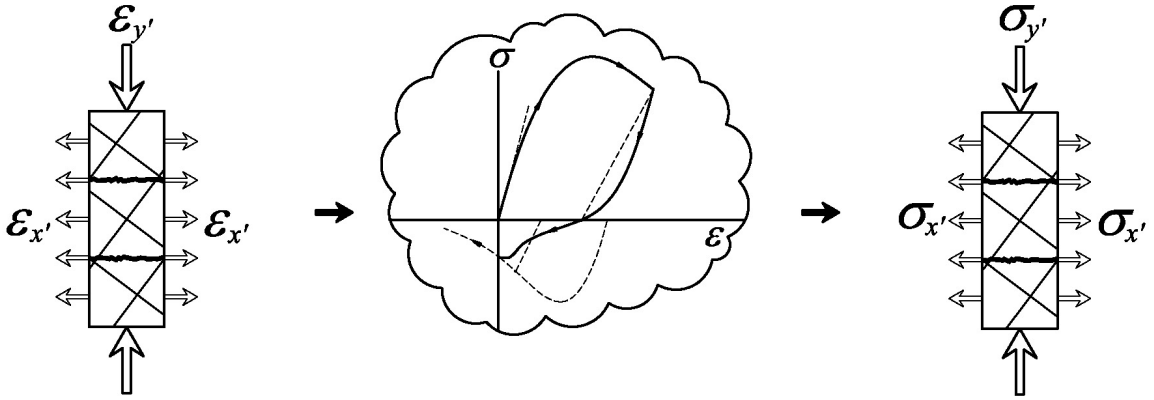

Figure 2.10. Calculation of stresses in concrete using the hysteretic constitutive model after formation of the second crack.

After the concrete stresses along the two struts (Figure 2.11) are calculated from the concrete constitutive model, the compressive stresses are reduced by appropriate compression softening and biaxial damage parameters (described in Chapter 3), and the final stress values in the two struts are back-transformed into the x-y coordinate system, and superimposed to obtain the concrete stress state in the x-y coordinates (Figure 2.12).

$$\sigma_{cAx} = \frac{0 + \sigma_{x'soft}}{2} + \frac{0 - \sigma_{cx'soft}}{2} \cdot cos2\theta_{crA} \tag{2.27}$$

$$\sigma_{cAy} = \frac{0+\sigma_{cx'soft}}{2} - \frac{0-\sigma_{cx'soft}}{2} \cdot cos2\theta_{crA} \tag{2.28}$$

$$\tau_{cAxy} = \frac{0-\sigma_{cx'soft}}{2} \cdot sin2\theta_{crA} \tag{2.29}$$

$$\sigma_{cBx} = \frac{0+\sigma_{cy'soft}}{2} + \frac{0-\sigma_{cy'soft}}{2} \cdot cos2\theta_{crB} \tag{2.30}$$

$$\sigma_{cBy} = \frac{0+\sigma_{cy'soft}}{2} - \frac{0-\sigma_{cy'soft}}{2} \cdot cos2\theta_{crB} \tag{2.31}$$

$$\tau_{cBxy} = \frac{0-\sigma_{cy'soft}}{2} \cdot sin2\theta_{crB} \tag{2.32}$$

$$\sigma_{cx} = \sigma_{cAx} + \sigma_{cBx} \tag{2.33}$$

$$\sigma_{cy} = \sigma_{cAy} + \sigma_{cBy} \tag{2.34}$$

$$\tau_{cxy} = \tau_{cAxy} + \tau_{cBxy} \tag{2.35}$$

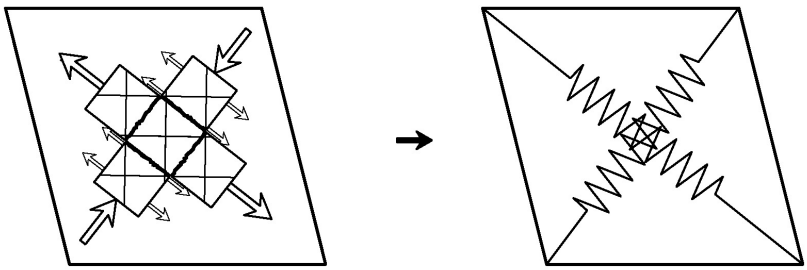

Figure 2.11. Representation of the two-fixed-strut mechanism after formation of the second crack

After determination of the concrete stress state in x-y coordinates, uniaxial stresses in the reinforcing steel bars developed as a result of normal strains in their longitudinal direction are calculated. For this purpose, the hysteretic uniaxial constitutive material model for reinforcing steel (described in Chapter 3) is applied in each of the two orthogonal (x and y) directions of reinforcement.

Finally, the calculated stress fields for concrete and reinforcing steel are superimposed to obtain the resulting x-y state of stress in the panel, corresponding to the applied strain field.

$$\sigma_x = \sigma_{cx} + \rho_{sx} \cdot \sigma_{sx} \tag{2.36}$$

$$\sigma_y = \sigma_{cy} + \rho_{sy} \cdot \sigma_{sy} \tag{2.37}$$

$$\tau_{xy} = \tau_{cxy} \tag{2.38}$$

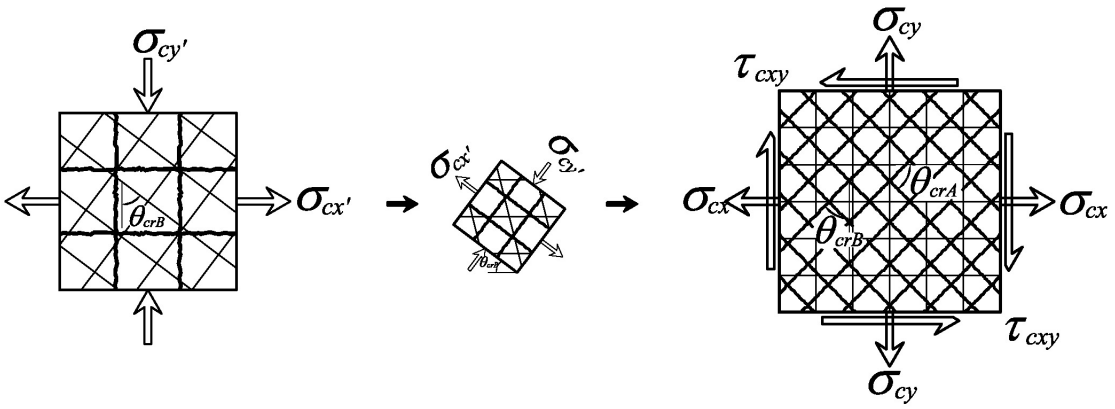

Figure 2.12. Back transformation of concrete stresses along the first and second strut, into the x-y state of concrete stress

2.5. Nonlinear Analysis Solution Strategy

The formulation of the proposed Fixed Strut Angle model described in the previous section, was implemented into a nonlinear analysis solution strategy for conducting nonlinear quasi-static analyses of RC panels using Matlab ("Matlab")

The nonlinear analysis solution strategy used in this study is an adaptation of the "arch-length" method, with a displacement controlled iterative strategy, based on incrementation of selected displacements components of the model (Clarke and Hancock 1990, Simons and Powell 1982). Details of this strategy are described in this section.

The strategy consists of two main stages, being the "incrementation stage" and the "equilibrium stage". While during the incrementation stage, new load and/or displacement values are imposed on system, during the equilibrium cycles, stress equilibrium of the system between external and internal forces is aimed to be satisfied for the imposed conditions.

2.5.1. Incrementation Cycle (First Iteration Cycle)

According to the strategy, each load step in the analysis starts with an incrementation cycle. In this cycle, incrementation of load (for load controlled analysis), incrementation of displacement (for displacement controlled analysis), or both (arc-length controlled analysis) can be applied to the system and a corresponding unbalanced (residual) magnitude is calculated for initiation of the equilibrium cycles.

Each incrementation cycle commences with the calculation of the tangent stiffness matrix of the system. For the panel model proposed, since a single constitutive panel element has three degrees of freedom (ε_x, ε_y and γ_{xy}.), the stiffness matrix is a 3x3 matrix with the following components:

$$\left[K_I\right]_i = \begin{bmatrix} \frac{\partial \sigma_x}{\partial \varepsilon_x} & \frac{\partial \sigma_x}{\partial \varepsilon_y} & \frac{\partial \sigma_x}{\partial \gamma_{xy}} \\ \frac{\partial \sigma_y}{\partial \varepsilon_x} & \frac{\partial \sigma_y}{\partial \varepsilon_y} & \frac{\partial \sigma_y}{\partial \gamma_{xy}} \\ \frac{\partial \tau_{xy}}{\partial \varepsilon_x} & \frac{\partial \tau_{xy}}{\partial \varepsilon_y} & \frac{\partial \tau_{xy}}{\partial \gamma_{xy}} \end{bmatrix} \tag{2.39}$$

The next step in the incrementation strategy is to define the reference external load vector $\left\{F_I\right\}_i$, which depends on the type of external loading that the model will be subjected to. For example, for analysis under applied shear stresses only (with no σ_x and σ_y applied), can be written as:

$$\left\{F_I\right\}_i = \begin{Bmatrix} 0 \\ 0 \\ 1 \end{Bmatrix} \tag{2.40}$$

The tangent displacement vector $\left\{\delta_I\right\}_i$ can be calculated using the stiffness matrix and the reference external load vector as:

$$\left\{\delta_I\right\}_i = \frac{\left\{F_I\right\}_i}{\left[K_I\right]_i} \tag{2.41}$$

The tangent displacement vector is used to determine the direction (sign) of displacements of the model under the applied external force vector, and the magnitudes of its terms are irrelevant. After the calculation of $\left\{\delta_I\right\}_i$, the initial load increment $\Delta\lambda_i^{j=1}$ can be calculated:

$$\Delta\lambda_i^{j=1} = \frac{-\left\{b_n\right\}^T \left\{\Delta\delta_R\right\}_i^{j=1}}{\left\{b_n\right\}^T \left\{\delta_I\right\}_i} \tag{2.42}$$

where $\{b_n\}$ is a vector with a unity term along the degree-of-freedom to be incremented for the displacement-controlled analysis, and zero along other degrees of freedom. The nominator of this expression represents the applied nodal displacement (or strain) increment along the controlled (n^{th}) degree of freedom of the model (Equation 2.43), in the case of displacement (strain) controlled analysis, where the applied nodal displacement increment of the controlled degree of freedom is controlled.

$$\Delta\delta_n = \{b_n\}^T \{\Delta\delta_R\}_i^{j=1} \tag{2.43}$$

Therefore, the initial load increment can be expressed as:

$$\Delta\lambda_i^{j=1} = \frac{-\Delta\delta_n}{\{b_n\}^T \{\delta_I\}_i} \tag{2.44}$$

After the calculation of initial load increment, the corresponding initial displacement increment can be calculated as:

$$\{\Delta\delta\}_{\mathrm{i}}^{\mathrm{j=1}} = \Delta\lambda_i^{j=1} \{\delta_I\}_i \tag{2.45}$$

and the following expressions can be used for the incrementation cycle:

$$\{\delta\}_{\mathrm{i}}^{\mathrm{j=1}} = \{\delta\}_{\mathrm{i-1}} - \{\Delta\delta\}_{\mathrm{i}}^{\mathrm{j=1}} \tag{2.46}$$

$$\lambda_i^{j=1} = \lambda_{\mathrm{i-1}} + \Delta\lambda_i^{j=1} \tag{2.47}$$

where $\{\delta\}$ represents the nodal displacement vector, *i* denotes the current load step, *j=1* denotes the first iteration (incrementation), and λ is a scalar to be multiplied with the reference external load vector to obtain the external force vector (F_{ext}). While the internal force vector is calculated using the stresses developed in the panel model for the strain field (nodal displacement vector) applied, the external force vector calculated:

$$\{F_{ext}\}_i^{j=1} = \lambda_i^{j=1}\{F_I\}_i \tag{2.48}$$

The difference between the internal and external load vectors is defined as the residual force vector $\{R\}$ for the incrementation cycle, as:

$$\{R\}_i^{j=1} = \{F_{int}\}_i^{j=1} - \{F_{ext}\}_i^{j=1} \tag{2.49}$$

If the residual force vector is larger than a specified tolerance, it should be reduced, by incrementing the nodal displacement vector and the external force multiplier λ through the equilibrium cycles, until the external and internal forces are balanced, within the specified magnitude of tolerance.

2.5.2. Equilibrium Iteration Cycles

Since the residual force vector is known at the end of the incrementation cycle, the residual displacement increment can be calculated as:

$$\{\Delta\delta_R\}_i^j = \frac{\{R\}_i^{j-1}}{[K_I]_i} \tag{2.50}$$

The incremental external force multiplier and nodal displacement vector can now be calculated from the residual displacement vector as:

$$\Delta\lambda_i^j = \frac{-\{b_n\}^T\{\Delta\delta_R\}_i^j}{\{b_n\}^T\{\delta_I\}_i} \tag{2.51}$$

$$\{\Delta\delta\}_i^j = \Delta\lambda_i^j\{\delta_I\}_i + \{\Delta\delta_R\}_i^j \tag{2.52}$$

After calculation of the incrementations, the nodal displacement vector and external force multiplier at the end of the current iteration cycle can be calculated as;

$$\{\delta\}_i^j = \{\delta\}_i^{j-1} + \{\Delta\delta\}_i^j \tag{2.53}$$

$$\lambda_i^j = \lambda_i^{j-1} + \Delta\lambda_i^j \tag{2.54}$$

After that, as was done in the incrementation stage, the external force vector F_{ext} and the internal force vector F_{int} are calculated, and the residual force is defined as the difference between these two as:

$$\{F_{ext}\}_i^j = \lambda_i^j \{F_I\}_i \tag{2.55}$$

$$\{R\}_i^j = \{F_{int}\}_i^j - \{F_{ext}\}_i^j \tag{2.56}$$

If the residual force vector is larger than a specified tolerance, the equilibrium cycles are continued until the external and internal forces are balanced, within the specified magnitude of tolerance. When this condition is satisfied, the load step is assumed converged, and the strategy is commenced for a new load step with a new incrementation cycle.

Graphical representations of the nonlinear analysis solution strategy described are illustrated in Figures 2.13 and 2.14. Further information on the solution strategy can be found in Clarke and Hancock (1990) and Simons and Powell (1982).

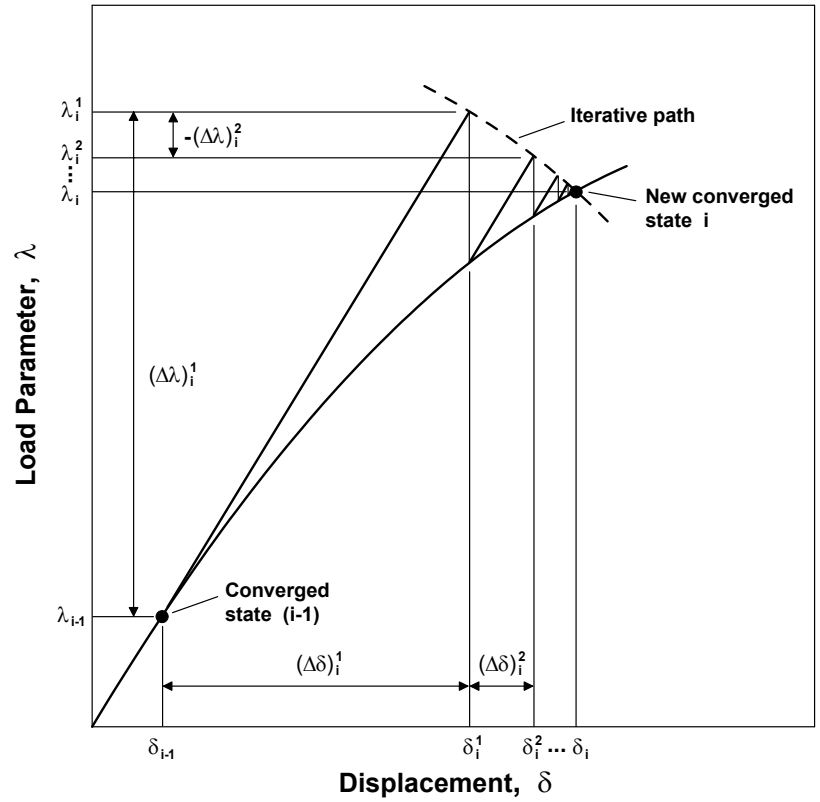

Figure 2.13. Representation of the nonlinear analysis solution strategy for a single degree of freedom system

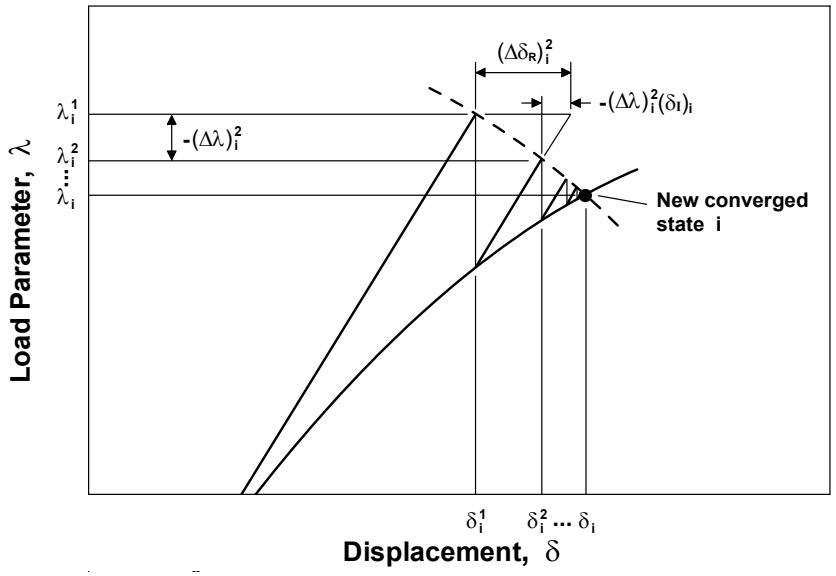

Figure 2.14 Representation of iterative equilibrium cycles

3. MATERIAL CONSTITUTIVE MODELS

The constitutive panel model proposed relates the panel response directly to uniaxial constitutive stress–strain behavior of concrete and reinforcing steel. Therefore, state-of-the-art hysteretic material constitutive relationships were implemented in the present model formulation. Details of the hysteretic constitutive models used for reinforcing steel and concrete, as well as the constitutive modeling approaches adopted to represent biaxial compression softening in concrete, tension stiffening behavior, and biaxial damage on concrete are described in the following sections.

3.1. Constitutive Model for Reinforcement

The uniaxial constitutive stress-strain relationship implemented in Fixed Strut Angle Model for reinforcing steel is the well-known nonlinear hysteretic model of Menegotto and Pinto (1973), extended by Filippou et al. (1983). The model is computationally efficient and capable of reproducing experimental results with accuracy.

In the Menegotto and Pinto (1973) model, the stress–strain (σ–ε) relationship is in the form of curved transitions (Figure 3.1), each from a straight-line asymptote with slope E_0 (modulus of elasticity) to another straight-line asymptote with slope $E_1=b.E_0$ (yield modulus) where the parameter b is the strain hardening ratio. The curvature of the transition curve between the two asymptotes is governed by a cyclic curvature parameter (R), which permits the Bauschinger's effect to be represented. The uniaxial hysteretic stress–strain relationship takes the form:

$$\sigma^* = b \cdot \varepsilon^* + \frac{(1-b)\cdot \varepsilon^*}{(1+\varepsilon^{*R})^{1/R}} \tag{3.1}$$

where

$$\varepsilon^* = \frac{\varepsilon - \varepsilon_r}{\varepsilon_0 - \varepsilon_r} \tag{3.2}$$

$$\sigma^* = \frac{\sigma - \sigma_r}{\sigma_0 - \sigma_r} \tag{3.3}$$

and

Equation (3.1) represents the curved transition from the elastic asymptote with slope E_0 to the yield asymptote with slope $E_1 = b.E_0$ (Figure 3.1). Parameters σ_r and ε_r are the stress and strain at the point of strain reversal, which also forms the origin of the asymptote with slope E_0. Parameters σ_0 and ε_0 are the stress and strain at the point of intersection of the two asymptotes. Parameter b is the strain hardening ratio, which is the ratio between the slopes E_1 and E_0, and R is the parameter that influences the curvature of the transition curve between the two asymptotes (and thus permits the Bauschinger's effect to be represented). As indicated on Figure 3.1, the strain and stress pairs (ε_r, σ_r) and (ε_0, σ_0) are updated after each strain reversal.

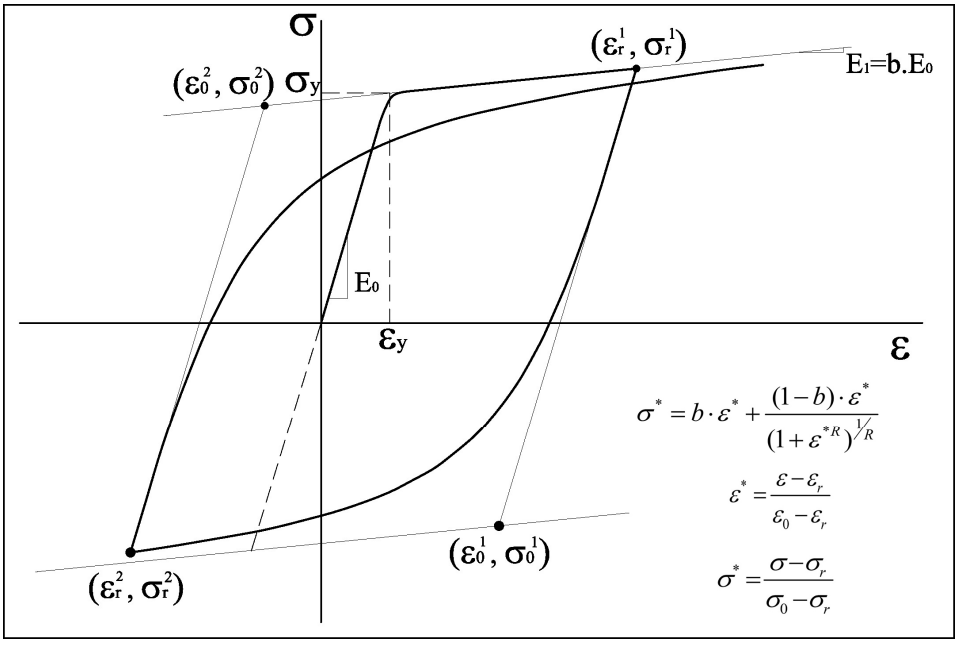

Figure 3.1. Constitutive model for steel (Menegotto and Pinto, 1973)

The tangent modulus E_t of the stress-strain relationship is obtained by differentiating the equations above, and is given by the following expression:

$$E_t = \frac{d\sigma}{d\varepsilon} = \left(\frac{\sigma_0 - \sigma_r}{\varepsilon_0 - \varepsilon_r}\right) \cdot \frac{d\sigma^*}{d\varepsilon^*} \tag{3.4}$$

$$\frac{d\sigma^*}{d\varepsilon^*} = b + \left[\frac{1-b}{\left(1+\varepsilon^{*R}\right)^{1/R}}\right] \cdot \left[1 - \frac{\varepsilon^{*R}}{1+\varepsilon^{*R}}\right] \tag{3.5}$$

where

The curvature parameter R is dependent on the absolute strain difference between the current asymptote intersection point and the previous maximum or minimum strain reversal point (Figure 3.2) depending on whether the current strain is increasing or decreasing, respectively. The expression for R takes the form suggested by Menegotto and Pinto:

$$R = R_0 - \frac{a_1 \cdot \xi}{a_2 + \xi} \tag{3.6}$$

Where R_0 is the value assigned to the parameter R for initial (or monotonic) loading, and a_1 and a_2 are experimentally determined parameters that represent the degradation of the curvature within subsequent cycles. The absolute strain difference between the current asymptote intersection point and the previous maximum or minimum strain reversal point is represented by the parameter ξ (Figure 3.2), which can be expressed as:

$$\xi = \left|\frac{\left(\varepsilon_m - \varepsilon_0\right)}{\varepsilon_y}\right| \tag{3.7}$$

where ε_m is the maximum or minimum strain, at the previous point of strain reversal, depending on whether the current strain is increasing or decreasing, respectively. Parameter ε_0 is the strain at the current intersection point of the two asymptotes, and parameter ε_y is the strain at monotonic yield point (Figure 3.2). As shown in Figure 3.2, both ε_m and ε_0 lie on the same asymptote, and ξ is updated following a strain reversal.

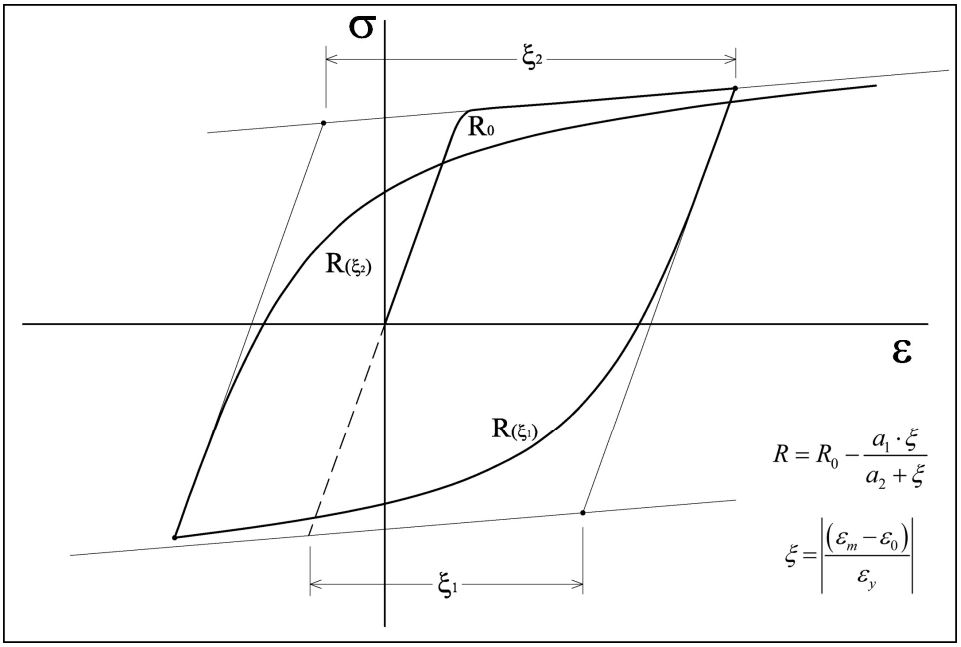

Figure 3.2. Degradation of cyclic curvature

Figure 3.3 shows an illustrative hysteretic stress-strain relationship, generated by the Menegotto and Pinto model, for a representative strain history.

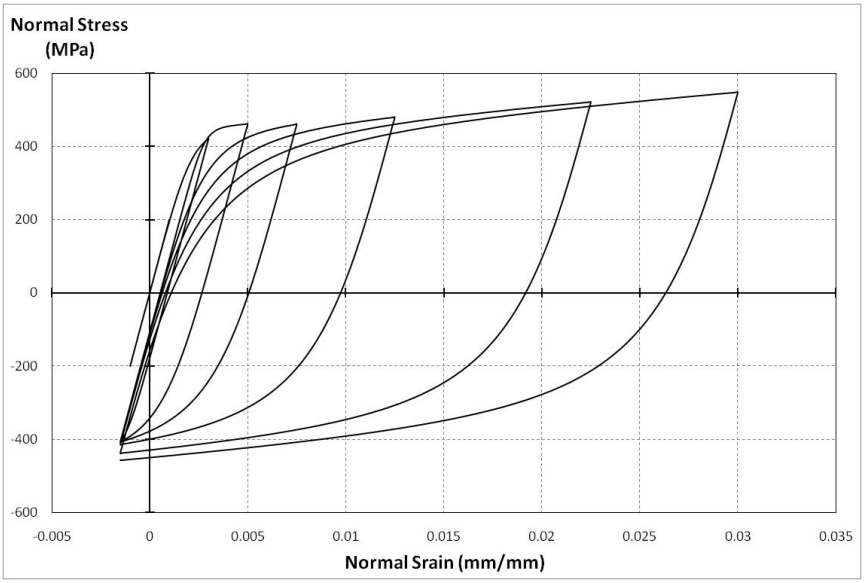

Figure 3.3.Illustration of Menegotto Pinto model

3.2. Constitutive Model for Concrete

The uniaxial hysteretic constitutive model proposed by Chang and Mander (1994) was adopted in the Fixed Strut Angle Model to represent the stress–strain behavior of concrete. The Chang and Mander model is an advanced, rule-based, generalized, and non-dimensional model that can simulate the hysteretic behavior of confined and unconfined, ordinary and high-strength concrete in both cyclic compression and tension. The model addresses important behavioral issues such as the hysteretic behavior in both cyclic compression and tension, the progressive degradation of stiffness of the unloading and reloading curves for increasing values of strain, and the effects of and gradual crack closure and tension stiffening on the behavior.

In the Chang and Mander model, the monotonic curve forms the envelope for the hysteretic stress-strain relationship. This is known as a reasonable assumption based on experimental results presented by Karsan and Jirsa (1969), and modeled by Mander et al. (1988a) for unconfined concrete in cyclic compression. Mander et al. (1988b) also performed tests for confined concrete and validated their model. Experiments by Gopalaratnman and Shah (1985) and Yankelevsky and Reinhardt (1987) have shown that this is also the case for concrete in cyclic tension. Thus, in the model by Chang and Mander, concrete in tension is modeled with a cyclic behavior similar to that in compression. The model envelopes for compression and tension have control on the slope of the stress-strain behavior at the origin, and the shape of both the pre-peak and post-peak branches of the stress-strain behavior. The shape of the envelopes can be feasibly altered while keeping the values of the peak stress and the strain at peak stress constant, allowing a refined calibration for modeling. In order to define the compression and tension envelopes, Chang and Mander model uses the Tsai's equation (Tsai, 1988), which is based on the equation by Popovics (1973), an equation that has proven to be very useful in describing the monotonic compressive stress-strain curve for concrete.

3.2.1. Compression Envelope Curve

The compression envelope curve of the Chang and Mander model is defined by the initial slope E_c, the peak coordinate ε'_c, f'_c, a parameter r from Tsai's (1988) equation

defining the shape of the envelope curve, and a parameter $x_{cr}^{-} > 1$ to define the spalling strain (Figure 3.4).

Both the compression and tension envelope curves can be written in non-dimensional form by the use of the following equations:

$$y(x) = \frac{n \cdot x}{D(x)} \tag{3.8}$$

$$z(x) = \frac{(1 - x^{r})}{D(x)^{2}} \tag{3.9}$$

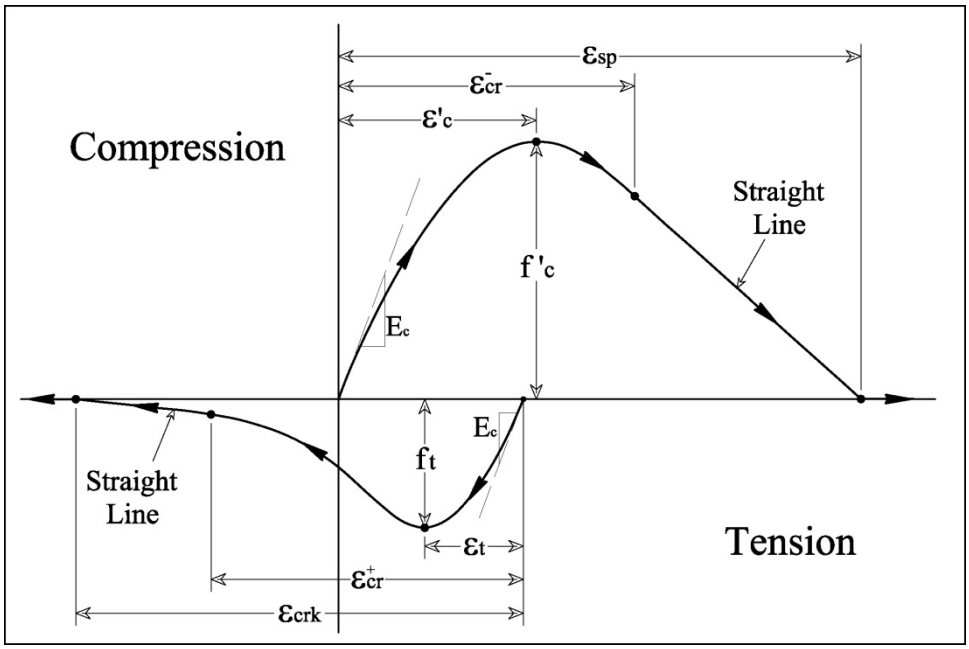

Figure 3.4.Compression and tension envelope curves of the model by Chang and Mander (1994)

where;

$$D(x) = 1 + \left(n - \frac{r}{r-1} \right) \cdot x + \frac{x^{r}}{r-1}, \quad r \neq 1 \tag{3.10}$$

$$D(x) = 1 + \left(n - 1 + \ln x\right) \cdot x^{r}, \quad r = 1 \tag{3.11}$$

And n and x are defined for the compression envelope as;

$$x^{-} = \left| \frac{\varepsilon_c}{\varepsilon_c^{'}} \right| \tag{3.12}$$

$$n^{-} = \left| \frac{E_c \cdot \varepsilon_c^{'}}{f_c^{'}} \right| \tag{3.13}$$

The non-dimensional spalling strain can be calculated by:

$$x_{sp} = x_{cr}^{-} - \frac{y(x_{cr}^{-})}{n^{-} \cdot z(x_{cr}^{-})} \tag{3.14}$$

In the equations above, ε_c is the concrete strain, $\varepsilon_c^{'}$ is the concrete strain at peak unconfined (or confined) stress, $f_c^{'}$ is the unconfined (or confined) concrete strength, E_c is the concrete initial modulus of elasticity, x^{-} is the non-dimensional strain on the compression envelope, x_{cr}^{-} is the non-dimensional critical strain on the compression envelope curve (used to define a tangent line up to the spalling strain), x_{sp} is the non-dimensional spalling strain, $y(x)$ is the non-dimensional stress function, $z(x)$ is the non-dimensional tangent modulus function (Figure 3.4)

The stress f_c and the tangent modulus E_t at any given strain on the compression envelope curve are defined by:

$$f_c = f_c^{-}(x^{-}) \tag{3.15}$$

$$E_t = E_t^{-}(x^{-}) \tag{3.16}$$

Where $f_c^-(x^-)$ and $E_t^-(x^-)$ are defined as;

If $x^- < x_{cr}^-$ (Tsai's equation)

$$f_c^- = f_c^- \cdot y(x^-) \tag{3.17}$$

$$E_t^- = E_c \cdot z(x^-) \tag{3.18}$$

If $x_{cr}^- \le x^- \le x_{sp}$ (Straight line)

$$f_c^- = f_c^{'} \cdot \left[y(x_{cr}^-) + n^- \cdot z(x_{cr}^-) \cdot (x^- - x_{cr}^-) \right] \tag{3.19}$$

$$E_t^- = E_c \cdot z(x_{cr}^-) \tag{3.20}$$

If $x > x_{sp}$ (Spalled)

$$f_c^- = E_t^- = 0 \tag{3.21}$$

Once the concrete is considered as spalled, the stresses are set to zero from that point on. Confined concrete can be considered not to spall; in such a case a large value of x_{cr}^- should be defined. The minus superscript in the equations above refers to the stress-strain behavior in compression.

The material parameters associated with the compression envelope curve of the model are the concrete strength $f_c^{'}$, the concrete strain at peak stress $\varepsilon_c^{'}$, the concrete initial modulus of elasticity E_c, the Tsai's parameter r defining the shape of the compression envelope, and the non-dimensional critical strain x_{cr}^- where the envelope curve starts following a straight line. All of these parameters can be controlled and manipulated based on specific experimental results for a refined calibration of the compression envelope. On

the other hand, Chang and Mander (1994) have proposed empirical relationships for the parameters E_c, $\varepsilon_c^{'}$ and r defined based on a detailed review of previous research. Parameters E_c, $\varepsilon_c^{'}$ and r associated with the unconfined compression envelope can be empirically related to the unconfined concrete strength $f_c^{'}$ (MPa) as:

Initial Modulus of elasticity:
$$E_c = 8200 f_c^{'3/8} \tag{3.22}$$

Strain at peak stress:
$$\varepsilon_c^{'} = \frac{\left(f_c^{'}\right)^{1/4}}{1120} \tag{3.23}$$

Shape Parameter:
$$r = \frac{f_c^{'}}{5.2} - 1.9 \tag{3.24}$$

3.2.2. Tension Envelope Curve

The shape of the tension envelope curve in the Chang and Mander model is the same as that of the compression envelope curve (Figure 3.4). The only difference is the shifted new origin ε_0, as explained in the following section. The non-dimensional parameters for the tension envelope curve are given by:

$$x^{+} = \left| \frac{\varepsilon_c - \varepsilon_0}{\varepsilon_t} \right| \tag{3.25}$$

$$n^{+} = \frac{E_c \cdot \varepsilon_t}{f_t} \tag{3.26}$$

The non dimensional cracking strain is given by;

$$x_{crk} = x_{cr}^{+} - \frac{y(x_{cr}^{+})}{n^{+} \cdot z(x_{cr}^{+})} \tag{3.27}$$

where ε_c is the concrete strain, ε_t is the concrete strain at peak tension stress, f_t is the concrete tensile strength, E_c is the concrete initial Young's modulus, x^+ is the non-dimensional strain on the tension envelope curve, x^+_{cr} is the critical strain on the tension envelope curve (used to define a tangent line up to the cracking strain), and x_{crk} is the cracking strain (Figure 3.4).

The stress f_c and the tangent modulus E_t for any given strain on the tension envelope curve are defined as:

$$f_c = f_c^+(x^+) \tag{3.28}$$

$$E_t = E_t^+(x^+) \tag{3.29}$$

Where $f_c^+(x^+)$ and $E_t^+(x^+)$ are defined as;

If $x^+ < x^+_{cr}$ (Tsai's equation)

$$f_c^+ = f_t \cdot y(x^+) \tag{3.30}$$

$$E_t^+ = E_c \cdot z(x^+) \tag{3.31}$$

If $x^+_{cr} \le x^+ \le x_{crk}$ (Straight line)

$$f_c^+ = f_t \cdot \left[y(x^+_{cr}) + n^+ \cdot z(x^+_{cr}) \cdot (x^+ - x^+_{cr}) \right] \tag{3.32}$$

$$E_t^+ = E_c \cdot z(x^+_{cr}) \tag{3.33}$$

If $x > x_{crk}$ (Cracked)

$$f_c^+ = E_t^+ = 0 \tag{3.34}$$

where the functions and are defined by Equations (3.8) and (3.9). When the concrete is cracked it is considered no longer to resist any tensile stress, as a result of crack opening, but on the other hand a gradual crack closure is considered to take place. Concrete experiencing tension stiffening can be considered not to crack completely, that is, a large value of x_{cr}^+ can be defined. The plus superscript refers to the stress-strain behavior in tension.

The parameters associated with the tension envelope curve include: the concrete tensile strength f_t, the strain at peak tensile stress ε_t, the parameter r defining the shape of the tension envelope curve, and the critical strain on the tension envelope curve x_{cr}^+ (where the envelope curve starts following a straight line) can also be controlled and calibrated based on specific experimental results or empirical relations proposed by other researchers (e.g., Collins and Mitchell, 1991; Belarbi and Hsu, 1994) to model the behavior of concrete in tension and the tension stiffening phenomenon.

3.2.3. Hysteretic Properties of the Model

In order to define the cyclic properties of concrete in compression, statistical regression analyses were performed by Chang and Mander (1994) on an extensive experimental database that included data from Sinha et al. (1964), Karsan and Jirsa (1969), Spooner and Dougill (1975), Okamoto et al. (1976) and Tanigawa and Uchida (1979). Based on the regression analyses, empirical relations were developed for key hysteretic parameters such as those for secant stiffness E_{sec} and plastic stiffness E_{pl} upon unloading from, and stress and strain offsets Δf and $\Delta\varepsilon$ upon return to the compression envelope (Figure 3.5). The hysteretic parameters for cyclic compression are given by:

$$E_{sec}^- = E_c \cdot \left(\frac{\left| \frac{f_{un}^-}{E_c \varepsilon_c'} \right| + 0.57}{\left| \frac{\varepsilon_{un}^-}{\varepsilon_c'} \right| + 0.57} \right) \tag{3.35}$$

$$E_{pl}^{-} = 0.1 \cdot E_c \cdot e^{\left(-2 \cdot \left|\frac{\varepsilon_{un}^{-}}{\varepsilon_c^{'}}\right|\right)} \tag{3.36}$$

$$\Delta f^{-} = 0.09 \cdot f_{un}^{-} \cdot \sqrt{\left|\frac{\varepsilon_{un}^{-}}{\varepsilon_c^{'}}\right|} \tag{3.37}$$

$$\Delta \varepsilon^{-} = \frac{\varepsilon_{un}^{-}}{1.15 + 2.75 \cdot \left|\frac{\varepsilon_{un}^{-}}{\varepsilon_c^{'}}\right|} \tag{3.38}$$

Where $\varepsilon_c^{'}$ is the strain at peak compressive stress, E_c is the initial modulus of elasticity, and f_{un} and ε_{un} are the unloading stress and strain.

Parameters such as the plastic strain upon unloading ε_{pl}, new stress f_{new} and tangent modulus E_{new} upon return to unloading strain from the envelope curve ε_{un}, and the strain ε_{re}, stress f_{re} and tangent modulus E_{re} at the point of return to the envelope curve are can be geometrically derived from these empirical relations (Figure 3.5) as:

$$\varepsilon_{pl}^{-} = \varepsilon_{un}^{-} - \frac{f_{un}^{-}}{E_{sec}^{-}} \tag{3.39}$$

$$f_{new}^{-} = f_{un}^{-} - \Delta f^{-} \tag{3.40}$$

$$E_{new}^{-} = \frac{f_{new}^{-}}{\varepsilon_{un}^{-} - \varepsilon_{pl}^{-}} \tag{3.41}$$

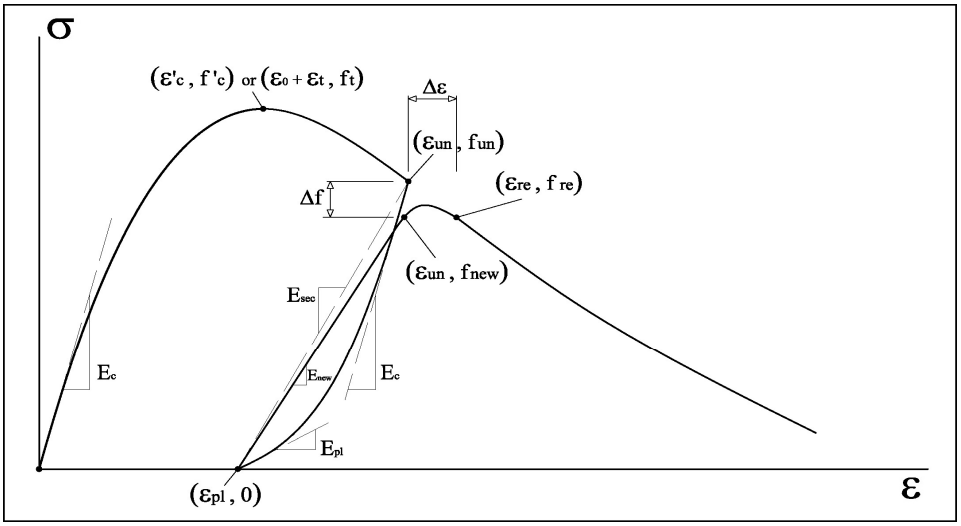

Figure 3.5. Hysteretic parameters of the model by Chang and Mander (1994)

$$\varepsilon_{re}^{-} = \varepsilon_{un}^{-} - \Delta\varepsilon^{-} \tag{3.42}$$

$$f_{re}^{-} = f^{-} \cdot \left(\left| \frac{\varepsilon_{re}^{-}}{\varepsilon_{c}^{'}} \right| \right) \tag{3.43}$$

$$E_{re}^{-} = E^{-} \cdot \left(\left| \frac{\varepsilon_{re}^{-}}{\varepsilon_{c}^{'}} \right| \right) \tag{3.44}$$

For cyclic behavior in tension, Chang and Mander modified the empirical relations defined in equations. (3.35) through (3.38), based on test results by Yankelevsky and Reinhardt (1987) as:

$$E_{sec}^{+} = E_c \cdot \left(\frac{\left| \frac{f_{un}^{+}}{E_c \varepsilon_t} \right| + 0.67}{\left| \frac{\varepsilon_{un}^{+} - \varepsilon_0}{\varepsilon_t} \right| + 0.67} \right) \tag{3.45}$$

$$E_{pl}^{+} = \frac{E_c}{\left| \frac{\varepsilon_{un}^{+} - \varepsilon_0}{\varepsilon_t} \right|^{1.1} + 1} \tag{3.46}$$

$$\Delta f^{+} = 0.15 \cdot f_{un}^{+} \tag{3.47}$$

$$\Delta \varepsilon^{+} = 0.22 \cdot \left(\varepsilon_{un}^{+} - \varepsilon_0 \right) \tag{3.48}$$

Where ε_t the strain at peak tensile stress, E_c is the initial modulus of elasticity and ε_0 is the shifted origin of the tensile envelope curve. The derived parameters for tension are thus:

$$\varepsilon_{pl}^{+} = \varepsilon_{un}^{+} - \frac{f_{un}^{+}}{E_{sec}^{+}} \tag{3.49}$$

$$f_{new}^{+} = f_{un}^{+} - \Delta f^{+} \tag{3.50}$$

$$E_{new}^{+} = \frac{f_{new}^{+}}{\varepsilon_{un}^{+} - \varepsilon_{pl}^{+}} \tag{3.51}$$

$$\varepsilon_{re}^{+} = \varepsilon_{un}^{+} - \Delta \varepsilon^{+} \tag{3.52}$$

$$f_{re}^{+} = f^{+} \cdot \left(\left| \frac{\varepsilon_{re}^{+} - \varepsilon_0}{\varepsilon_t} \right| \right) \tag{3.53}$$

$$E_{re}^{+} = E^{+} \cdot \left(\left| \frac{\varepsilon_{re}^{+} - \varepsilon_0}{\varepsilon_t} \right| \right) \tag{3.54}$$

In terms of modeling generalized hysteretic behavior, the constitutive model uses smooth “connecting” curves for unloading and reloading between the compression and tension envelope curves, and smooth “transition” curves for partial unloading and

reloading between the connecting curves (Fig. 4.15). The connecting and transition curves are geometrically defined such that they commence at the prescribed starting point (e.g., ε_{un} , f_{un} in Fig. 4.13) with a prescribed initial slope (e.g., E_c), and end up at a prescribed final (target) point (e.g., $\varepsilon_{pl}, 0$) with a prescribed final slope (e.g., E_{pl}). Both connecting and transition curves have slope continuity with uniform sign of curvature (second strain derivative of the curve equation) in between the starting and final points.

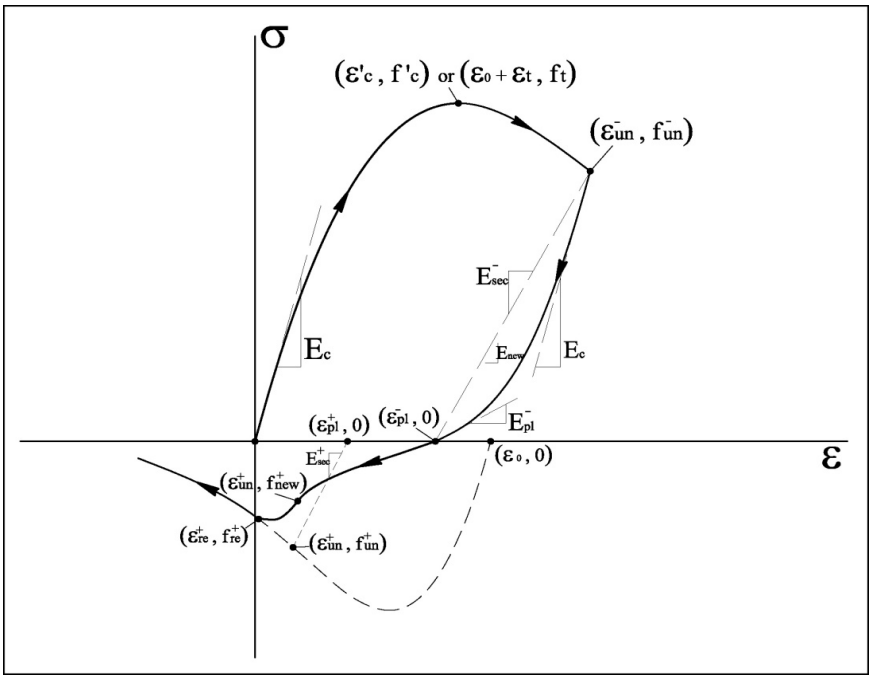

Figure 3.6. Unloading from the compression envelope curve

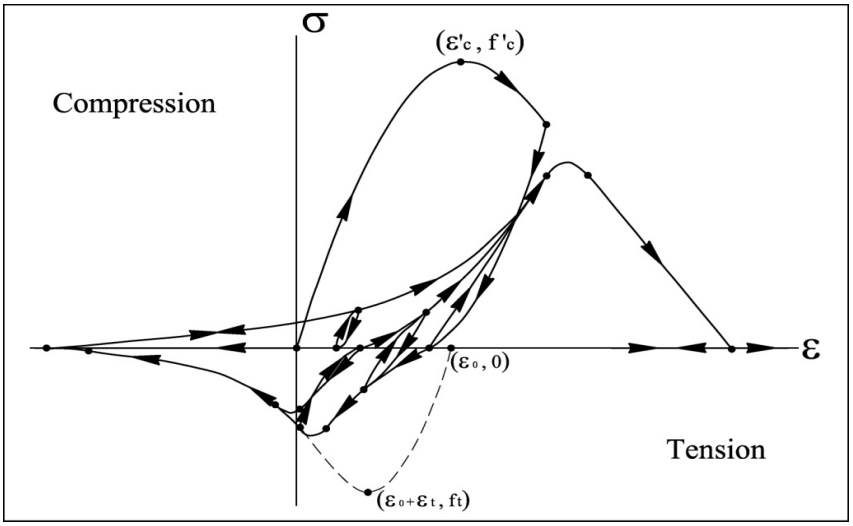

Figure 3.7. Continuous hysteresis in compression and tension

Further details of the model can be found in the referenced report of Chang and Mander (1994)

3.3. Compression Softening of Concrete

An important consideration in modeling the behavior of a RC panel element under membrane actions is incorporating the compression softening effect. Since the behavior of concrete under biaxial stress state was first identified by Kupfer, Hilsdorf and Rüsch in 1964, the softening effect has been experimentally observed by many other researchers, (e.g., Vecchio and Collins, 1986), and were represented by analytical models mainly in the form of reduction (softening) in the compressive stresses in concrete along the principal compression direction of RC panels, due to presence of tensile strains in the perpendicular principal direction. Some compression softening models have also included softening in the compressive strain (e.g., Belarbi and Hsu, 1995; Vecchio and Collins, 1993), reducing the strain at the peak compressive stress for concrete. Although all of these compression softening models were formulated for the case of monotonic loading, many of them were implemented into cyclic analysis methods (Belarbi 1995, Vecchio 1993).

The compression softening models adopted for the proposed Fixed Strut Angle panel model are described in the following subsections.

3.3.1. Vecchio and Collins (1993)

Vecchio and Collins (1993) used a large experimental database from tests on RC panels to propose two different models to represent compression softening behavior, one considering compression softening in both stresses and strains, and the second considering softening effect only in stresses.

3.3.1.1. Model A: In this approach, both compressive stresses and strains, along the principal compression direction, are reduced by the same β_m coefficient, where the softening coefficient β_m is defined as:

$$\beta_m = \frac{1}{1 + K_c \cdot K_f} \tag{3.64}$$

where,

$$K_c = 0.35 \cdot \left(\frac{-\varepsilon_1}{\varepsilon_2} - 0.28 \right)^{0.80} \geq 1.0 \tag{3.65}$$

$$K_f = 0.1825 \sqrt{f'_c} \geq 1.0 \tag{3.66}$$

and ε_1 and ε_2 are the strains in the principal tensile and compressive stress directions, respectively.

3.3.1.2. Model B: In this approach, only compressive stress along the principal compression direction is reduced by the β_m coefficient, providing a simpler model implementation. The softening coefficient β_m is defined in this case as:

$$\beta_m = \frac{1}{1 + K_c} \tag{3.67}$$

$$K_c = 0.27 \cdot \left(\frac{\varepsilon_1}{\varepsilon_0} - 0.37 \right) \tag{3.68}$$

where,

and ε_1 is the tensile strain in the principal tensile stress direction and ε_0 is the strain corresponding to peak stress of concrete in compression.

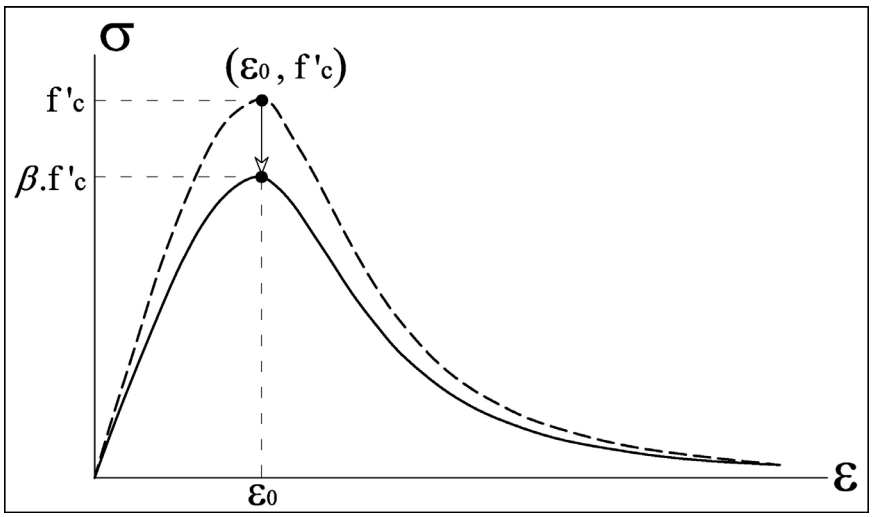

Figure 3.8. Softening effect modeled with Model B

3.3.2. Belarbi and Hsu (1995)

In the mid-1990's Belarbi and Hsu (1995) performed 22 full-size panel tests, where panel specimens were subjected to compression in one direction and tension in the other, for comprehensive experimental observations on biaxial concrete behavior. As a result of these tests, Belarbi and Hsu derived following equations, for simulating the softening effects of tensile strains perpendicular to the stress-strain behavior of concrete in the principal compressive stress direction. The softening coefficient for compressive stresses was expressed as:

$$\zeta_{\sigma_o} = \frac{0.9}{\sqrt{1 + k_\sigma \cdot \varepsilon_r}} \tag{3.69}$$

where k_σ is 250 for sequential loading and 400 for proportional loading, The softening coefficient for the compressive strain at peak compressive stress value was expressed as:

$$\zeta_{\varepsilon_o} = \frac{0.9}{\sqrt{1+k_\varepsilon \cdot \varepsilon_r}} \tag{3.70}$$

where k_ε is 0 for sequential loading and 500 for proportional loading, and ε_r is the tensile strain perpendicular to the compressive stress direction.

In this study, the so-called Model B by Vecchio and Collins (1993), which considers only a reduction in peak compressive stress, was implemented in the Fixed Strut Angle constitutive panel model proposed, since Vecchio and Collins (1993) observed that more complicated models (including also reduction in the strain at peak stress) are only marginally better for incorporating the compression softening effect, and also due to the simplicity of Model B for implementation into a cyclic panel model.

3.4. Tension Stiffening Effect on Concrete and Steel

The contribution of cracked concrete to the tensile resistance of RC members is known as the effect of tension stiffening. The concrete between the cracks, which is still bonded to the reinforcing steel bars, contributes to the tensile resistance of the member. The tension stiffening phenomenon plays a significant role in reducing the post-cracking deformations of reinforced concrete structures, and has been proven by researchers (e.g., Vecchio and Collins, 1988; Stevens , 1987; Collins and Mitchell, 1991;, Belarbi and Hsu, 1994; Pang and Hsu, 1995; Hsu and Zhang, 1996; Mansour et al., 2002; Hsu and Zhu, 2002) to influence considerably the post-cracking stiffness, yield capacity and shear behavior of reinforced concrete members.

.

In formulation of the constitutive panel model proposed, two alternative tension stiffening models available in the literature were incorporated. The first tension stiffening model used is the model by Belarbi and Hsu (1994). As investigated in detail by Belarbi

and Hsu (1994), modeling of the tension stiffening phenomenon must consider two effects simultaneously. First, an average (smeared) tensile stress-strain curve must be considered for cracked concrete; and second, the stress-strain curve of bare mild steel bars must be replaced by an average (smeared) stress-strain curve for steel bars stiffened by concrete between cracks.

In the Belarbi and Hsu model, the tensile stress-strain behavior of concrete is considered as linear up to cracking and, a descending curve is defined for the post-cracked stress-strain region, the equation of which is independent of reinforcement parameters. The average stress-strain relationship proposed by Belarbi and Hsu (1994) for concrete in tension takes the form:

$$\text{For } \varepsilon_c \le \varepsilon_{cr}, \qquad \sigma_c = E_c \varepsilon_c$$

$$\text{For } \varepsilon_c > \varepsilon_{cr}, \qquad \sigma_c = f_{cr}\left(\frac{\varepsilon_{cr}}{\varepsilon_c}\right)^{0.4}$$

where E_c is the initial Young's modulus of the average stress-strain relationship, f_{cr} is concrete tensile cracking stress, and ε_{cr} is the concrete strain at cracking.

Belarbi and Hsu (1994) also identified how the average stress-strain relationship of reinforcing steel bars surrounded by concrete is different than the stress-strain relationship of bare steel bars. The most important difference was found to be the lowering of the yield stress, as yielding of a reinforced concrete element occurs when the steel stress at the cracked section reaches the yield strength of the bare bar. At the same time, the average steel stress smeared along the length of the element reaches a level lower than that of the yield stress of the bare bar. Based on experimental data from the RC panels, the reduction of the yield stress of bars embedded in concrete were found to be empirically dependent on the cross-sectional area ratio of the longitudinal steel in the panel, the ratio of the elastic modulus of steel to the elastic modulus of concrete, and the ratio of concrete cracking

stress to the steel yield stress. The effective (reduced) yield stress for embedded reinforcing bars is expressed, in terms of the elastic modulus ratio n (E_s/E_c), the reinforcement ratio ρ, concrete cracking stress f_{cr}, and bare bar yield stress f_y, as:

$$f_{yeff} = f_y \cdot \left[1 - 1.314 \cdot \frac{n^{0.434}}{\rho^{1.084}} \cdot \left(\frac{f_{cr}}{f_y} \right)^{1.517} \right] \tag{3.71}$$

The second tension stiffening model incorporated in the present Fixed Strut Angle panel model is the model by Stevens (1987). In the Stevens model, average tensile stress–strain behavior of concrete is also considered as linear up to cracking, after which an exponential curve is defined. Parameters defining the post-crack stress-strain behavior include a so-called homogeneity ratio called (α), as well as the cracking stress (f_{cr}) and cracking strain (ε_{cr}) of concrete:

$$f_c = f_{cr} \cdot \left[(1-\alpha) \cdot e^{-\lambda_t \cdot (\varepsilon_c - \varepsilon_{cr})} + \alpha \right] \tag{3.72}$$

where,

$$\alpha = 75 \cdot \frac{\rho_s}{d_b} \quad , \quad \lambda_t = \frac{270}{\sqrt{\alpha}} \tag{3.73}$$

The effective yield stress of reinforcing steel bars is defined by Stevens (1987) to be dependent on bar diameter (d_b) and concrete cracking stress (f_{cr}) as:

$$f_{yeff} = f_y - \Delta f_{ycr} \tag{3.74}$$

where

$$\Delta f_{ycr} = \frac{75}{d_b} \cdot f_{cr} \tag{3.75}$$

Due to disparities in the formulation of the two tension stiffening models for concrete and reinforcing steel, graphical comparisons between the two is useful. When the average (smeared) tensile stress–strain behavior of cracked concrete is considered, as illustrated in

Figure 3.9, while the Belarbi and Hsu (1994), model yields lower tensile values for relatively lower values of tensile strain, it predicts higher tensile stresses for higher strains, compared with the model by Stevens (1987), independently of the reinforcement ratio used for the Stevens model.

When the effective (reduced) tensile yield stress of reinforcing bars embedded in concrete is considered, as illustrated in Figure 3.10, while the Belarbi and Hsu (1994) model predicts considerable amounts of reduction in the yield stress, especially for lower reinforcement ratios, compared with the model by Stevens (1987), the Stevens model predicts overall, a very a slight influence of tension stiffening on the yield stress of reinforcement.

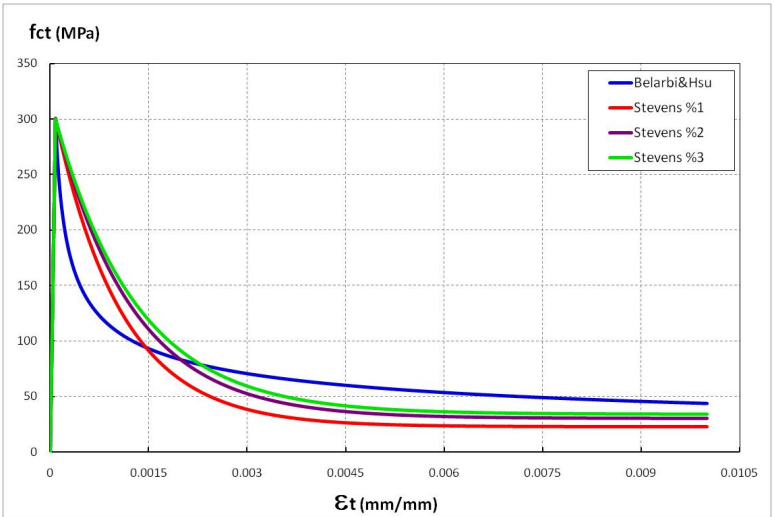

Figure 3.9. Comparison of tension stiffening models

3.5. Biaxial Damage on Concrete

An important consideration in modeling the behavior of a RC panel element under membrane actions is incorporating the cyclic damage effects on concrete subjected to biaxial loading. This cyclic damage on concrete is represented via a damage coefficient. Unlike compression softening and tension stiffening parameters, the damage coefficient is a cyclic-strain-history-dependent parameter, and is not considered in analysis of concrete under monotonic loading.

The damage coefficient is a parameter that considers the effect of the history of compressive strains, which are in perpendicular direction to a specific compressive stress direction considered (e.g., along a compression strut) for concrete. The damage coefficient is therefore defined for biaxial loading, and does not apply for uniaxial concrete stress-strain behavior. The damage coefficient, similar to the compression softening coefficient, is applied as a multiplier to the concrete compressive stress, softening the stress-strain behavior of concrete in compression.

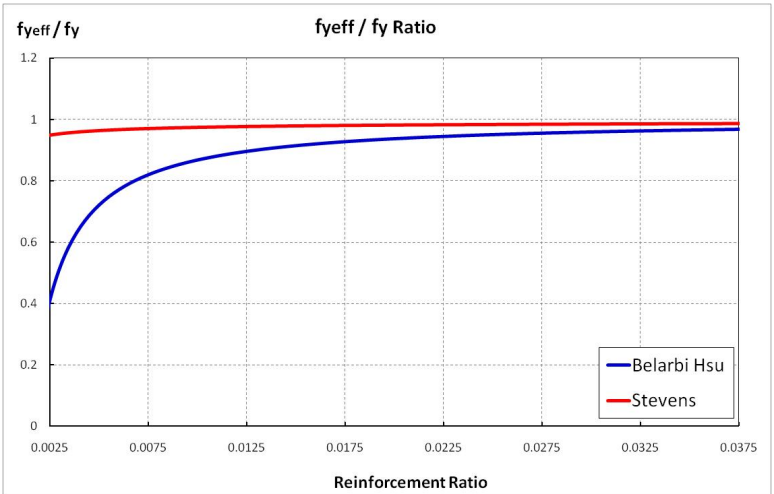

Figure 3.10. Comparison of tension stiffening effects

There are two empirical models available in literature for the damage coefficient; one by Stevens (1987), and the other by Mansour and Hsu (2002). The formulation proposed by Stevens uses the ratio of the difference between the maximum value of the compressive strain experienced ($\varepsilon_{\perp max}$) and the current compressive strain ($\varepsilon_{\perp}$) (if any) in the direction perpendicular to the compressive (strut) direction considered, to the peak compressive stress, ($\varepsilon_c^{'}$) in concrete, as:

$$\beta_{damage} = (1 + 0.5 \cdot x) \tag{3.76}$$

$$x = \frac{\varepsilon_{\perp max} - \varepsilon_{\perp}}{\varepsilon_c^{'}} \tag{3.77}$$

The final softening parameter used in this study considering both compression softening and biaxial damage parameters, based on the Stevens (1987) formulation for biaxial damage, takes the form:

$$\beta = \beta_m \cdot \frac{1}{\beta_{damage}} \tag{3.78}$$

On the other hand, the biaxial damage formulation proposed by Mansour and Hsu (2002) uses the ratio of the maximum value of the compressive strain experienced in the direction perpendicular to the compressive (strut) direction considered, to the peak compressive stress, $(\varepsilon_c^{'})$ in concrete, as:

$$\beta_{damage} = (1 - 0.4 \cdot \frac{\varepsilon_{\perp \max}}{\varepsilon_c^{'}}) \tag{3.79}$$

The final softening parameter used in this study considering both compression softening and biaxial damage parameters, based on the Mansour and Hsu (2002) formulation for biaxial damage, takes the form:

$$\beta = \beta_m \cdot \beta_{damage} \tag{3.80}$$

It should be mentioned that the two biaxial damage formulations have yielded very similar results for the panels investigated within the scope of this analytical study.

The constitutive material models described in this chapter, as well as the formulation of the Fixed Strut Angle constitutive panel model and the nonlinear analysis solution strategy (both described in Chapter 2), were implemented in Matlab ("Matlab") for conducting nonlinear quasi-static analyses of RC panel specimens using the constitutive panel model formulation proposed. Calibration of the proposed model and comparison of model results with results of cyclic tests performed on RC panel specimens is presented in Chapter 4.

4. COMPARISON OF MODEL RESULTS WITH EXPERIMENTAL DATA

This Chapter presents information on experimental calibration of the Fixed Strut Angle panel model, and detailed comparisons of the model results with cyclic test results from the literature on six RC panel specimens, at both global and local response levels.

Results of parametric sensitivity studies performed to identify the sensitivity of the model results to variation and uncertainties in material parameters are also provided.

As well, detailed discussions of the analytical results are presented to evaluate the effectiveness and shortcomings of the proposed model, in simulating the cyclic response of RC panels.

4.1. Cyclic Panel Tests in the Literature

As outlined in Chapter 1, very few cyclic panel tests are available in literature. Three set of cyclic panel tests were identified (Stevens, 1987, Mansour, 2001, Ohmori et al., 1989), and two of these three test programs are considered within the scope of this analytical study. Because of the lack of information about the tests performed by Ohmori et al., those tests couldn't be modeled in the scope of this study. The first of these two test programs was conducted by Stevens using the "Shell Element Tester" facility at the University of Toronto in the mid-1980's and the other by Mansour and Hsu in early 2000 using the "Universal Element Tester" facility at the University of Houston. Further details on these test programs are presented in the next two sections.

4.1.1. Tests by Stevens (1987)

These were one of the first reversed cyclic panel tests, with 3 membrane elements tested using the "Shell Element Tester" (Figure 4.2) at the University of Toronto. All of these tests were conducted under stress control, and the test panels were square, with

1625x1625 mm dimensions and 285 mm thickness. The testing equipment was configured for loading principal (normal) stresses on the specimens. All panel reinforcement was arranged orthogonally in x and y directions, and this was referred to as "45° reinforcement" by other researchers (Mansour and Hsu 2005) (Figure 4.1).

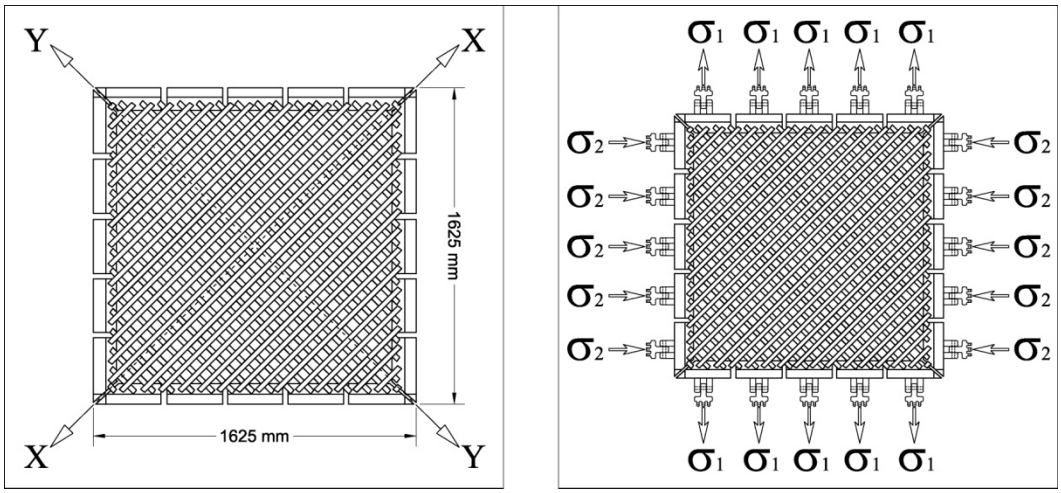

Figure 4.1. Panel and loading geometry for Stevens (1987) specimens



Figure 4.2. Shell Element Tester (University of Toronto)

Properties of the panel specimens tested in the scope of this experimental program are listed in table 4.1. In this test program, there were two different parameters investigated; the loading type and reinforcement ratio. While specimens SE8 and SE10 were used to examine the effect of loading type on panel response, specimens SE8 and SE9 were used to investigate the effect of reinforcement ratio.

Table 4.1. Test parameters of Stevens

Specimen :	SE8	SE9	SE10
Loading Type :	$\sigma_x = 0$ $\sigma_y = 0$ $\tau_{xy} = Reversed\ Cyclic$	$\sigma_x = 0$ $\sigma_y = 0$ $\tau_{xy} = Reversed\ Cyclic$	$\sigma_x = -\left\lvert \tau_{xy} / 3 \right\rvert$ $\sigma_y = -\left\lvert \tau_{xy} / 3 \right\rvert$ $\tau_{xy} = Reversed\ Cyclic$
ρ_x :	$\rho_x = 0.03$	$\rho_x = 0.03$	$\rho_x = 0.03$
ρ_y :	$\rho_y = 0.01$	$\rho_y = 0.03$	$\rho_y = 0.01$
σ_x :	$\sigma_{yx} = 492\,MPa$	$\sigma_{yx} = 422\,MPa$	$\sigma_{yx} = 422\,MPa$
σ_y :	$\sigma_{yy} = 479\,MPa$	$\sigma_{yy} = 422\,MPa$	$\sigma_{yy} = 479\,MPa$
f'_c :	$37\,MPa$	$44.2\,MPa$	$34\,MPa$
ε_{co} :	0.0026	0.0026	0.0023
f'_{ct} :	$2\,MPa$	$2.2\,MPa$	$2\,MPa$
ε_{ct} :	0.0001	0.0001	0.00013

4.1.2. Tests by Mansour and Hsu (2005)

Mansour and Hsu (2005) also performed reversed cyclic panel tests at the University of Houston. There are two important characteristics of this research program. First, these tests (12 full-size reversed cyclic panel tests) were performed under strain control, which revealed the sudden stiffness drop as an effect of first cracking on panel response. Second, the test program was aimed to investigate the effect of reinforcement orientation to the overall behavior.

Although the orientation of reinforcement was a test variable in this experimental program, only 3 panels (the CA series), among the total of 12, having orthogonal reinforcement in X and Y directions (45° reinforcement) were considered within the scope of this analytical study. All three of these panel specimens had 1397x1397 mm dimensions

and 178 mm thickness. The testing equipment called the "Universal Element Tester" (Figure 4.4) was configured for application of principal (normal) strains to the test specimens.

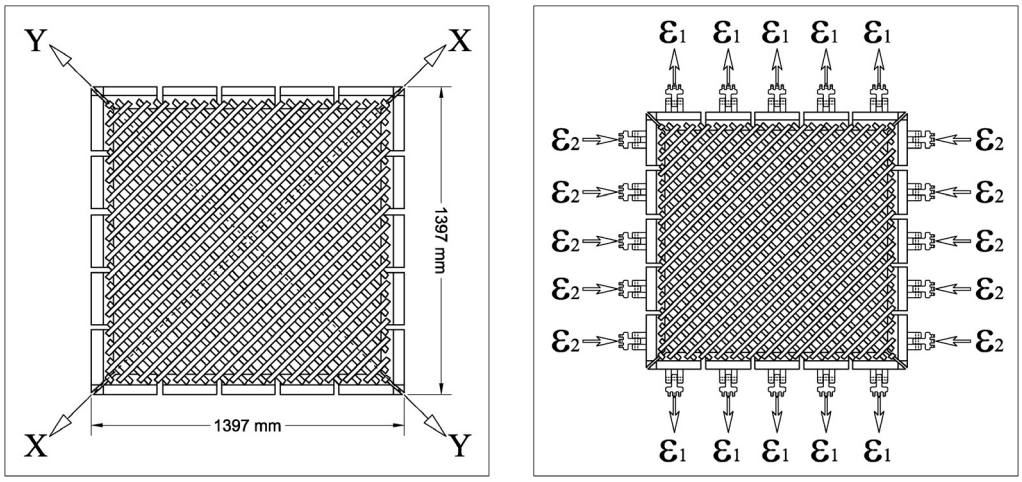

Figure 4.3. Configuration of panel tests by Mansour and Hsu (2005)

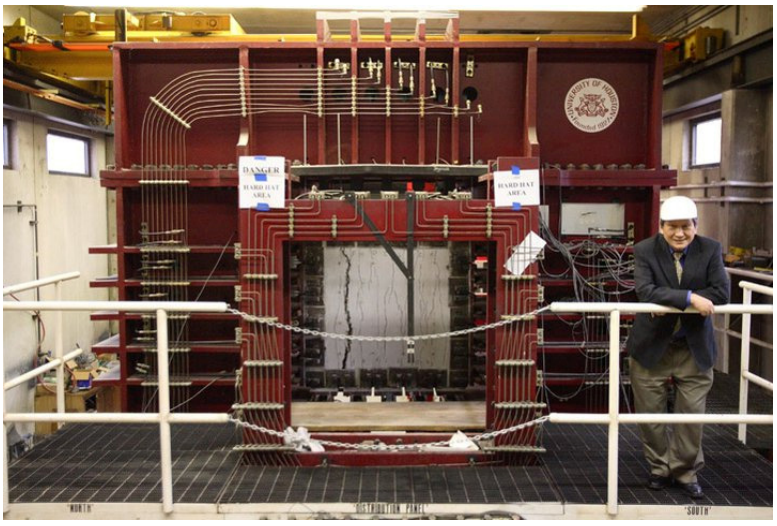

Figure 4.4. Universal Element Tester (University of Houston)

Properties of the three 45° panel specimens investigated are presented in Table 4.2. The only variable among these three specimens is the reinforcement ratio.

4.2. Comparisons of Model Results with Test Results of Stevens

In this section, global and local response comparisons between the test results for the SE-series specimens and the Fixed Strut Angle Model results are presented. All test results plotted in this section are graphically-digitized plots of the original microfilmed plots available in Stevens (1987).

Table 4.2. Test parameters of Mansour and Hsu

Specimen :	CA2	CA3	CA4
Loading Type :	$\sigma_x = 0$ $\sigma_y = 0$ $\tau_{xy} = Reversed\ Cyclic$	$\sigma_x = 0$ $\sigma_y = 0$ $\tau_{xy} = Reversed\ Cyclic$	$\sigma_x = 0$ $\sigma_y = 0$ $\tau_{xy} = Reversed\ Cyclic$
ρ_x :	$\rho_x = 0.0077$	$\rho_x = 0.017$	$\rho_x = 0.027$
ρ_y :	$\rho_y = 0.0077$	$\rho_y = 0.017$	$\rho_y = 0.027$
σ_x :	$\sigma_{yx} = 424\,MPa$	$\sigma_{yx} = 425\,MPa$	$\sigma_{yx} = 453.4\,MPa$
σ_y :	$\sigma_{yy} = 424\,MPa$	$\sigma_{yy} = 425\,MPa$	$\sigma_{yy} = 453.4\,MPa$
f'_c :	$45MPa$	$44.5MPa$	$45MPa$
ε_{co} :	0.0025	0.0024	0.0028
f'_{ct} :	$2.2\,MPa$	$2.2\,MPa$	$2.2\,MPa$
ε_{ct} :	0.00008	0.00008	0.00008

4.2.1. Global Comparisons

In this section, the overall shear stress τ_{xy} versus shear strain γ_{xy} behavior of the test specimens are compared with the analytical model results, and discussion of the results is presented.

4.2.1.1. Specimen SE8: When the overall shear stress versus shear strain behavior of the specimen is concerned, it is seen that the behavior is captured reasonably well by the model (Figure 4.5). Although the overall capacity is underestimated at approximately 87% of test result, that the geometry of the loading and unloading curves, cracking stresses, and stiffness characteristics are well-predicted. In addition, the pinching effect, which is known as a characteristic feature of shear behavior, is also predicted accurately. Since the SE8 specimen has 1% reinforcement ratio in the y direction and 3% in the x direction, while the

reinforcement in y direction has yielded, the reinforcement in x direction remained linear elastic. Yielding of reinforcement in y direction not only limited the capacity, but also generated a ductile behavior for the specimen.

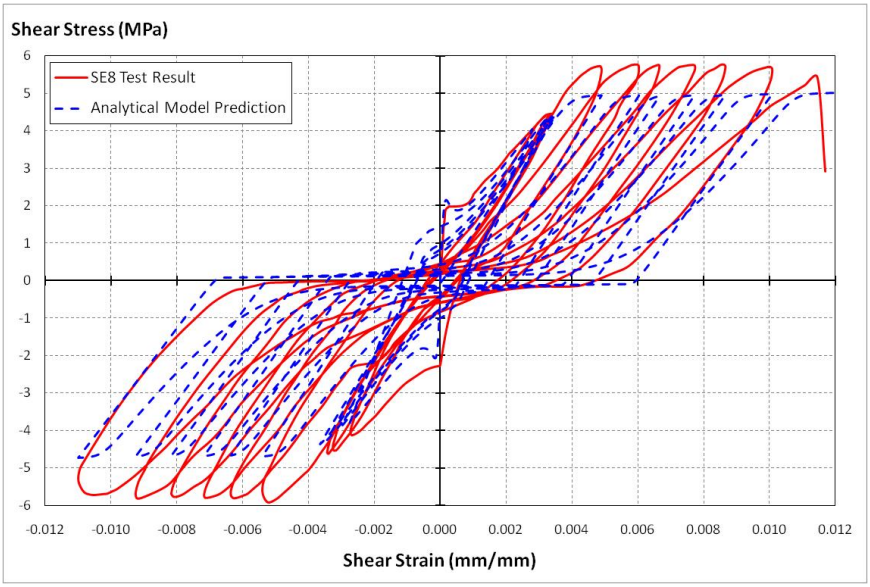

Figure 4.5. Specimen SE8, shear stress vs. shear strain comparison

4.2.1.2. Specimen SE9: General behavior of specimen SE9 is captured by the proposed model with reasonable accuracy (Figure 4.6). Although it appears that the capacity is overestimated by the model, it is believed that there is an imperfection in the test results, related to the yield strength of the steel used. According to coupon tests performed by the researchers, the yield strength of the steel is 422 MPa. On the other hand, the test results show that the reinforcement yields at approximately 325 MPa during the test. While the model results fits much more closely with the test results when 325 MPa yield strength is used, for the comparison presented, reported coupon test results were used for calibration of the model.

Although the shear stress capacity appears overestimated by the model due to the reason explained above, pinching characteristics, cracking stresses, and stiffness properties are all well-predicted (Figure 4.6). However, for this specimen, the width of the loading and unloading curves was predicted to be less than the test results. The main reason of this discrepancy may be attributed with variation in the cyclic behavior of concrete, which is predicted to govern the overall response of this specimen. Since the specimen has 3%

reinforcement in both directions, in the model of this specimen, the concrete compression struts are able to reach their maximum "softened and damaged" compressive stress capacity, prior to yielding of steel. However, since the tests were stress-controlled, none of these tests were continued until the failure mode of the specimens was clearly indentified.

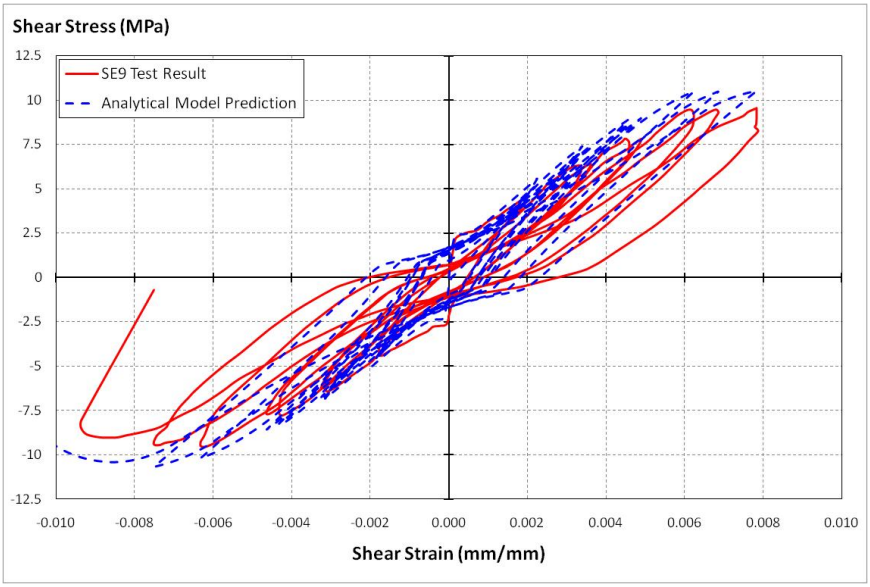

Figure 4.6. SpecimenSE9, shear stress vs. shear strain comparison

4.2.1.3. Specimen SE10: Specimen SE10 was the one of the most important specimens of this study, with its unequal reinforcement ratio in x and y directions, and with applied σ_x and σ_y compressive stresses which are both proportional to applied shear stress. Specimen SE10 is a replication of specimen SE8, with 1% reinforcement ratio in y direction and 3% reinforcement in x direction, the only difference being the σ_x and σ_y compressive stresses applied. The shear stress capacity of this specimen is predicted at 89% of the test result (Figure 4.7). Except this reasonable error in capacity prediction, other features including cracking stress, stiffnesses of the loading and unloading curves, and pinching are all predicted accurately as seen in Figure 4.7.

4.2.2. Local Response Comparisons

In this section, local response features including normal strain in x direction ε_x, normal strain in y direction ε_y, principal strain direction θ_p and concrete principal stress

direction θ_{cr} measured for all specimens are compared with analytical model results, and discussion of the results is presented.

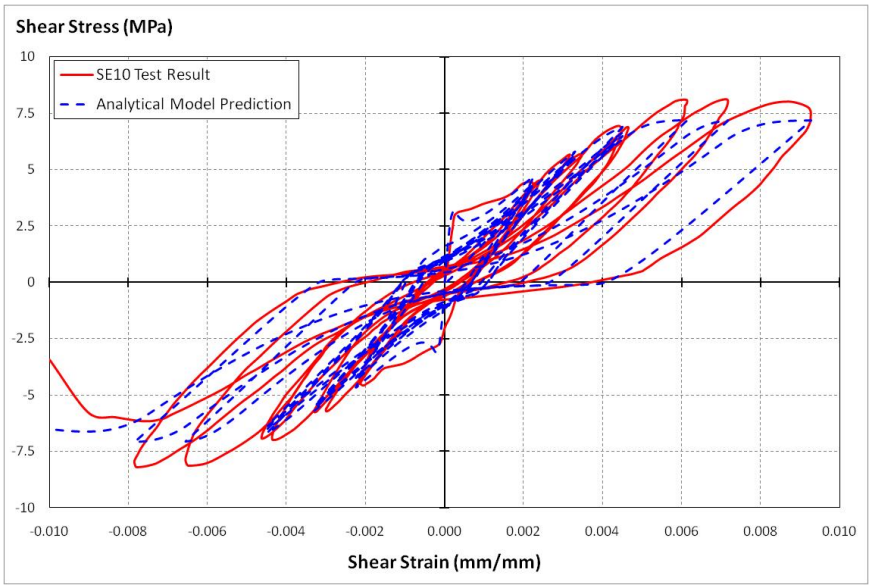

Figure 4.7. Specimen SE10, shear stress vs. shear strain comparison

4.2.2.1. Specimen SE8: When the normal strains in x direction are considered, a sudden increase at approximately the 900th step is identified in the test results (Figure 4.8). This increase believed to correspond to the first yield of reinforcement in y direction. In the model, the reinforcement in x direction remained linear elastic. Except this inconsistency, the general strain history in the x direction is predicted reasonably well (Figure 4.8).

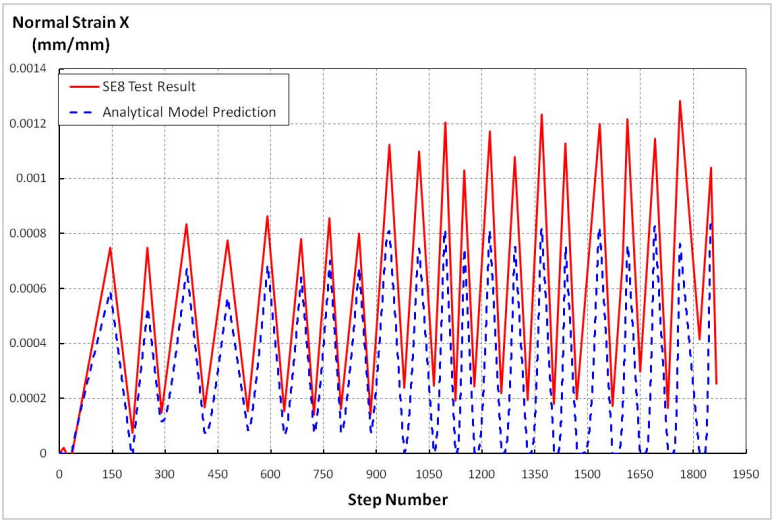

Figure 4.8. Specimen SE8, comparison of normal strains in x direction

When the normal strains in the y direction are observed, it is seen that the strain history is captured accurately; with an ascending trend starting around 900th step which is again corresponds to yielding of reinforcement in the y direction (Figure 4.9).

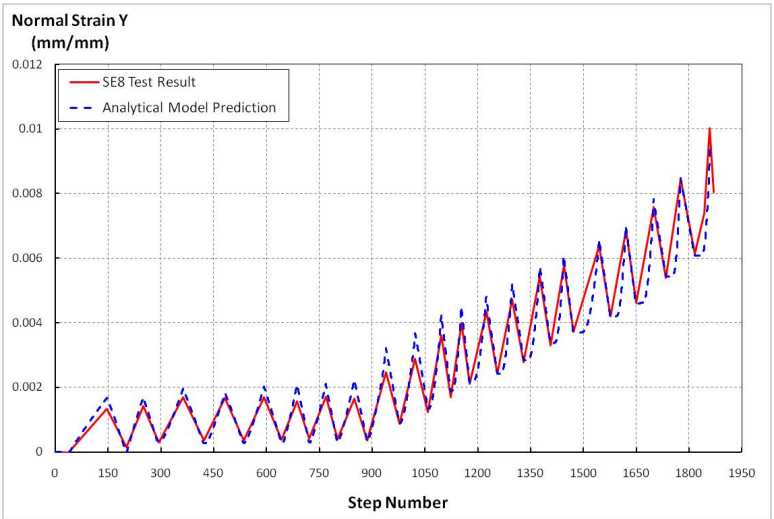

Figure 4.9. Specimen SE8, comparison of normal strains in y direction

When the principal strain directions are compared for specimen SE8, as illustrated in Figure 4.10, the principal strain direction history is predicted reasonably well. Only a slight underestimation at the beginning of the analysis (for small shear strain values) was observed.

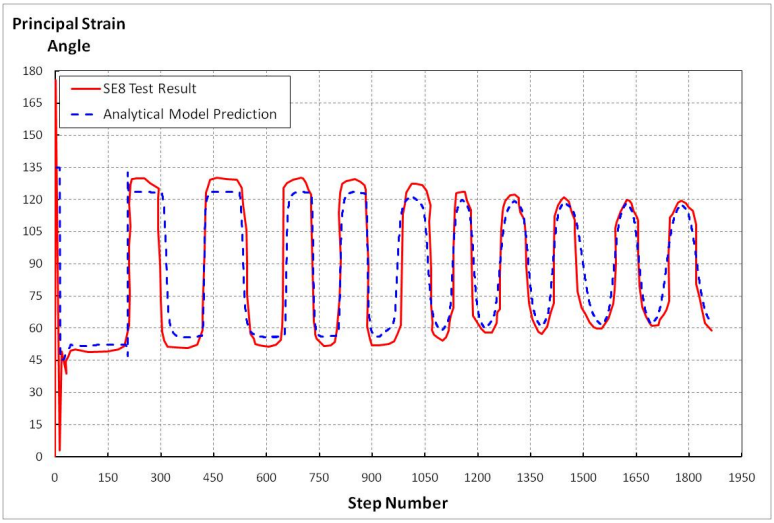

Figure 4.10. Specimen SE8, comparison of principal strain directions

When the normal strains in y direction versus shear stress relationships are compared, it is observed that the model results are in good agreement with the test results (Figure 4.11).

When the principal strain direction versus shear strain behaviors are compared, it is seen that with very few exceptions, the cyclic analytical model response is in good agreement with the envelope of the test measurements (Figure 4.12). The test result given in the figure is the envelope of the test measurements for specimen, SE8, as the original cyclic plot (Stevens, 1987) was too congested for digitizing purposes.

When the principal stress direction in concrete versus shear stress behaviors are compared, since the proposed model uses fixed principal stress directions (parallel to cracks) approach, the model prediction for principal stress angle in concrete does not deviate from the two crack directions. There exists variation in the test measurements, probably due to aggregate interlock action along cracks, although these deviations are typically associated with unloading and reloading branches, and the upper bound for principal stress angles do not vary significantly with the magnitude of the shear stress (Figure 4.13). Given that the fixed principal stress direction approach in the model greatly simplifies its formulation and allows cyclic analysis, this approach seems feasible in terms of a balance between accuracy and simplicity. It must be mentioned that the test result given in the figure is the envelope of the test measurements for the specimen, as the original cyclic plot (Stevens, 1987) was too congested for digitizing purposes.

4.2.2.2. Specimen SE9: When the normal strains in the x direction are compared for specimen SE9, although the general ascending trend is captured, moderate discrepancies exist between the test results and model predictions (Figure 4.14).

When the normal strains in y direction are compared, the general ascending trend is captured again, with increasing discrepancies at later stages of loading (Figure 4.15). At this point, it should be clarified that the normal strains predicted by the model in x and y directions are almost identical.

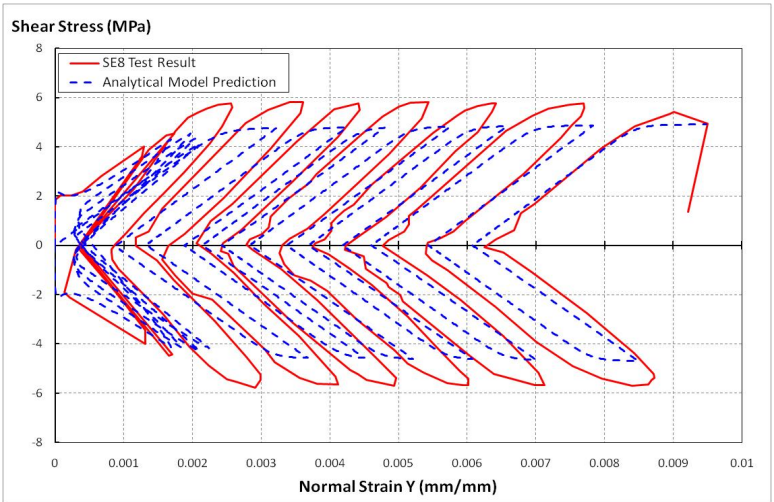

Figure 4.11. Specimen SE8, comparison of shear stress vs. normal strains in y direction

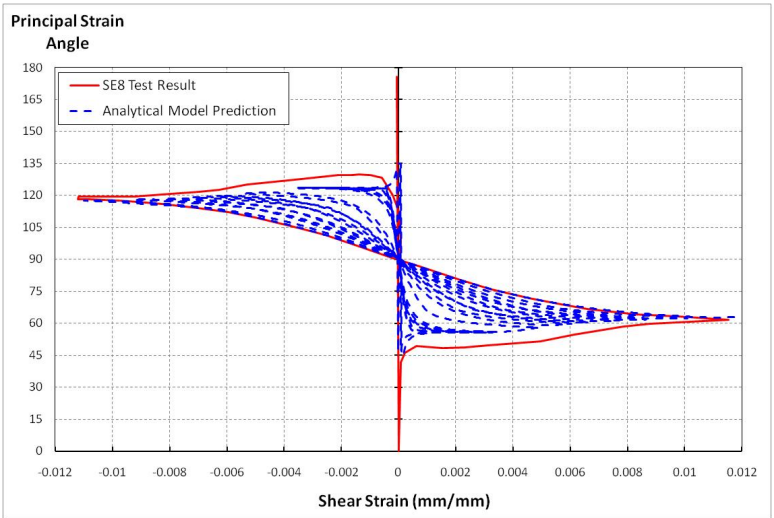

Figure 4.12. Specimen SE8, comparison of principal strain direction vs. shear strain

Considering that the specimen had equal reinforcement ratios in both directions and pure shear loading is applied, the model predictions are mechanically consistent. Therefore, differences between normal strains measured in the x and y directions during the test may be attributed to imperfections in the test conditions.

When the principal strain directions are compared the SE specimen, as depicted in Figure 4.16, the test results are well-predicted by the model.

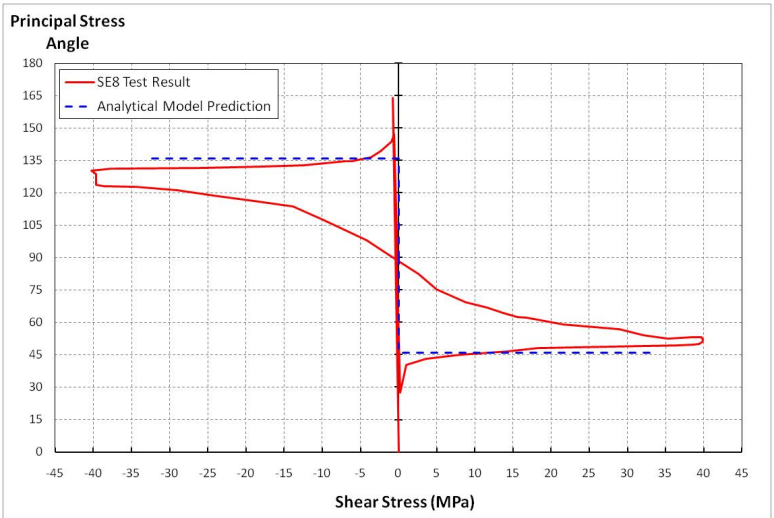

Figure 4.13. Specimen SE8, comparison of principal stress direction in concrete vs. shear stress

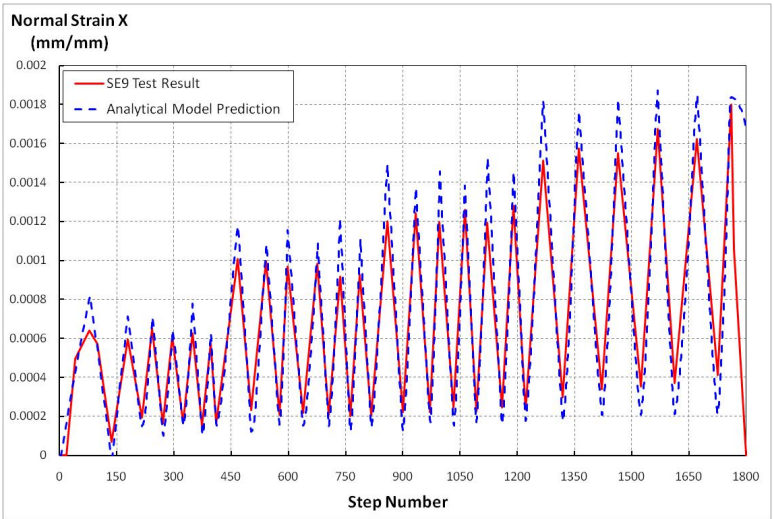

Figure 4.14. Specimen SE9, comparison of normal strains in x direction

When the shear stress versus normal strain in y direction behaviors are compared (Figure 4.17), the level of underestimation for strains in y direction (previously shown in Fig. 4.15) can be observed more clearly.

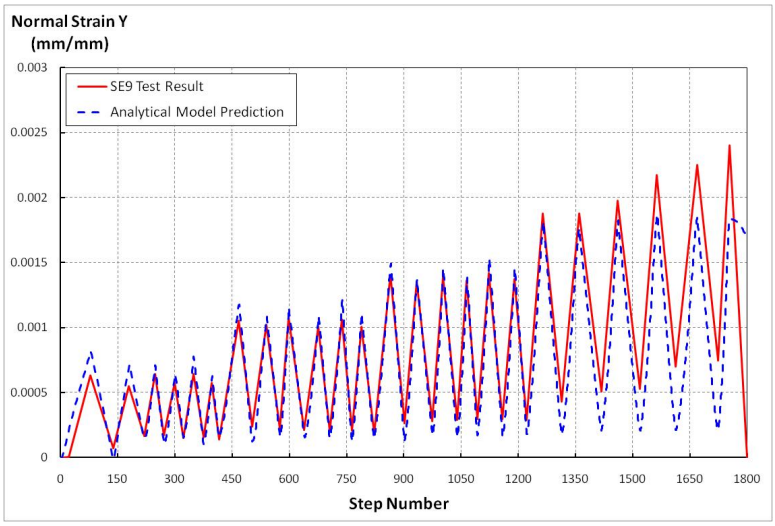

Figure 4.15. Specimen SE9, comparison of normal strains in y direction

For Specimen SE9, since the reinforcement ratio is equal for both directions and pure shear stress is applied to the specimen, the principal strain direction predicted by the model does not deviate significantly with shear strain, as the pure shear stress state imposed on the model results in approximately a pure shear strain state, if the reinforcement ratios and material properties of reinforcing steel are the same in x and y directions. In the analysis, except for the transition zones, the principal strain angle is therefore fixed at approximately 45° or 135°, and does not deviate.

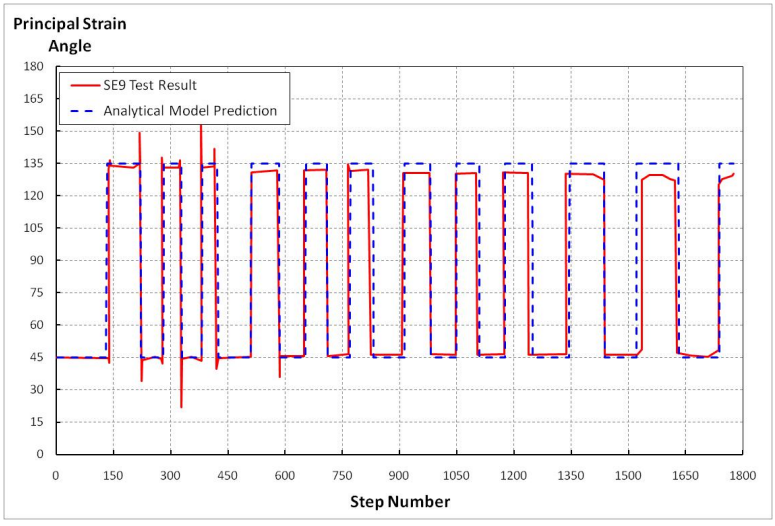

Figure 4.16. Specimen SE9, comparison of principal strain directions

When the model results are compared with the test result, this can be observed to be a reasonable representation of the behavior (Figure 4.18), since the principal strain directions measured in the test also do not deviate significantly, except in transition regions from one loading direction to the other. Again, the test result given in the figure is the envelope of the test measurements for the specimen.

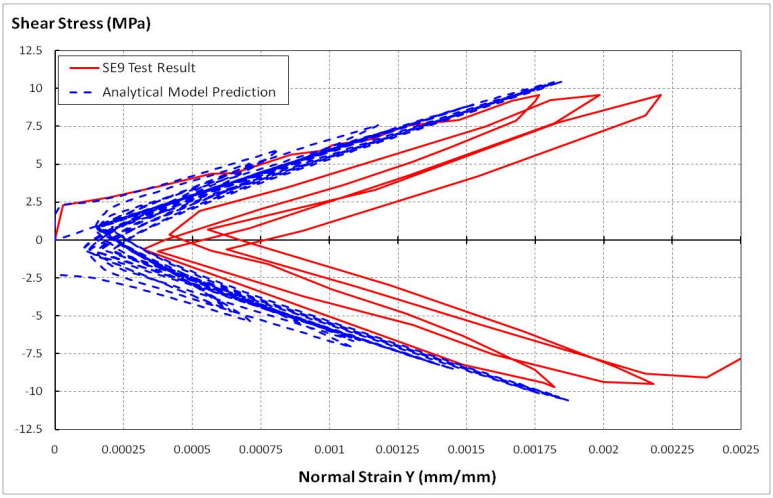

Figure 4.17. Specimen SE9, comparison of shear stress vs. normal strains in y direction

Since the symmetrically reinforced specimen was subjected to pure shear stresses, the principal stress directions in concrete predicted by the model are naturally 45° and 135° during the entire loading history. This prediction is in agreement with the test results, as shown in Figure 4.19. The fixed principle stress direction assumption of the model again seems appropriate.

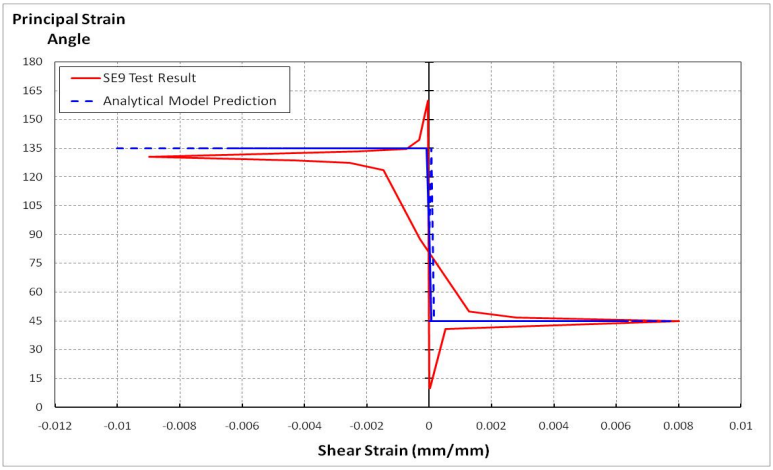

Figure 4.18. Specimen SE9, comparison of principal strain direction vs. shear strain

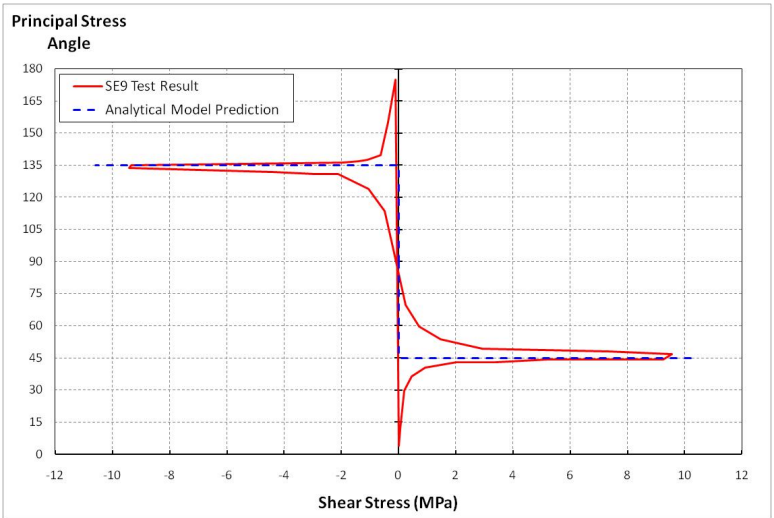

Figure 4.19. Specimen SE9, comparison of principal stress direction in concrete vs. shear stress

4.2.2.3. Specimen SE10: For specimen SE10, when the normal strains in x direction are compared, an under prediction, at approximately 80% of the measured peak strains, is observed. However, the general response is well-captured (Figure 4.20).

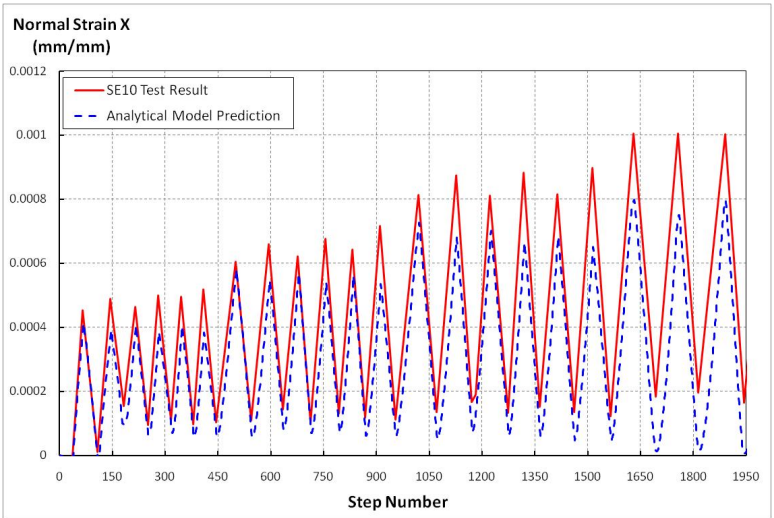

Figure 4.20. Specimen SE10, comparison of normal strains in x direction

When the normal strains in y direction are compared, the model now yields an over prediction of the measured values, although the general trend remains to be captured well (Figure 4.21).

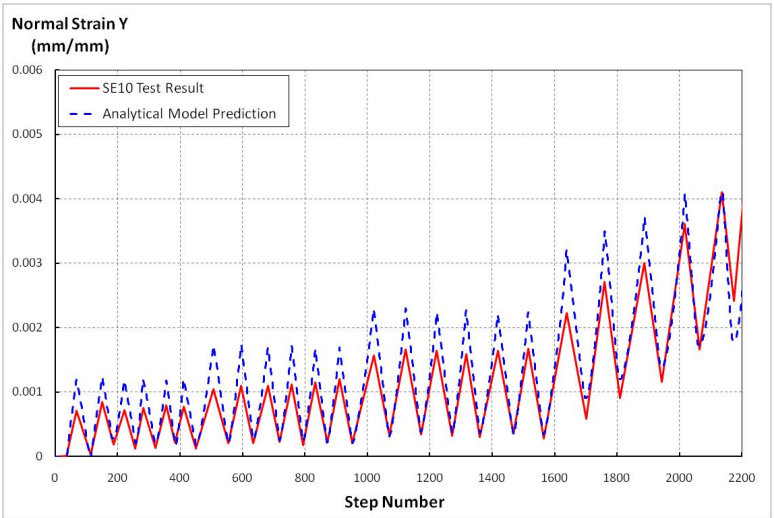

Figure 4.21. Specimen SE10, comparison of normal strains in y direction

When the principal strain directions are compared, as shown in Figure 4.22, the experimental measurements are predicted with reasonable accuracy overall, with moderate underestimation of the measured principal strain angles.

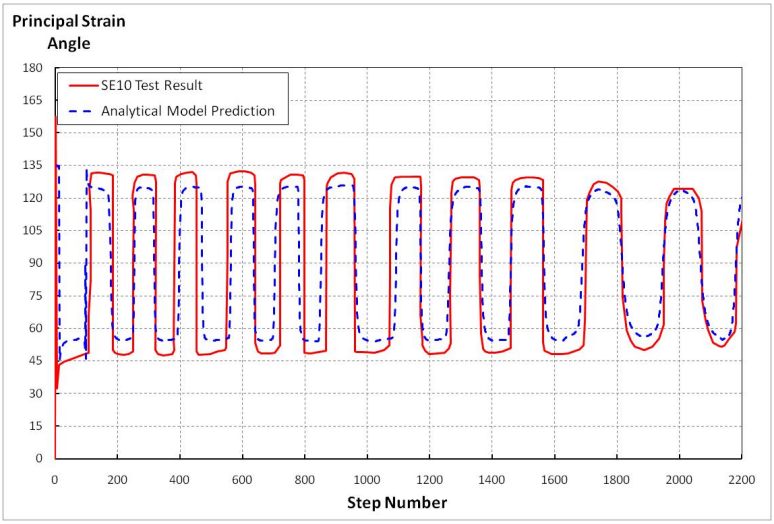

Figure 4.22. Specimen SE10, comparison of principal strain directions

When the normal strains in y direction vs. shear stresses responses are compared, it the slight underestimation in the shear stresses and the slight overestimation in normal strains in y direction can be identified more clearly (Figure 4.23). However, the overall response is well-predicted.

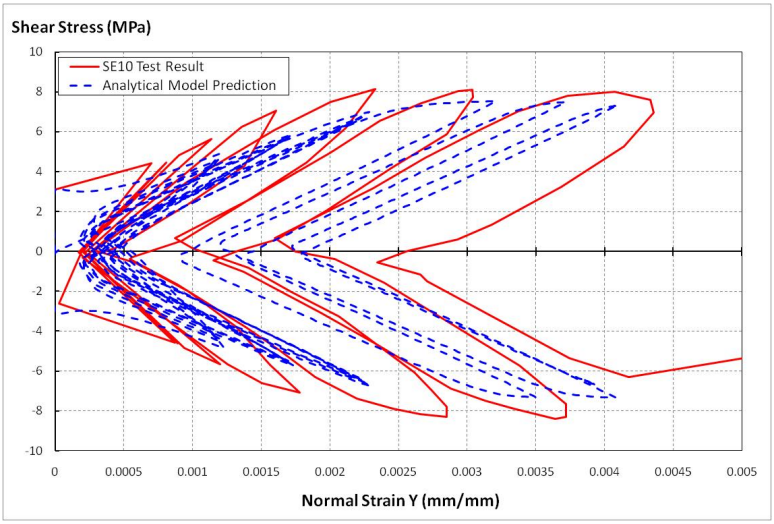

Figure 4.23. Specimen SE10, comparison of shear stress vs. normal strains in y direction

When the principal strain direction versus shear strain behaviors are compared, it can be seen that, the cyclic response prediction of the model is close to the envelope of the test results (Figure 4.24). As for the previous specimens, the test result given in the figure is the envelope of the cyclic test measurements.

As well, as observed for the other specimens the fixed principal concrete stress directions, predicted by the model is overall in good agreement with the envelope of the test measurements, as shown in Figure 4.25, validating the fixed strut angle modeling approach used.

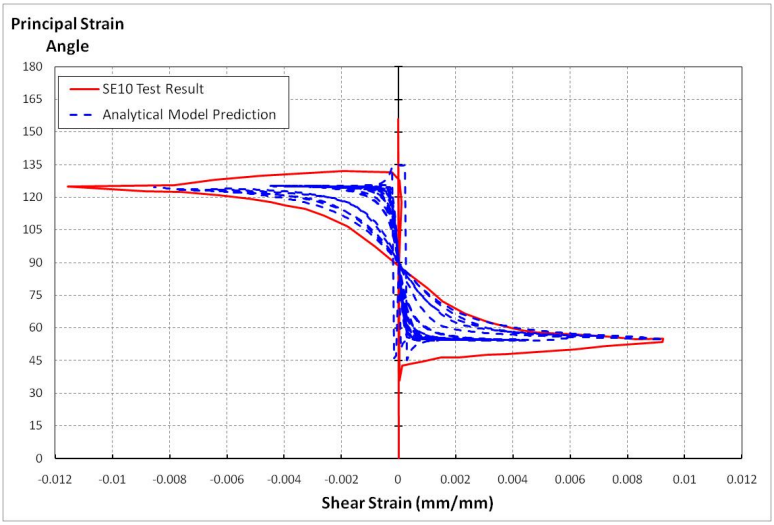

Figure 4.24. Specimen SE10, comparison of principal strain direction vs. shear strain

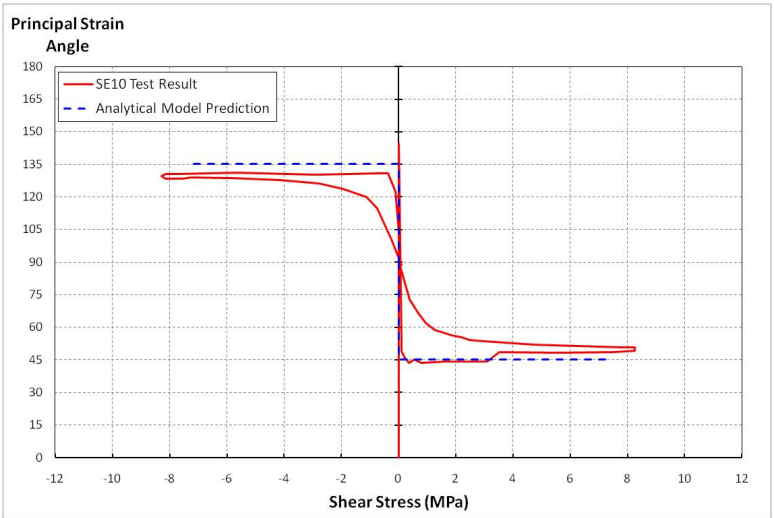

Figure 4.25. Specimen SE10, comparison of principal stress direction in concrete vs. shear stress

4.3. Comparisons of Model Results with Test Results of Mansour and Hsu (2005)

In this section, results of three panel tests conducted by Mansour and Hsu (2005) at the University of Houston are compared with predictions of the Fixed Strut Angle model proposed. The experimental data used for the comparisons are of two types; the global shear stress versus shear strain data are digitized plots from Mansour and Hsu (2005), and the data used for local response comparisons were provided by the Muhammad Mansour (personal communication).

Material properties used for the calibration of the model were reported values in Mansour and Hsu (2005). These properties are tabulated in Table 4.2.

For calibration of the model for these test specimens, it must be mentioned that the test results for the stress-strain curves of concrete and reinforcing steel bars were not reported by Mansour and Hsu, as was the case for Stevens (1987). Therefore, only peak stress and strain and peak stress values for concrete were used for calibration of the material parameters of the concrete model. Parameters associated with the shape of the concrete stress-strain curve were calibrated based on the concrete constitutive model Saatçioğlu and Razvi (1992). The stress-strain curve for concrete in tension was calibrated based on the tension stiffening model of Belarbi and Hsu (1995). For the effective yield

strength of reinforcing steel bars embedded in concrete, the bare bar yield strength value reported in Table 4.2 was also reduced according to the tension stiffening model of Belarbi and Hsu (1995).

Since the analyses are conducted using a single constitutive panel element, the model results are sensitive to the shape of the stress-strain relationships adopted for concrete and reinforcing steel, which may introduce sources of uncertainty in this case. Detailed sensitivity studies on the model response are presented in Section 4.5.

4.3.1. Global Comparisons

In this section, the measured overall shear stress τ_{xy} vs. shear strain γ_{xy} behavior of the specimens tested by Mansour and Hsu (2005) are compared with analytical results obtained using the Fixed Strut Angle model, and the results are discussed.

4.3.1.1. Specimen CA2: Specimen CA2 has the smallest reinforcement ratio in both directions, with a value of 0.77%. When the test results are compared with model predictions, the model seems to underestimate the shear stress capacity of the specimen, at approximately 82% of the measured value. Other features of the response including the shapes of the unloading and reloading curves, stiffnesses characteristics, cracking stress values and pinching behavior (to some extent) are captured with reasonable accuracy (Figure 4.26). It should be mentioned that since the specimen has relatively low amount of reinforcement in both directions, the behavior dominated by the nonlinear behavior of the reinforcing steel. As later explained in the section on sensitivity studies, such behavior of lightly reinforced specimens are highly influenced by reinforcement yield strength. Therefore, the shear stress capacity prediction for this specimen is influenced by the calibrated effective yield strength value used for the reinforcing steel bars, which may involve uncertainties.

4.3.1.2. Specimen CA3: Specimen CA3 has a reinforcement ratio of 1.77% in both directions. The analytical model predicts the overall shear stress versus shear strain behavior of this specimen with high accuracy, with all its stiffness, pinching and cracking stress attributes (Figure 4.27).

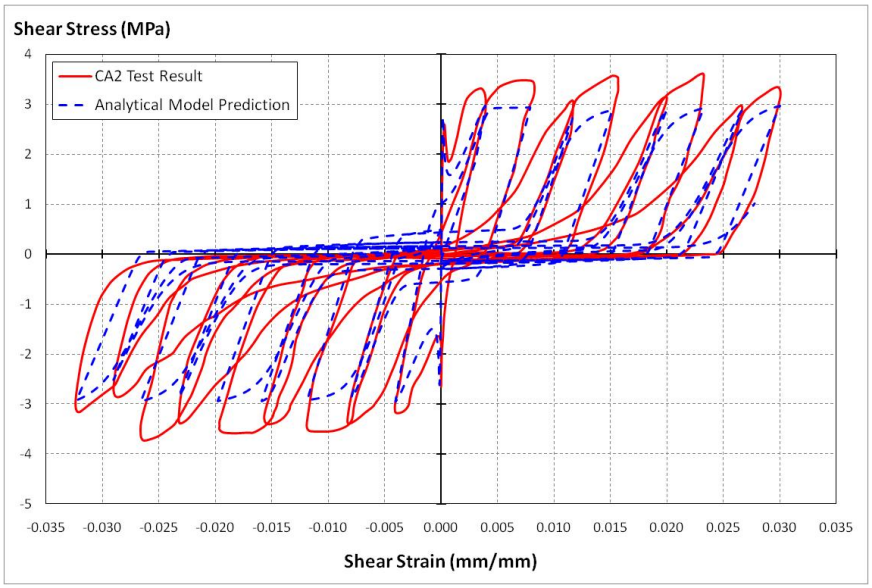

Figure 4.26. Specimen CA2, shear stress vs. shear strain comparison

The only difference is associated with the shape of the envelope of the response, which was found to be influenced both by the shape of the concrete stress–strain behavior in compression and the effective yield strength of reinforcing steel.

4.3.1.3. Specimen CA4: Specimen CA4 had the largest reinforcement ratio, with the value of 2.77% percent in both directions. The model predicts the overall shear stress versus shear strain behavior of this specimen reasonably well, with slight discrepancies in cyclic stiffness characteristics. Features including the pinching effect, cracking stress, and shear stress capacity are all captured accurately (Figure 4.28).

4.3.2. Local Response Comparisons

Since the reinforcement ratios are same in both directions for the CA-series specimens, it is expected that the normal strains in x and y directions should be almost the same, when the specimens are subjected a state of pure shear stress. However, although the model results consistently follow this type of behavior, test results for all specimens yield different values for normal strain histories in x and y directions, presumably due to imperfections in the test setup. Detailed comparisons are provided in this section separately for the three specimens.

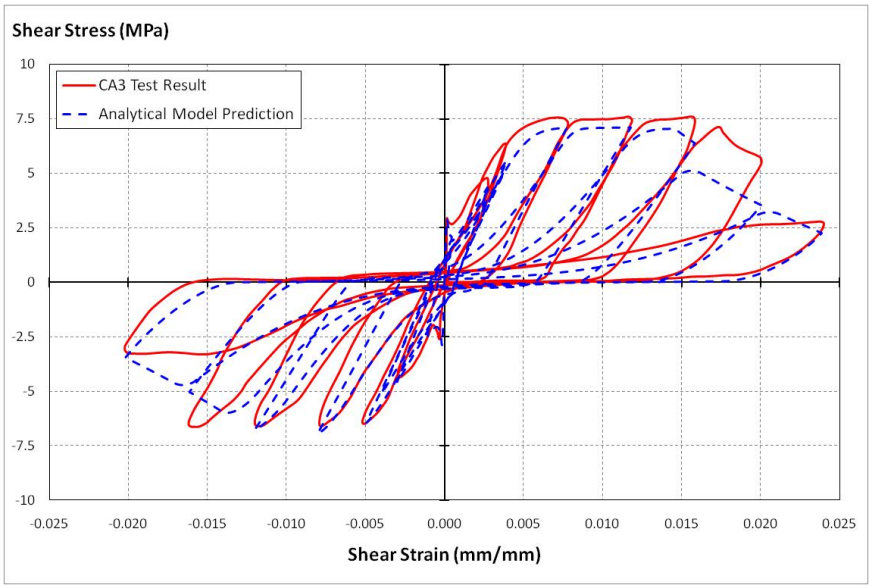

Figure 4.27. Specimen CA3, shear stress vs. shear strain comparison

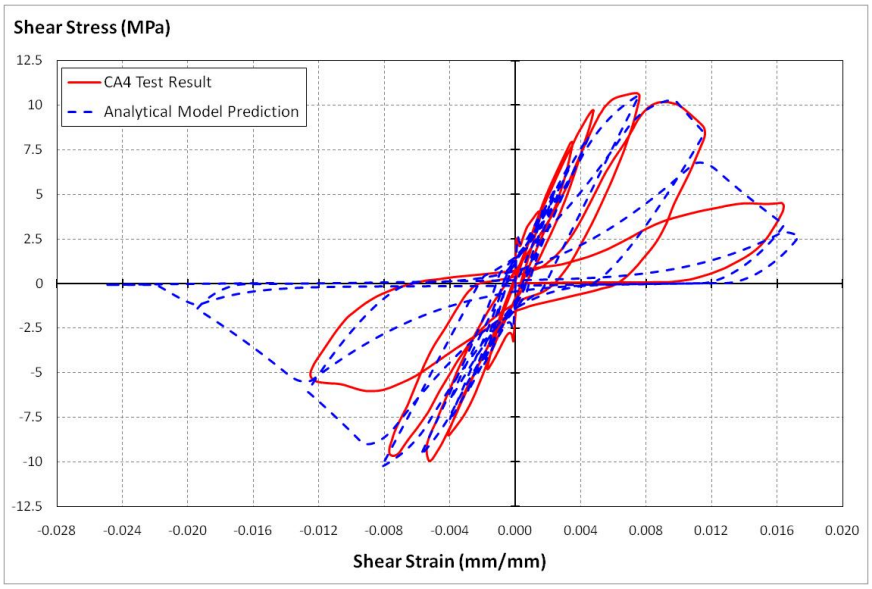

Figure 4.28. Specimen CA4, shear stress vs. shear strain comparison

4.3.2.1. Specimen CA2: As described in the previous subsection, shear stress values predicted by the model underestimate the test results at approximately 82%. On the other hand, when the normal strains in x direction are compared, the strains are well predicted by the model during initial phases of loading, although under predicted during later stages (Figure 4.29). The residual (plastic) normal strain value at the end of the test is underestimated at approximately 80% of the test result.

When normal strains in y direction are compared, a similar correlation between the test results and the model predictions is observed. Strains which are initially well-predicted by the model do not increase with the same rate of that of the test results (Figure 4.30). The residual (plastic) normal strain value predicted by the model is at approximately 80% of the test result.

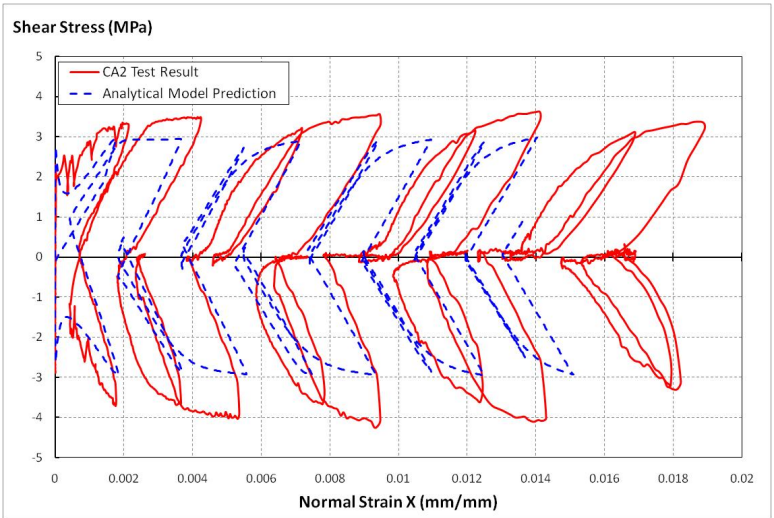

Figure 4.29. Specimen CA2, comparison of shear stresses vs. normal strains in x direction

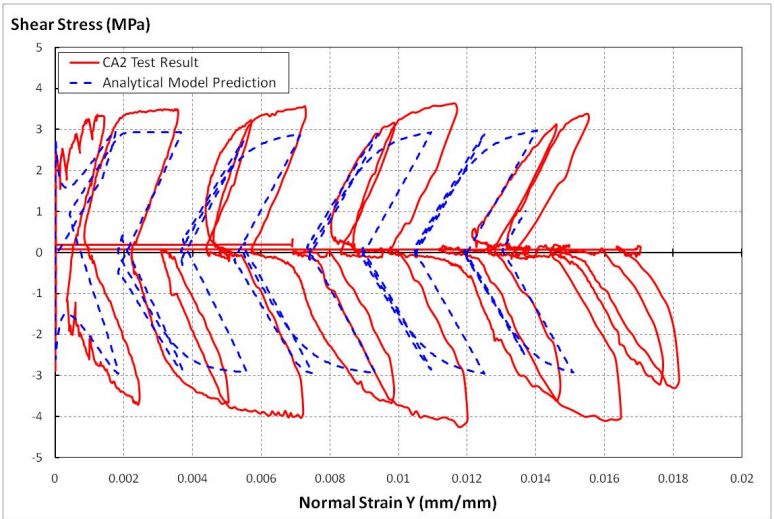

Figure 4.30. Specimen CA2, comparison of shear stresses vs. normal strains in y direction

4.3.2.2. Specimen CA3: Although shear stress versus shear strain behavior is well-predicted by the model for Specimen CA3, the model largely underestimates the normal

strains in x and y directions. The residual (plastic) strains predicted by model are at approximately 40% of the test results (Figures 4.31 and 4.32).

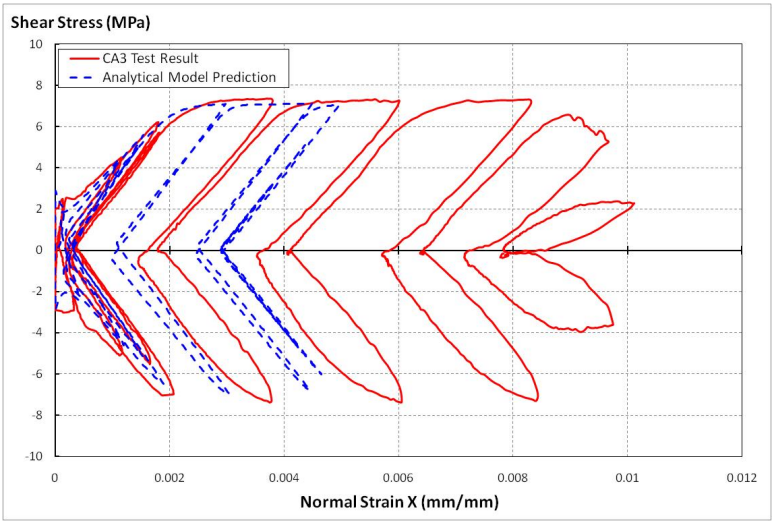

Figure 4.31. Specimen CA3, comparison of shear stresses vs. normal strains in x direction

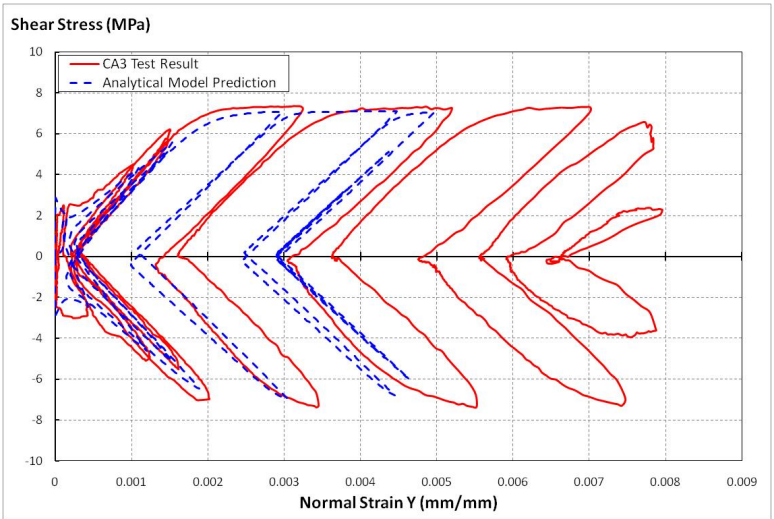

Figure 4.32. Specimen CA3, comparison of shear stresses vs. normal strains in y direction

4.3.2.3. Specimen CA4: Local response results obtained using the analytical model differs significantly from the test measurements. Since specimen CA4 had the largest reinforcement ratio among the three specimens, (2.77%), the model has not predicted any yielding in the reinforcement during the entire loading history. Test observations also revealed no yielding of reinforcement; however, in the test measurements, a significant increase in strain values is revealed, reaching up to 10 times of the elastic range of strain

values. Since such inconsistency is not observed in the analytical results, the model underestimates the measured residual strain in x direction by approximately 10 times (Figure 4.33).

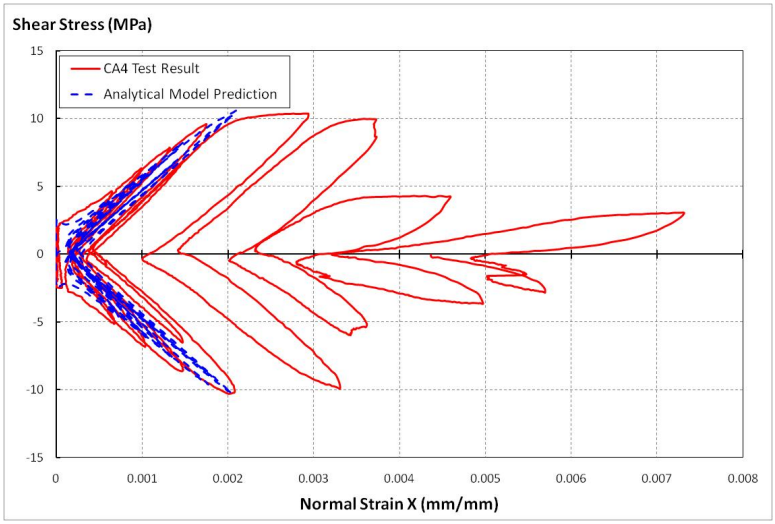

Figure 4.33. Specimen CA4, comparison of shear stresses vs. normal strains in x direction

In the y direction, while the analytical model predicts almost the same strain values as those in the x direction, the measured strains in y direction are almost half of the strains in x direction (Figure 4.34). This inconsistency in the test results may be again attributed to imperfections in the test setup or in material properties of the test specimens.

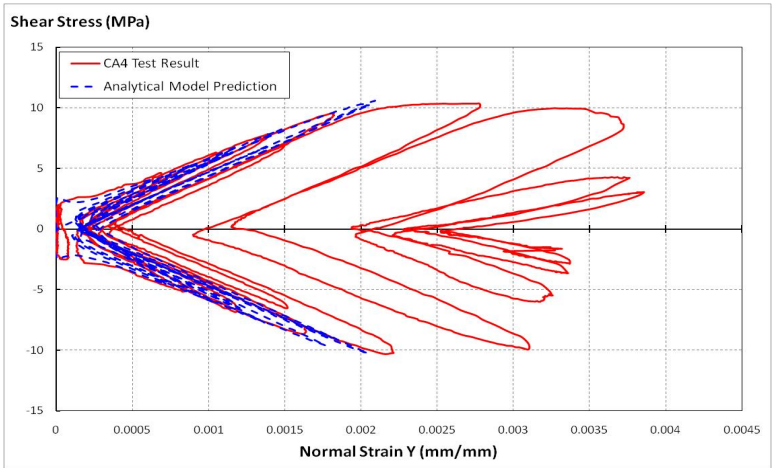

Figure 4.34. Specimen CA4, comparison of shear stresses vs. normal strains in y direction

4.4. General Discussion of Model Results and Effectiveness

All of these comparisons can be used to reveal the following attributes of the proposed Fixed Strut Angle panel model (FSAM);

- The proposed FSAM, with its robust material constitutive relationships, can provide reasonably accurate cyclic stiffness predictions for the all panel specimens investigated in this study, independently from the reinforcement ratio, loading type, or loading history.

- The proposed FSAM can predict shear stress and strain at cracking, accurately. Nevertheless, it should be mentioned that the prediction of cracking strain or stress (as well as crack direction) is highly sensitive the adopted stress–strain behavior for concrete in tension, necessitating careful calibration.

- The proposed FSAM can predict the overall shear stress capacity of a panel with reasonable accuracy. For the panel specimens considered, shear capacity predictions range between 80% and 90% of test results, indicating that the model consistently underestimates the shear capacity, although with small error. This is expected, since the model formulation follows a zero shear aggregate interlock assumption. Incorporating a constitutive model to represent cyclic shear aggregate interlock could improve the accuracy; however, the results reveal that the zero aggregate assumption is reasonable for the panels investigated. The FSAM can also predict the failure mode of the panel specimens investigated, as shown in the global comparisons for the CA series panels by Mansour and Hsu (2005).

- Results of the FSAM are highly sensitive to the parameters used in calibration of the constitutive material models. Material behavioral coefficients associated with compression softening, tension stiffening, and cyclic damage also influence the model results to a large extent. Considering that the model is only a three-degree-of-freedom system allowing minimal redundancy or redistribution in the behavior, it is believed that such sensitivity to material parameters can be reduced when the FSAM is used as a constitutive model implemented into a global Finite Element formulation.

As well, the material behavioral coefficients used in this study were proposed by prior researchers. New coefficients and empirical relationships obtained upon further research can improve the effectiveness of the model, as the model's simple formulation allows the flexibility to easily incorporate new constitutive models and material behavioral coefficients.

As far as local response (strain) estimations are concerned, it appears the FSAM is not capable of providing accurate predictions of local responses. However, it should be mentioned, the test measurements of local strain responses compared with the model predictions have possess inconsistencies; including different strain readings on two faces of panel specimen or different strain readings, up to three times, for in two orthogonal directions for a symmetrically reinforced panel subjected to pure shear. When these experimental inconsistencies are considered, it is difficult to conclude on the accuracy (or weakness) of the model in predicting local responses.

Compared with previously-developed cyclic panel models, the FSAM can be deemed effective for predicting the cyclic behavior of RC panels, considering both its comparable accuracy and relative simplicity.

4.5. Parametric Sensitivity Studies on the Fixed Strut Angle Model

Since the results of the FSAM were found to be sensitive to the parameters used in calibration of the constitutive material models, parametric studies were conducted to investigate the sensitivity of the model results to variations in material constitutive parameters, the estimation of which typically involves a level of uncertainty.

Three significant parameters were selected from the constitutive models used for both concrete and reinforcing steel, and the influence of these parameters on the overall shear stress versus shear strain behavior predicted by the model was investigated. Since the model results were found to be also highly sensitive to reinforcement ratios in x and y directions, the effect of each material parameter was investigated considering two different reinforcement ratios in a panel, $\rho_{sx}=\rho_{sy}=0.0075$, and $\rho_{sx}=\rho_{sy}=0.03$.

4.5.1. Effect of Concrete Parameters

As described in Chapter 3, the Chang and Mander (1994) constitutive model for concrete defines the monotonic compressive backbone curve of concrete, with the help of six main parameters, including:

- $f'c$: Compressive Strength of concrete
- ε_{co} : Strain value corresponds to peak stress value
- E_c : Elastic modulus of concrete
- r : Parameter defines the shape of envelope curve
- x_{cr}: Parameter defines the post peak behavior

Three of those parameters, $f'c$, Ec and x_{cr}, define the compressive strength of concrete, shape of envelope curve, and post peak geometry of envelope curve, respectively. The sensitivity of the FSAM results to these three parameters are investigated in the following subsections.

4.5.1.1. Effect of Concrete Post Peak Behavior on Overall Behavior: The post-peak (descending) geometry of the compressive stress-strain envelope of concrete is controlled by the x_{cr} parameter. Since this parameter controls the transition between the Tsai-equation-based curve and the linear descending region of the envelope, different types of post-peak behavior can been generated for different values of x_{cr}, including an asymptotic descending curve or linear descending behavior with different slopes. Values of 1.5, 1.14 and 10000 were chosen to investigate the sensitivity of the proposed model to x_{cr}.

The effect of parameter x_{cr} on the compressive envelope of the concrete stress-strain relationship is plotted in Figure 4.35.

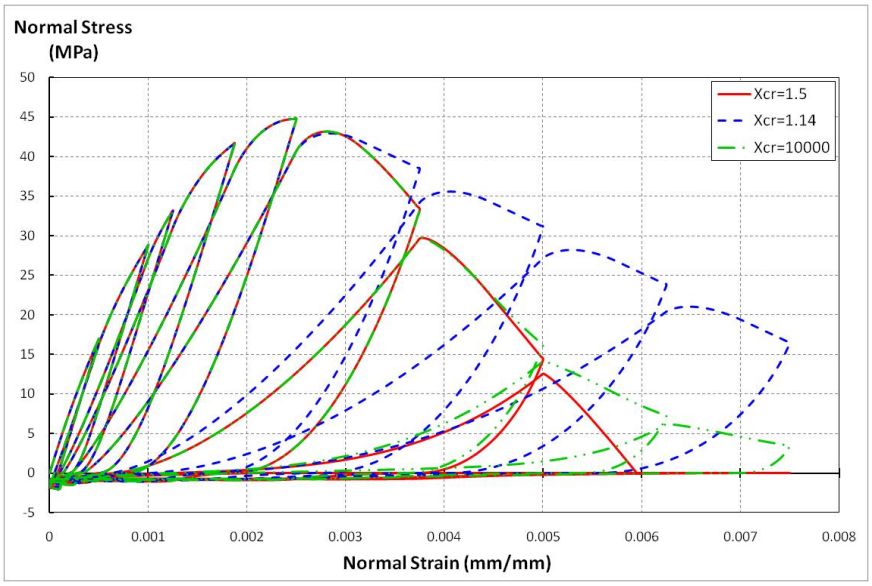

Figure 4.35. Effect of used post peak parameters on the compressive envelope of concrete

Result of six different analyses for two reinforcement ratios considered and the three values used for parameter x_{cr} are presented in Figure 4.36.

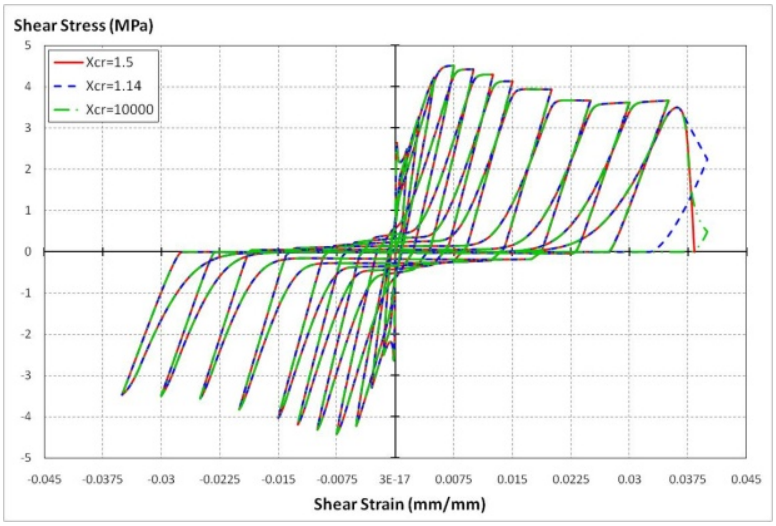

a-) $\rho_{sx}=\rho_{sy}=0.0075$

Based on the analysis results, following remarks can be made:

- Since the reinforcement ratio of the panel directly dictates the type of behavior, when the reinforcement ratio is 0.75%, the behavior is dominated by steel yielding, and the concrete stress-strain relationship does not propagate into the descending region.

Therefore, no significant influence of post-peak stress-strain behavior of concrete on the overall response is observed (Figure 4.36a).

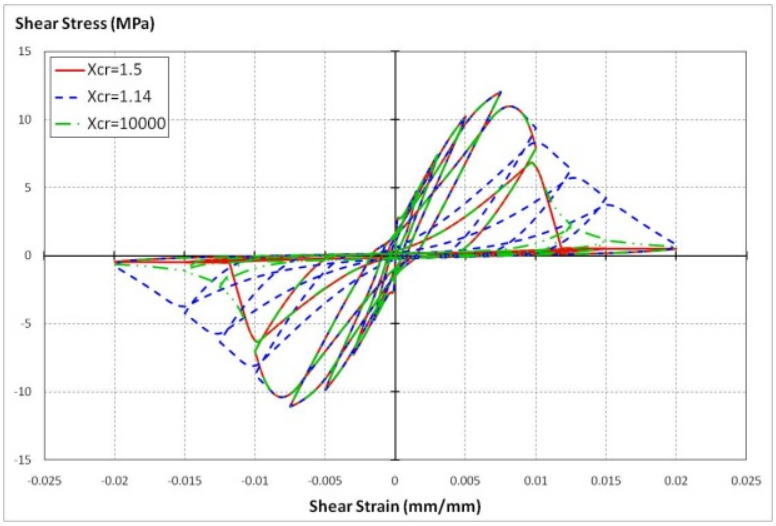

b-) $\rho_{sx}=\rho_{sy}=0.03$

Figure 4.36. Effect of parameter x_{cr} on the overall response prediction of the FSAM

- When the reinforcement ratio is 3%, the behavior of the panel is governed by concrete stress-strain behavior, clearly showing the effect of parameter x_{cr} on the model response (Figure 4.36b).

4.5.1.2. Effect of Peak Compressive Stress (Strength) of Concrete on Overall Behavior: Compressive strength of concrete is controlled by parameter *f'c*. Values of 45 MPa and 34 MPa were chosen to investigate the sensitivity of the model to the concrete compressive strength.

The effect of parameter *f'c* on the compressive envelope of the concrete stress-strain relationship is plotted in Figure 4.37.

Result of six different analyses for two reinforcement ratios considered and the two values used for parameter *f'c* are presented in Figure 4.38.

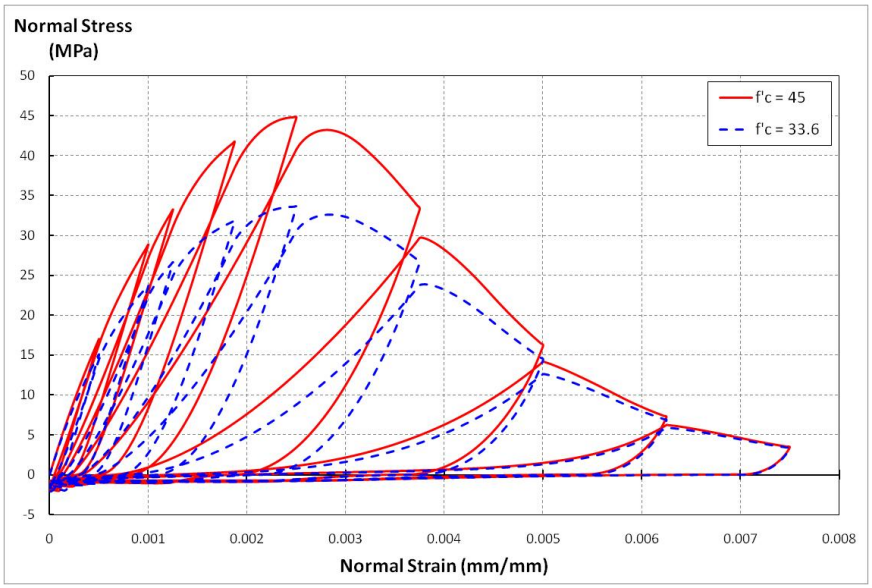

Figure 4.37. Effect of parameter *f'c* on the compressive stress-strain envelope of concrete

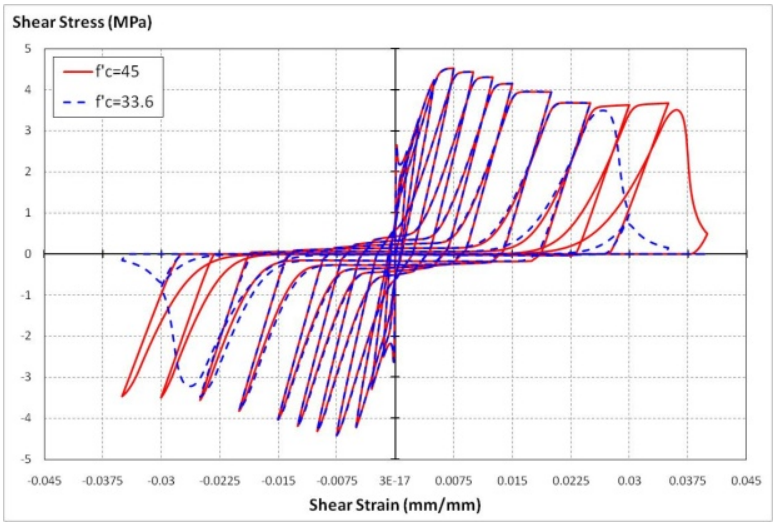

a-) $\rho_{sx}=\rho_{sy}=0.0075$

Based on the analysis results, following remarks can be made:

- When the reinforcement ratio is 0.75%, the behavior is dominated by steel yielding; no significant influence of concrete compressive strength on the overall response is observed (Figure 4.38a).

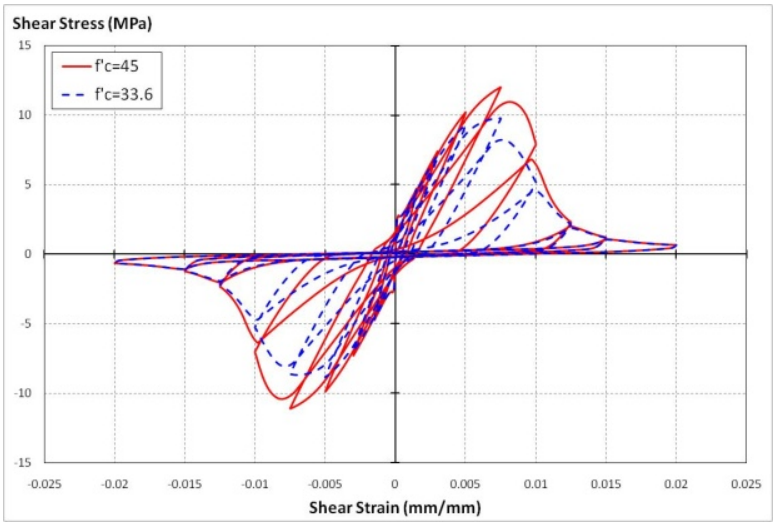

b-) $\rho_{sx}=\rho_{sy}=0.03$

Figure 4.38. Effect of concrete compressive strength on the overall response prediction of the FSAM

- When the reinforcement ratio is 3%, the behavior of the panel is governed by concrete stress-strain behavior, clearly showing the effect of concrete compressive strength on the model response. For this analysis, it can be observed that 25% decrease in concrete compressive strength causes 19% decrease in the shear stress capacity of the panel (Figure 4.38b).

4.5.1.3. Effect of Modulus of Elasticity of Concrete on Overall Behavior: The initial modulus (Modulus of Elasticity) of concrete is controlled by parameter E_c, which also influences the shape of the concrete stress-strain relationship. Values of 31000 MPa and 62000 MPa were chosen to investigate the sensitivity of the model to the elastic modulus of concrete.

The effect of parameter E_c on the compressive envelope of the concrete stress-strain relationship is plotted in Figure 4.39.

Result of six different analyses for two reinforcement ratios considered and the two values used for parameter E_c are presented in Figure 4.40.

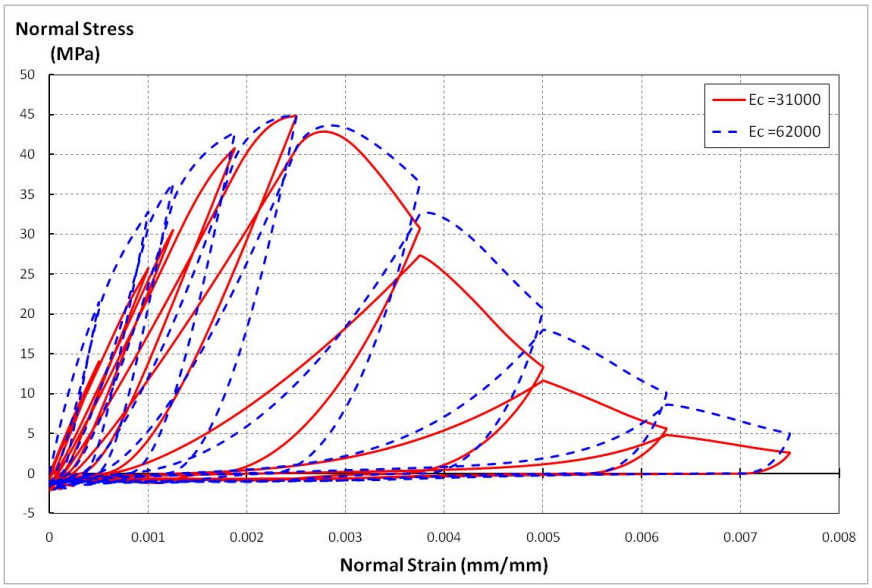

Figure 4.39. Effect of parameter E_c on the compressive stress-strain envelope of concrete

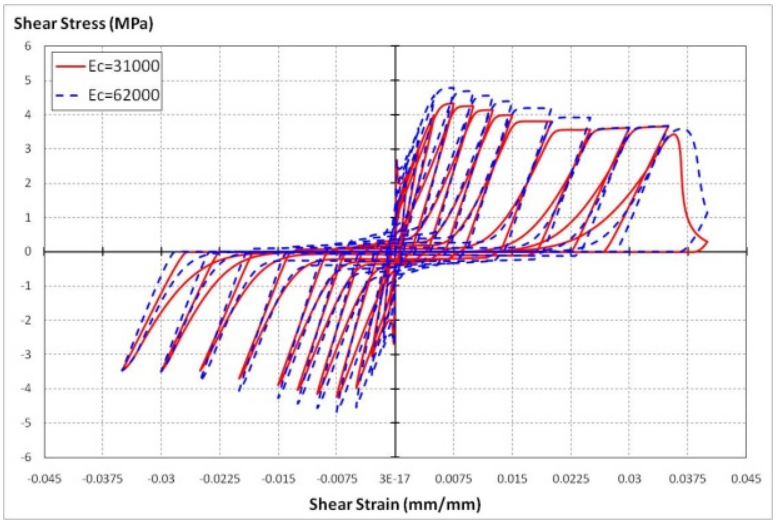

a-) $\rho_{sx}=\rho_{sy}=0.0075$

Based on the analysis results, following remarks can be made:

- Even when the reinforcement ratio is 0.75%, the predicted response is moderately sensitive to the elastic modulus of concrete, indicating that careful calibration of this parameter is provides a more reliable response prediction. (Figure 4.40a).

- When the reinforcement ratio is 3%, the behavior of the panel is governed by concrete stress-strain behavior, clearly showing the effect (although again moderate) of concrete elastic modulus on the model response. (Figure 4.40b).

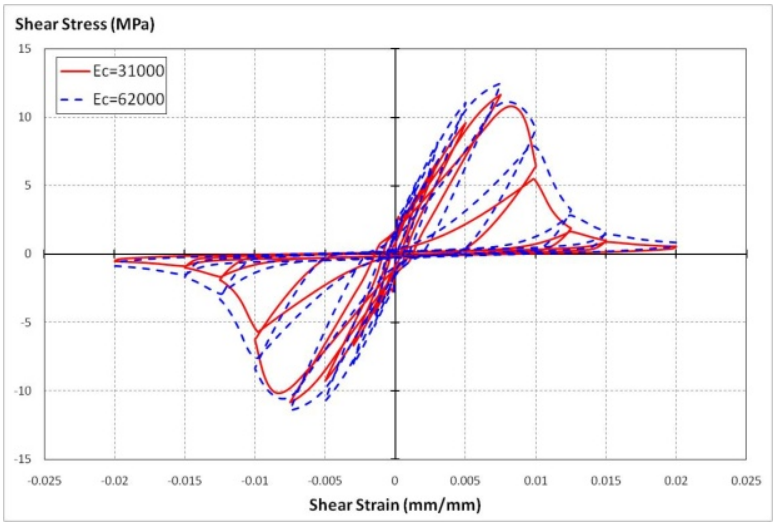

b-) $\rho_{sx}=\rho_{sy}=0.03$

Figure 4.40. Effect of concrete elastic modulus on the overall response prediction of the FSAM

4.5.2. Effect of Steel Parameters

As described in Chapter 3, the Menegotto and Pinto (1973) constitutive model for reinforcing steel defines the hysteretic behavior of reinforcing steel with two (elastic and yield) asymptotes and curved transitions in between, using of seven main parameters, including:

- σ_y :Yield stress
- ε_y :Yield strain
- E_{st} :Elastic modulus
- b :Parameter controlling strain hardening
- R_0, a_1 and a_2 : Parameter controlling the Bauschinger's effect

Three of those parameters, σ_y, a_2 and b, define the yield stress of steel, the amount of strain hardening, and the intensity of the Bauschinger's effect, respectively. The sensitivity of the FSAM results to these three parameters is investigated in the following subsections.

4.5.2.1. Effect of Yield Stress of Reinforcing Steel on Overall Behavior: The yield stress of steel is controlled by parameter f_y, and is the most important parameter for defining the behavior of steel. There may be uncertainties in calibration of this parameter, due to tension stiffening effects. Values of 300 MPa and 450 MPa were chosen to investigate the sensitivity of the model to the yield stress of reinforcing steel.

The effect of steel yield stress on the cyclic stress-strain behavior of reinforcing steel is shown in Figure 4.41.

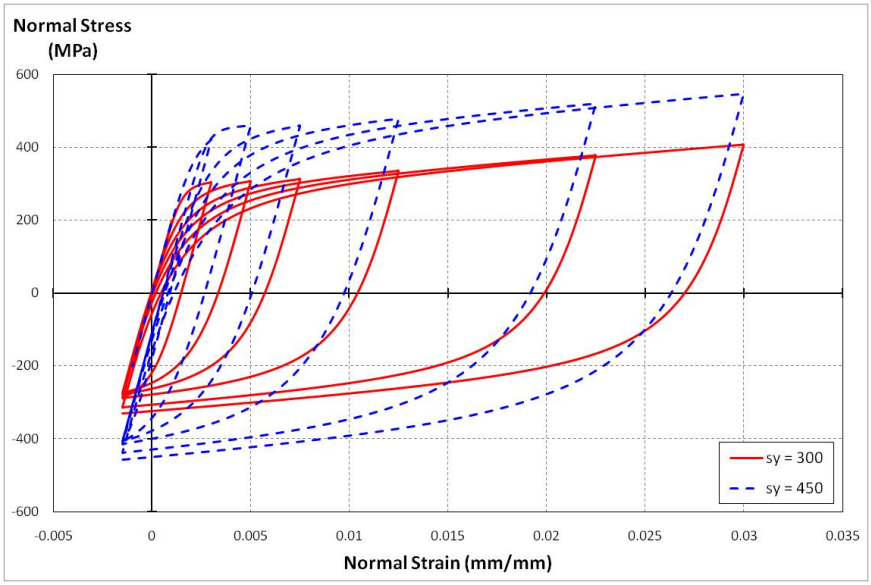

Figure 4.41. Effect of yield strength parameters on the tensile envelope of steel reinforcement

Result of six different analyses for two reinforcement ratios considered and the two values used for parameter f_y are presented in Figure 4.42.

Based on the analysis results, following remarks can be made:

- When the reinforcement ratio is 0.75%, the response is dominated by steel stress-strain behavior. Therefore, variation in the yield stress of steel creates a significant difference in the overall response. In this case, a 33% decrease in yield stress of creates a 23% decrease in the shear stress capacity prediction of the model (Figure 4.42a).

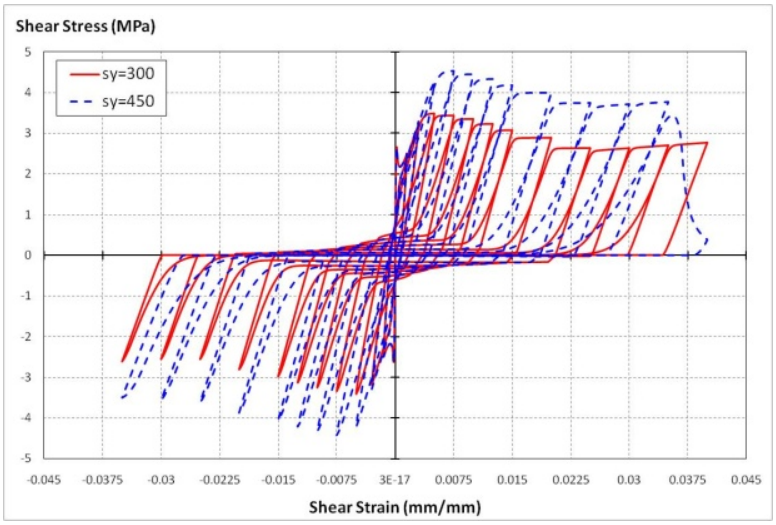

a-) $\rho_{sx}=\rho_{sy}=0.0075$

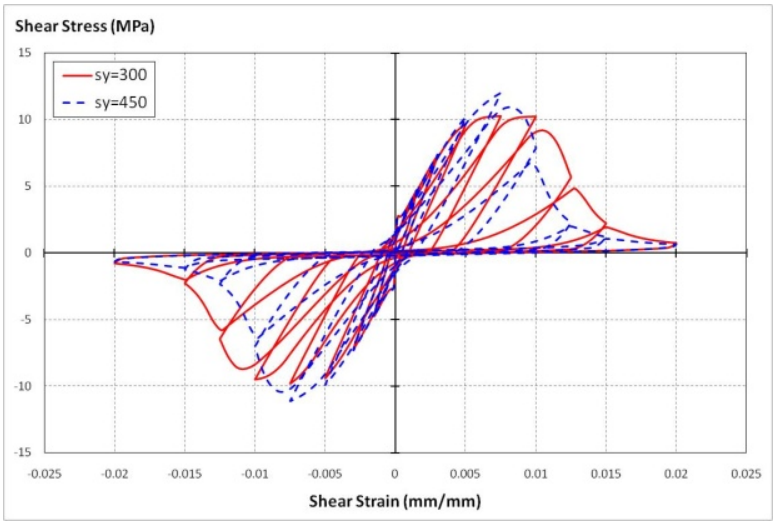

b-) $\rho_{sx}=\rho_{sy}=0.03$

Figure 4.42. Effect of steel yield stress on overall response of the FSAM

- Even when the reinforcement ratio is as high as 3% and the behavior of the panel is governed by concrete stress-strain behavior, a significant change in the steel yield

stress can change the failure mode of the panel, and the failure mode can be transformed into a mixed type failure, where nonlinear behavior of steel and concrete together control the response (Figure 4.42b), or even steel-yielding type of failure

4.5.2.2. Effect of Strain Hardening Properties of Reinforcing Steel on Overall Behavior: The kinematic strain hardening ratio of reinforcing steel is controlled by parameter *b*, the calibration of which is also subject to uncertainty due to tension stiffening effects. Values of 0.015 and 0.03 were chosen to investigate the sensitivity of the model to the strain hardening in reinforcing steel.

The effect of kinematic strain hardening on the cyclic stress-strain behavior of reinforcing steel is shown in Figure 4.43.

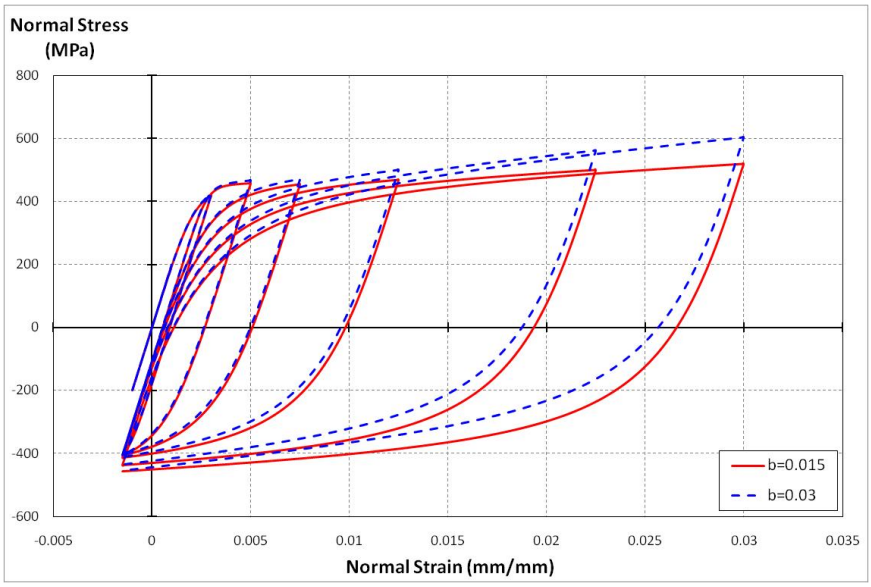

Figure 4.43. Effect of steel strain hardening parameters on the cyclic stress-strain behavior of reinforcing steel

Result of six different analyses for two reinforcement ratios considered and the two values used for parameter *b* are presented in Figure 4.44.

Based on the analysis results, following remarks can be made:

- When the reinforcement ratio is 0.75%, the effect of strain hardening on the response can be observed as both as a difference in capacity for further loading cycles and a difference in the shear strain at failure (Figure 4.44a).

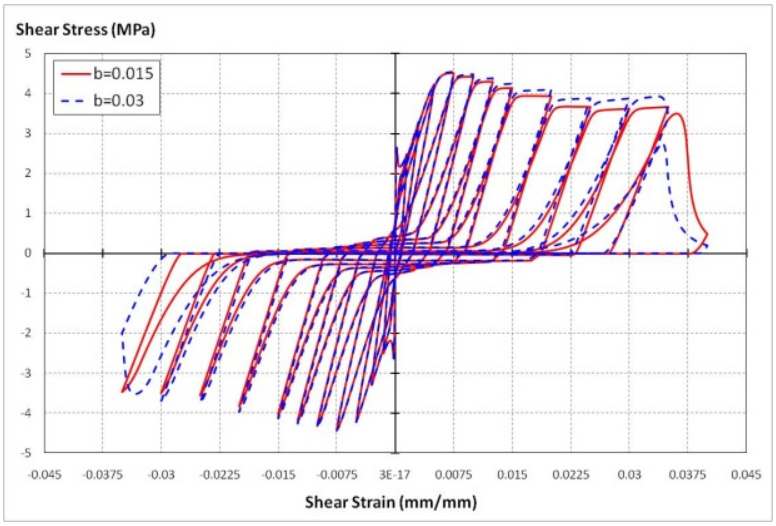

a-) $\rho_{sx}=\rho_{sy}=0.0075$

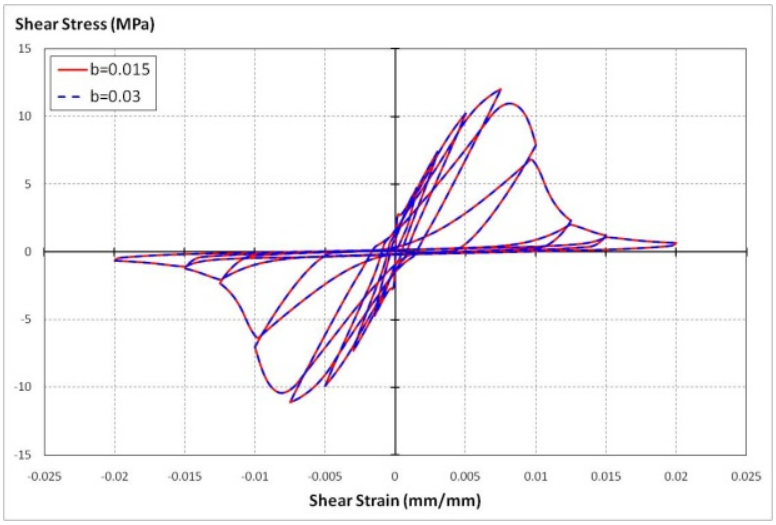

b-) $\rho_{sx}=\rho_{sy}=0.03$

Figure 4.44. Effect of steel strain hardening on the overall response predicted by the FSAM

- When the reinforcement ratio is high as 3%, and the behavior of the panel is governed by concrete stress-strain behavior, no influence of strain hardening on the response is observed (Figure 4.44b).

4.5.2.3. Effect of Bauschinger's Effect Properties of Reinforcing Steel on Overall Behavior: The Bauschinger's effect on the stress-strain behavior of reinforcing steel is typically controlled by parameter a_2, which significantly affects the curvature of the unloading and reloading branches of the stress-strain relationship. There may be uncertainties in calibration of parameter a_2 in the absence of cyclic stress-strain test results for reinforcing steel bars. In the literature, the two values typically used for calibration of parameter a_2 are 0.15 and 0.0015. These values were chosen to investigate the sensitivity of the model to the Bauschinger's effect on reinforcing steel.

The influence of the Bauschinger's effect on the cyclic stress-strain behavior of reinforcing steel is shown in Figure 4.45.

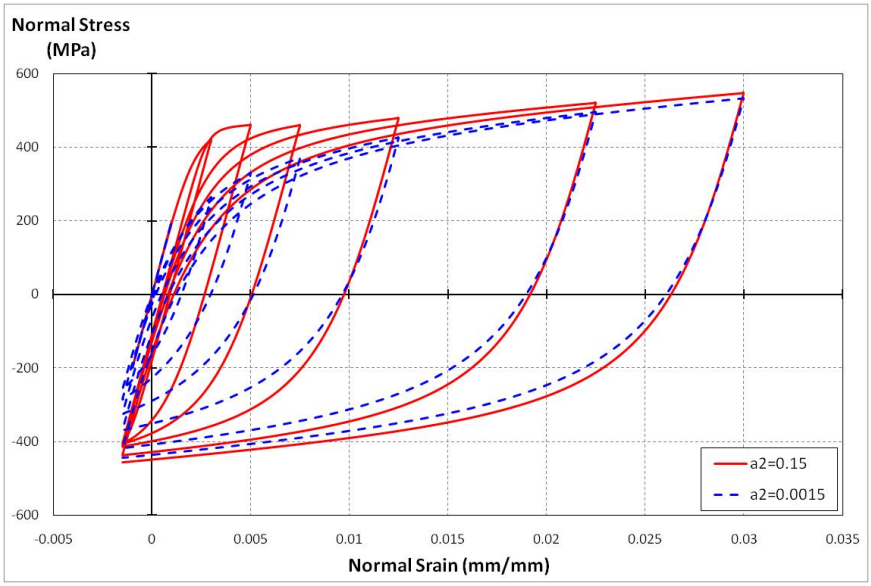

Figure 4.45. Effect of Bauschinger's effect on the cyclic stress-strain behavior of reinforcing steel

Result of six different analyses for two reinforcement ratios considered and the two values used for parameter a_2 are presented in Figure 4.46.

The analysis results reveal that the Bauschinger's effect, independently from the reinforcement ratio, significantly influences the cyclic response prediction of the FSAM. It does not only influence the shear stress capacity, but may also control the failure more (steel yielding versus concrete crushing) of the panel, implying that careful calibration of

this parameter is important. In this study, the accurate response prediction were obtained upon using a value of 0.15 for parameter a_2, which is the originally-proposed most widely used value in the literature for calibration of this parameter (Menegotto and Pinto, 1974).

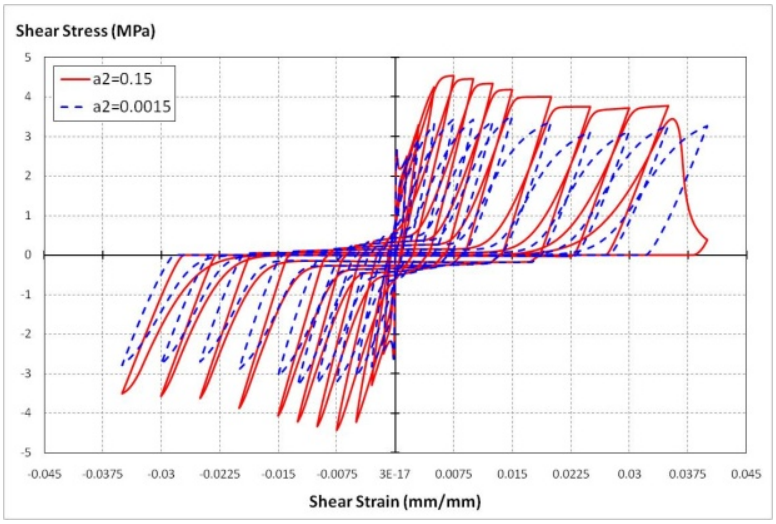

a-) $\rho_{sx}=\rho_{sy}=0.0075$

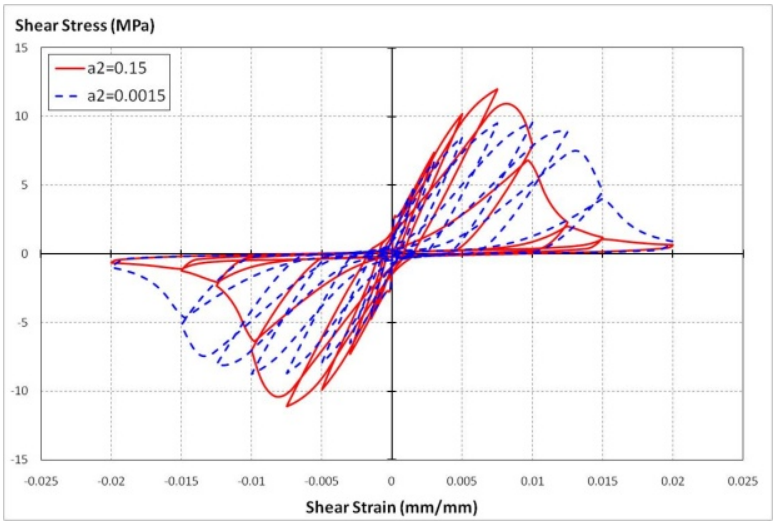

b-) $\rho_{sx}=\rho_{sy}=0.03$

Figure 4.46. Effect of Bauschinger's Effect in reinforcing steel on overall response predicted by the FSAM

5. SUMMARY AND CONCLUSIONS

5.1. Overview

A novel constitutive model (the Fixed Strut Angle Model – FSAM) is proposed in this study for simulating the cyclic shear behavior of reinforced concrete (RC) panel elements. The constitution of the FSAM is based on interpretation of previously-developed reinforced concrete panel models, as well as the results of panel tests available in the literature.

A detailed review of available constitutive panel models in the literature was first conducted, identifying the behavioral characteristics of each, as well as their shortcomings and inconsistencies. A new and simple constitutive formulation was then proposed, one which can simulate with reasonable accuracy, the cyclic behavior of reinforced concrete panel elements with different reinforcement configurations under generalized in-plane loading conditions.

The model formulation was incorporated into a nonlinear solution strategy and correlation studies were conducted for a detailed comparison of model results with the results of cyclic panel tests available in the literature, at both local and global response levels. Parametric studies were also performed to identify the sensitivity of the model results to variation and uncertainties in material parameters.

5.2. Conclusions

Based on the results of this analytical study, the following conclusions were reached:

- The FSAM is the simplest constitutive formulation that is capable of simulating the reversed cyclic stress–strain response of a reinforced concrete panel element. Despite its simple formulation and well-defined assumptions, results of the correlation studies conducted indicate that the FSAM consistently provides reasonably accurate

response predictions RC panels with various reinforcement ratios, subjected to various loading conditions. The model was shown to capture the overall behavioral attributes RC panels, including cyclic shear stress versus shear strain behavior, cracking stress, stiffness, cyclic stiffness degradation, pinching, ductility, and failure mode.

- Results of the comparisons reveal that shear stress capacity predictions of the FSAM range between 80% and 90% of test results, indicating that the model consistently underestimates the shear capacity, although with relatively small error. This is expected, since the model formulation follows a zero shear aggregate interlock assumption. Incorporating a constitutive model to represent cyclic shear aggregate interlock could improve the accuracy; however, the results reveal that the zero aggregate assumption is reasonable for the panels investigated.

- It appears the FSAM is not capable of providing consistently accurate predictions of local deformations. However, when experimental inconsistencies in local strain measurements are considered, it is difficult to conclude on the accuracy (or weakness) of the model in predicting local deformations.

- The formulation of the FSAM does not involve inherent complexities, which make its revision, or further improvement, difficult. The flexible formulation of the FSAM allows revisions including implementation of different constitutive material models and shear aggregate interlock relationships, as well as incorporation of different compression softening, tension stiffening, and biaxial damage parameters. However, the state-of-the-art constitutive material models used in this study for concrete and reinforcing steel have been shown to be very satisfactory in simulating the material behavior and failure modes of the RC panels investigated.

- Parametric sensitivity studies have shown that the model is highly sensitive to calibration of material parameters. Material behavioral coefficients associated with compression softening, tension stiffening, and cyclic damage also influence the model results to a large extent. Considering that the model is only a three-degree-of-freedom system allowing minimal redundancy or redistribution in the behavior, it is

believed that such sensitivity of the analytical results to material parameters can be reduced when the FSAM is used as a constitutive model implemented into a global finite element formulation.

With all these features, the Fixed Strut Angle Model provides an excellent balance between accuracy and simplicity. The model is presented as a simple and effective alternative to existing constitutive panel models in the literature.

5.3. Recommendations for Future Research

The following can be recommended as the scope of further research in the area:

- The proposed FSAM can be easily implemented into a two-dimensional finite-element analysis formulation, for efficient and practical cyclic response prediction of reinforced concrete walls with various geometries and reinforcement details.

- Appropriate cyclic constitutive relationships for shear aggregate interlock and bond slip can be incorporated in the formulation of the model, in order to investigate the effects of such behavioral features in the response of reinforced concrete panels or walls.

REFERENCES

Belarbi, A. and T.C. Hsu, "Constitutive Laws of Concrete in Tension and Reinforcing Bars Stiffened By Concrete", *ACI Structural Journal*, Vol. 91, No. 4, pp. 465-474, July 1994.

Belarbi, A. and T.C. Hsu, "Constitutive Laws of Softened Concrete in Biaxial Tension Compression", *ACI Structural Journal*, Vol. 119, No. 12, pp. 3590-3610, September-October 1995.

Chang, G.A. and J.B. Mander, *Seismic Energy Based Fatigue Damage Analysis of Bridge Columns: Part I-Evaluation of Seismic Capacity*, NCEER Report No. 94-0006, National Center for Earthquake Engineering Research, 1994.

Clarke, M.J. and G.J. Hancock, "A Study of Incremental-Iterative Strategies for Non-Linear Analyses", *International Journal for Numerical Methods in Engineering*, Vol. 29, pp. 1365-1391, 1990.

Collins, M.P. and D.Mitchell, *Prestressed Concrete Structures*, Prentice Hall, New Jersey, USA, 1991.

Filippou, F.C., E.G. Popov and V.V. Bertero, *Effects of Bond Deterioration on Hysteretic Behavior of Reinforced Concrete Joints*, EERC Report No. UCB/EERC-83/19, University of California, Berkeley, 1983.

Gérin, M. and P. Adebar, "Simple Rational Model for Reinforced Concrete Subjected to Seismic Shear", *ASCE Journal of Structural Engineering*, Vol. 83, No. 2, pp. 219-231, December 1993.

Gopalaratnman, V.S. and S.P. Shah, "Softening Response of Plain Concrete under Direct Tension", *Journal of the American Concrete Institute*, Vol. 82, No. 3, pp. 310-323, 1985.

Hsu, T.C., "Softened Truss Model Theory for Shear and Torsion", *ACI Structural Journal*, Vol. 85, No. 6, pp. 624-635, November-December 1988.

Hsu, T.C. and L. Zhang, "Tension Stiffening in Reinforced Concrete Membrane Elements", *ACI Structural Journal*, Vol. 93, No. 1, pp. 108-115, January-February 1996.

Hsu, T.C. and R.H. Zhu, "Softened Membrane Model for Reinforced Concrete Elements in Shear", *ACI Structural Journal*, Vol. 99, No. 4, pp. 460-469, July-August 2002.

Hsu, T.C. and M.Y. Mansour, "Failure Mechanism of Reinforced Concrete Under Cyclic Loading", *ACI Special Publications*, Vol. 206, pp. 1-25, April 2002.

Karsan, I.D. and J.O. Jirsa, "Behavior of Concrete under Compressive Loadings", *ASCE Journal of the Structural Division*, Vol. 95, No. ST12, pp. 2543-2563, 1969.

Kupfer, H., H.K. Hilsdorf and H. Rüsch, "Behavior of Concrete under Biaxial Stresses", *ACI Structural Journal*, Vol. 66, No. 8, pp. 656-666, August 1969.

Mander, J.B., M.J.N Priestley and R. Park, "Theoretical Stress-Strain Model for Confined Concrete", *ASCE Journal of Structural Engineering*, Vol. 114, No. 8, pp. 1804-1826, 1988a.

Mander, J.B., M.J.N Priestley and R. Park, "Observed Stress-Strain Model of Confined Concrete", *ASCE Journal of Structural Engineering*, Vol. 114, No. 8, pp. 1827-1849, 1988b.

Mansour, M.Y., *Behavior of reinforced concrete elements under cyclic shear: Experiments to theory*, Ph.D. Thesis, Department of Civil Engineering, University of Houston, 2001.

Mansour, M.Y., T.C. Hsu and J.Y. Lee, "Pinching Effect in Hysteretic Loops of R/C Shear Elements", *ACI Special Publications*, Vol. 205, pp. 293-321, January 2002.

Mansour, M.Y. and T.C. Hsu, "Behavior of Reinforced Concrete Elements under Cyclic Shear", *ASCE Journal of Structural Engineering*, Vol. 131, No. 1, pp. 44-53, January 2005.

Matlab v.7.6.0.324 (R2008a), The Math-Works, Inc., Massachusetts USA, 2008.

Mau, S.T. and T.C. Hsu, "Shear Design and Analysis of Low-Rise Structural Walls", *ACI Structural Journal*, Vol. 83, No. 2, pp. 306-315, March 1986.

Mau, S.T. and T.C. Hsu, "Shear Behavior of Reinforced Concrete Framed Wall Panels With Vertical Loads", *ACI Structural Journal*, Vol. 84, No. 3, pp. 228-234, May 1987.

Menegotto, M. and E. Pinto, "Method of Analysis for Cyclically Loaded Reinforced Concrete Plane Frames Including Changes in Geometry and Non-Elastic Behavior of Elements under Combined Normal Force and Bending", Proceedings, *IABSE Symposium on Resistance and Ultimate Deformability of Structures Acted on by Well-Defined Repeated Loads*, Lisbon, Portugal, 1973.

Mitchell, D. and M.P. Collins, "Diagonal Compression Field Theory – A Rational Model for Structural Concrete in Pure Torsion", *ACI Structural Journal*, Vol. 71, No. 8, pp. 396-408, August 1974.

Ohmori, N., T. Takahashi, N. Inoue, K. Kurihara and S. Watanabe, "Experimental studies on nonlinear behaviors of reinforced concrete panels subjected to cyclic in-plane shear", *Trans AIJ*, Vol. 403, pp. 105-117, 1989.

Okamoto, S., S. Shiomi and K. Yamabe, "Earthquake Resistance of Prestressed Concrete Structures", *AIJ Proceedings, Annual Convention*, pp. 1251-1252, 1976.

Palermo, D. and F.J. Vecchio, "Compression Field Modeling of Reinforced Concrete Subjected to Reversed Loading: Formulation", *ACI Structural Journal*, Vol. 100, No. 5, pp. 616-625, September-October 2003.

Pang, D. and T.C. Hsu, "Behavior of Reinforced Concrete Membrane Elements in Shear", *ACI Structural Journal*, Vol. 92, No. 6, pp. 665-677, November-December 1995.

Pang, D. and T.C. Hsu, "Fixed Angle Softened Truss Model for Reinforced Concrete", *ACI Structural Journal*, Vol. 93, No. 2, pp. 197-207, March-April 1996.

Popovics, S., "A Numerical Approach to the Complete Stress-Strain Curve of Concrete", *Cement and Concrete Research*, Vol. 3, No. 4, pp. 583-599, 1973.

Powell, G. and J. Simons, "Improved Iteration Strategy for Nonlinear Structures", *International Journal for Numerical Methods in Engineering*, Vol.17, pp. 1455-1467, 1981.

Saatçioğlu, M. and S. Razvi, "Strength and Ductility of Confined Concrete", *ASCE Journal of Structural Engineering*, Vol. 118, No. 6, pp. 1590-1607, November 1992.

Sinha B.P., K.H. Gerstle and L.G. Tulin, "Stress-Strain Relations for Concrete under Cyclic Loading", *Journal of the American Concrete Institute*, Vol. 61, No. 2, pp. 195-211, 1964.

Spooner, D.C. and J.W. Dougill, "A Quantitative Assessment of Damage Sustained in Concrete During Compression Loading", *Magazine of Concrete Research*, Vol. 27, No. 92, pp. 151-160, 1975.

Stevens, N.J., *Analytical Modeling of Reinforced Concrete Subjected to Monotonic and Reversed Loadings*, Ph.D. Thesis, Department of Civil Engineering, University of Toronto, 1987.

Stevens, N.J., M. Uzumeri and M.P. Collins, "Reinforced concrete subjected to reversed cyclic shear-Experiments and constitutive model", *ACI Structural Journal*, Vol. 88, No. 2, pp. 135-146, March-April 1991.

Tanigawa, Y. and Y. Uchida, "Hysteretic Characteristics of Concrete in the Domain of High Compressive Strain", *AIJ Proceedings, Annual Convention*, pp. 449-450, 1979.

Tsai W.T., "Uniaxial Compressional Stress-Strain Relation of Concrete", *ASCE Journal of Structural Engineering*, Vol. 114, No. 9, pp. 2133-2136, 1988.

Vecchio, F.J. and M.P. Collins, "The Modified Compression-Field Theory for Reinforced Concrete Elements Subjected to Shear", *ACI Structural Journal*, Vol. 83, No. 2, pp. 219-231, March 1986.

Vecchio, F.J. and M.P. Collins, "Predicting the Response of Reinforced Concrete Beams Subjected to Shear Using Modified Compression Field Theory", *ACI Structural Journal*, Vol. 85, No. 3, pp. 258-268, May-June 1988.

Vecchio, F.J. and M.P. Collins, "Compression Response of Cracked Reinforced Concrete", *ASCE Journal of Structural Engineering*, Vol. 83, No. 2, pp. 219-231, December 1993.

Vecchio F.J., "Disturbed Stress Field Model for Reinforced Concrete: Formulation", *ASCE Journal of Structural Engineering*, Vol. 126, No. 9, pp. 1070-1077, September 2000.

Yankelevsky, D.Z. and H.W. Reinhardt, "Response of Plain Concrete to Cyclic Tension", *ACI Materials Journal*, Vol. 84, No. 5, pp. 365-373, 1987.